AD-A103 932 SYSTEMS RESEARCH LABS INC DAYTON OH RESEARCH APPLICA--ETC F/G 21/2
APPLICATION OF COHERENT ANTI-STOKES RAMAN SCATTERING TO COMBUST--ETC(U)
FEB 81 L P GOSS, G L SWITZER F33615-77-C-2019
UNCLASSIFIED SRL-6948 AFWAL-TR-80-2122 NL

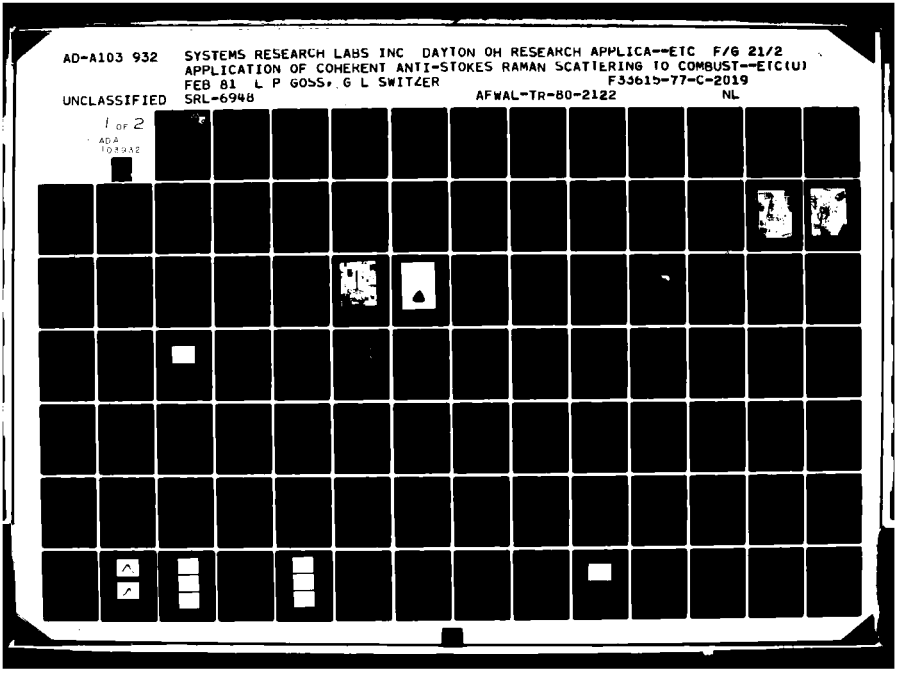

AFWAL-TR-80-2122

APPLICATION OF COHERENT ANTI-STOKES RAMAN SCATTERING TO COMBUSTION MEDIA

Larry P. Goss
Gary L. Switzer

Research Applications Division
Systems Research Laboratories, Inc.
2800 Indian Ripple Road
Dayton, Ohio 45440

February 1981

TECHNICAL REPORT AFWAL-TR-80-2122
Final Report for Period 31 May 1977 - 30 July 1980

AERO PROPULSION LABORATORY
AIR FORCE WRIGHT AERONAUTICAL LABORATORIES
AIR FORCE SYSTEMS COMMAND
WRIGHT-PATTERSON AIR FORCE BASE, OH 45433

NOTICE

When Government drawings, specifications, or other data are used for any purpose other than in connection with a definitely related Government procurement operation, the United States Government thereby incurs no responsibility nor any obligation whatsoever; and the fact that the Government may have formulated, furnished, or in any way supplied the said drawings, specifications, or other data, is not to be regarded by implication or otherwise as in any manner licensing the holder or any other person or corporation, or conveying any rights or permission to manufacture, use, or sell any patented invention that may in any way be related thereto.

This report has been reviewed by the Office of Public Affairs (ASD/PA) and is releasable to the National Technical Information Service (NTIS). At NTIS, it will be available to the general public, including foreign nations.

This technical report has been reviewed and is approved for publication.

PAUL W. SCHREIBER
Energy Conversion Branch
Aero Space Power Division

W. M. ROQUEMORE
Fuels Branch, Fuels and Lub Div
Aero Propulsion Laboratory

FOR THE COMMANDER

ROBERT D. SHERRILL
Chief, Fuels and Lubrication Division
Aero Propulsion Laboratory

ARTHUR V. CHURCHILL
Chief, Fuels Branch
Fuels and Lubrication Division
Aero Propulsion Laboratory

"If your address has changed, if you wish to be removed from our mailing list, or if the addressee is no longer employed by your organization, please notify AFWAL/POSF, W-PAFB, OH 45433 to help us maintain a current mailing list."

Copies of this report should not be returned unless return is required by security considerations, contractual obligations, or notice on a specific document.

SECURITY CLASSIFICATION OF THIS PAGE (When Data Entered)

REPORT DOCUMENTATION PAGE

READ INSTRUCTIONS BEFORE COMPLETING FORM

1. REPORT NUMBER: AFWAL-TR-80-2122	2. GOVT ACCESSION NO.: AD-A10
3. RECIPIENT'S CATALOG NUMBER: 3932	
4. TITLE (and Subtitle): APPLICATION OF COHERENT ANTI-STOKES RAMAN SCATTERING TO COMBUSTION MEDIA	5. TYPE OF REPORT & PERIOD COVERED: Final Technical Report, 31 May 1977 — 30 July 1980
	6. PERFORMING ORG. REPORT NUMBER: SRL-6948 Final
7. AUTHOR(s): Larry P. Goss, Gary L. Switzer	8. CONTRACT OR GRANT NUMBER(s): F33615-77-C-2019
9. PERFORMING ORGANIZATION NAME AND ADDRESS: Systems Research Laboratories, Inc., 2800 Indian Ripple Road, Dayton, OH 45440	10. PROGRAM ELEMENT, PROJECT, TASK AREA & WORK UNIT NUMBERS: Project 2301, Task S1, Work Unit 03; Project 3048, Task 05, Work Unit 66
11. CONTROLLING OFFICE NAME AND ADDRESS: Aero Propulsion Laboratory (AFWAL/POSF), Air Force Wright Aeronautical Laboratories (AFSC), Wright-Patterson AFB, OH 45433	12. REPORT DATE: February 1981
	13. NUMBER OF PAGES: 167
14. MONITORING AGENCY NAME & ADDRESS (if different from Controlling Office)	15. SECURITY CLASS. (of this report): UNCLASSIFIED
	15a. DECLASSIFICATION/DOWNGRADING SCHEDULE

16. DISTRIBUTION STATEMENT (of this Report)

Approved for public release; distribution unlimited.

17. DISTRIBUTION STATEMENT (of the abstract entered in Block 20, if different from Report)

18. SUPPLEMENTARY NOTES

19. KEY WORDS (Continue on reverse side if necessary and identify by block number)

Simultaneous Temperature-Concentration Measurements, Coherent Anti-Stokes Raman Scattering (CARS), Application of Nd:YAG and Dye Lasers, Polarization Background Cancellation, Hardened CARS System, Turbulence Effects, Combustion Diagnostics, Diagnostics of Practical Combustors

20. ABSTRACT (Continue on reverse side if necessary and identify by block number)

A laboratory-based system utilizing the Nd:YAG laser has been developed to investigate the Coherent Anti-Stokes Raman Scattering (CARS) of molecular gases in combustion. Single-shot and simultaneous experimental measurements of species concentration and temperature of combustion media are reported and compared with other optical techniques and theoretical predictions. The adverse effects of beam propagation through turbulence are investigated and discussed.

DD FORM 1 JAN 73 1473 EDITION OF 1 NOV 65 IS OBSOLETE

SECURITY CLASSIFICATION OF THIS PAGE (When Data Entered)

A transportable hardened CARS system, constructed to operate in adverse environments, has been used to conduct a series of investigations in a practical combustion tunnel. Temperature and number-density measurements made as a function of fuel-air flow, position in the combustion tunnel, and fuel variation--including both gaseous and liquid fuels--are reported.

PREFACE

This final report was prepared by the Research Applications Division of Systems Research Laboratories, Inc., 2800 Indian Ripple Road, Dayton, OH 45440, under Contract No. F33615-77-C-2019, Project 2301, Task S1, Work Unit 03, with Mr. Paul W. Schreiber (AFWAL/POOC) as Government Project Monitor and Project 3048, Task 05, Work Unit 66, with Dr. W. M. Roquemore (AFWAL/POSF) as Government Project Monitor. The research was conducted by Dr. Larry P. Goss, Mr. Gary L. Switzer, Mr. Darryl D. Trump, Mr. Dennis A. Mummert, Dr. Won B. Roh, and Mr. Carl G. Meyers, Jr. This report describes efforts performed during the period 31 May 1977 - 30 July 1980. The report was submitted in October 1980.

TABLE OF CONTENTS

LIST OF ILLUSTRATIONS

LIST OF ILLUSTRATIONS (Cont'd)

LIST OF ILLUSTRATIONS (Cont'd)

LIST OF ILLUSTRATIONS (Cont'd)

LIST OF ILLUSTRATIONS (Concluded)

LIST OF TABLES

Section 1

INTRODUCTION

This report describes the results of theoretical and experimental investigations of the coherent anti-Stokes Raman scattering (CARS) process of molecular gases which were conducted under USAF Contract F33615-77-C-2019.

A program is in progress at the AFWAL Aero Propulsion Laboratory (APL) to evaluate combustor models in environments which simulate many of the features in gas-turbine combustors. This program involves the selection and evaluation of appropriate diagnostic techniques for making time-averaged and time-resolved point measurements of velocity, temperature, and major species concentration in simulated, practical combustion environments.

Of the various optical diagnostic techniques, coherent anti-Stokes Raman spectroscopy (CARS) is considered to be one of the more promising methods for making temperature and species-concentration measurements in combustion environments. Favorable results have been obtained by various investigators using laboratory-type flame sources.[1-4] In addition, a preliminary evaluation of this technique using the large-scale AFWAL/APL combustor has been made,[5,6] and the results are very encouraging in view of the large scale, hostile, gas-turbine-type combustion environment in which the sensitive optical system was operated. Researchers at United Technologies Research Center have made successful temperature measurements using the BOXCARS technique in a large-scale furnace-type combustor.[7] Investigators at Shell Research Limited Thornton Research Centre have demonstrated the feasibility of using CARS to measure temperatures in a reciprocating engine.[8]

The overall objective of this contract was to establish the CARS technique as a valid combustion diagnostic tool through fundamental laboratory studies and to demonstrate the practicality of CARS through in situ testing of an environmentally hardened CARS system developed during the program.

Section 2 contains a short comprehensive review of the CARS theory to serve primarily as background material for the remaining sections.

Section 3 describes the fundamental laboratory equipment and studies which were undertaken. These include: 1) linewidth determinations by integrated power measurements; 2) flame-breakdown measurements; 3) single-shot thermometry; 4) reference-scheme studies, 5) simultaneous temperature and species-concentration measurements, and 6) turbulence effects and an experimental arrangement for their compensation.

Section 4 describes the construction, evaluation, and applications of the hardened CARS system for combustion diagnostics on the AFWAL/APL large-scale practical combustor. This includes temperature and species-concentration profiles of the combustor, comparisons of the CARS results with probe measurements, and an overall evaluation of the performance of the system in a hostile, dynamic environment.

Section 2

THEORY

In this section, highlights in the theory of the CARS process are presented in order to bring out the essential features in the analyses of the experimental data. A more complete description of the theory can be found in Refs. 9-10.

Due to the nonlinear nature of the response of a medium to strong external stimuli, the polarization induced in a medium subjected to intense light waves contains not only the frequency components of the incident waves but also linear combinations of these frequencies. This induced polarization containing many frequency components acts, in turn, as the source of a secondary wave containing the same number of frequency components.

In CARS experiments, two laser beams are used as the incident waves, one wave having the higher frequency at ω_1 (called the pump beam) and the other having the lower frequency (called the Stokes beam). Of the many secondary waves generated in the medium, the one used as the signal in a CARS experiment has the frequency at $2\omega_1 - \omega_2$ (the anti-Stokes beam). As a result of a resonance which occurs in the induced polarization when the difference frequency of the two laser beams is equal to a Raman-active vibrational frequency (ω_v) of a molecule in the medium (i.e., $\omega_1 - \omega_2 = \omega_v$), the CARS signal generated at $\omega_3 = 2\omega_1 - \omega_2$ ($= \omega_1 + \omega_v$) undergoes a resonant enhancement in intensity. Depending upon the linewidth of the laser beams employed in the experiment, slightly different versions of the theory are applicable in the analysis of the CARS process.

In the case of monochromatic incident waves, the nonlinear polarization induced at the anti-Stokes frequency is

$$P^{(3)}(t) = 3\chi^{(3)} E_1^2 E_2^* e^{i[(2k_1 - k_2) - (2\omega_1 - \omega_2)t]} \qquad (1)$$

with

$$\chi^{(3)} = \chi^{NR} + \sum_{v,J} \frac{N\Delta_{v,J} c^4}{3\hbar\omega_2^4} \left(\frac{d\sigma}{d\Omega}\right)_{v,J} \left[\frac{1}{\omega_{v,J} - (\omega_1 - \omega_2) - i\Gamma_{v,J}}\right] \qquad (2)$$

and

$$N\Delta_{v,J} = N_{v,J} - N_{v+1,J} \tag{3}$$

where $\chi^{(3)}$ is the third-order CARS susceptibility; χ^{NR} is the nonresonant third-order susceptibility; $d\sigma/d\Omega$ is the spontaneous Raman cross section; $\omega_{v,J}$ is the angular frequency of the Q-branch Raman transition; N is the molecular number density; and subscripts v and J indicate, respectively, vibrational and rotational quantum numbers of the energy level to which various parameters are related. Moreover, in thermal equilibrium, the molecular distribution is Boltzmann, i.e.,

$$N_{v,J} = \frac{N\,(2J+1)\,g_I}{Q}\, e^{-E_{v,J}/kT} \tag{4}$$

where Q is the partition function and g_I is the nuclear-spin degeneracy.

When Maxwell's equations which describe the propagation of electromagnetic waves are solved for the anti-Stokes wave after substitution of the third-order polarization as given in Eq. (1), it can be shown that the intensity of the anti-Stokes wave generated in an interaction length x is given, in the case of a phase-matched interaction, by

$$I_3 = \left(\frac{4\pi^2\omega_3}{c^2}\right)^2 |3\chi^{(3)}|^2\; I_1^2\; I_2 x^2 \tag{5}$$

Since the CARS intensity is proportional to $I_1^2\, I_2$, one can achieve a degree of spatial resolution in the measurement by focusing the incident laser beams. The lateral dimension of the laser beams (called spot size for Gaussian beams) gives the lateral resolution, and the length of the focal zone (confocal parameter for Gaussian beams) gives the longitudinal resolution along the beam direction. In such situations it is more appropriate and convenient to deal with the total power of the anti-Stokes beam rather than the intensity. Thus, in the case of the focused Gaussian beams, the anti-Stokes power generated can be approximated by

$$P_3 = \left(\frac{4\pi\omega_1\omega_3}{c^3}\right)^2 |3\chi^{(3)}|^2 P_1^2 P_2 \qquad (6)$$

where P_1 and P_2 are the power of the pump and Stokes beams, respectively.

Since the measurement of the power of the anti-Stokes wave as given by Eq. (6) will yield information for $\chi^{(3)}$ which, in turn, is related to $N_{v,J}$ by Eqs. (2) - (4), it should be possible to determine the number density for various states of any Raman-active molecular species present in the combustion media. This, in fact, forms the basis for the application of the CARS process to gas diagnostics--particularly in combustion media.

In the case of nonmonochromatic incident waves, the analysis is best carried out in the frequency domain. Since in actual experimental systems the incident beams are not really monochromatic, this case is more representative of a real experimental situation. In fact, the data presented in this paper were obtained using Gaussian beams from a single-mode ruby laser at the frequency ω_1 and a broadband dye laser centered at frequency ω_2. The measured linewidth of the single-mode pump laser was ~ 0.034 cm^{-1}; consequently, it was assumed to be monochromatic. This approximation turns out to be satisfactory for the applications under discussion. In this approximation, the spectral power density of the anti-Stokes wave becomes

$$P_3(\omega_3 + \delta) = \left(\frac{4\pi\omega_1\omega_3}{c^3}\right)^2 |3\chi^{(3)}(\omega_1, \omega_1, -\omega_2 + \delta)|^2 P_1^2 P_2(-\omega_2 + \delta) \qquad (7)$$

Equation (7), when convolved with an instrument slit function, then can be used to calculate normalized CARS spectra as a function of temperature.

For number-density measurements the bandpass of the signal-analyzing spectrometer was increased to allow measurement of the energy in the entire Q-branch. If the spectral power density of the broadband dye laser is assumed to be constant over the Q-branch, then the integrated anti-Stokes power (P_{INT}) becomes

$$P_{INT} = \int_{-\infty}^{\infty} P_3\,(\omega_3 + \delta)d\delta = K\,\frac{N^2 F(T)}{\Gamma_{eff}} \qquad (8)$$

where

$$\Gamma_{eff} \equiv \frac{\Gamma}{1 + \frac{1}{F(T)} \sum_{J>J'} \sum \frac{\Gamma^2 G_{JJ'}(T)}{(\omega_J - \omega_{J'})^2 + 4\Gamma^2}},$$

$$F(T) = \sum_J \Delta_J^2,\quad G_{JJ'}(T) = 8\Delta_J\Delta_{J'},$$

and

$$K = \left(\frac{12\pi\omega_1\omega_3}{c^3}\right)^2 \left(\frac{c^4}{3\hbar\omega_2^4}\,\frac{d\sigma}{d\Omega}\right)^2 P_1^2\,P_2$$

In evaluating the integral in Eq. (8), the Raman linewidth (Γ) was assumed to be constant for all lines and the contribution of the hot bands was neglected.

Species number densities were determined by comparing P_{INT} measured in the combustion gas with $(P_{INT})_c$ values generated in a calibration cell containing a known number density of the same species. The calculation of F(T) required knowledge of the combustion gas temperature, and $F(T_c)$ was determined from the temperature of the calibration gas (T_c). In addition, knowledge of Γ_{eff} as a function of pressure, temperature, and composition was required. Since those data were not available, only an estimated value of Γ_{eff} could be used. This value, obtained by assuming the linewidth to be proportional to the collisional frequency of the molecule, is

$$\Gamma_{eff} \propto \sigma_o\,\bar{v}(T)\,N_T^{\eta(T)} \qquad (9)$$

where σ_o is assumed to be a constant optical cross section; $\bar{v}(T)$ is the average molecular velocity; N_T is the total gas density; and $\eta(T)$ is a broadening parameter. From laboratory measurements the value of $\eta(300\ K)$ for N_2 and O_2

was determined to be ~ 0.8.[5] At combustion temperatures the value of η was assumed to be equal to 1 due to the increased separation between populated J levels. By incorporating these assumptions for Γ_{eff} into Eq. (8) and normalizing by taking the ratio $P_{INT}/(P_{INT})_c$, one obtains the expression used for determining species number density

$$N = \frac{P_c}{kT_c}\left(\frac{P_{INT}}{(P_{INT})_c}\right)^{\frac{1}{2}} \cdot \left(\frac{F(T_c)}{F(T)} \cdot \frac{T_c \cdot^3 p}{k \cdot^2 T \cdot^5 p_c}\right)^{\frac{1}{2}} \qquad (10)$$

where p and p_c are the pressures of the combustion and calibration gases, respectively, and k is the Boltzmann constant. The quantity indicated by the second bracket in Eq. (10) can be viewed as a correction factor to the number density which is required to offset the effects upon F(T) and Γ_{eff} between T_c and T. This factor is plotted in Fig. 1 for N_2 and O_2 at T_c = 300 K and p = p_c = 1 atm. The number densities obtained from this equation were then converted to mole fractions using the ideal gas law and the CARS-determined flame temperature.

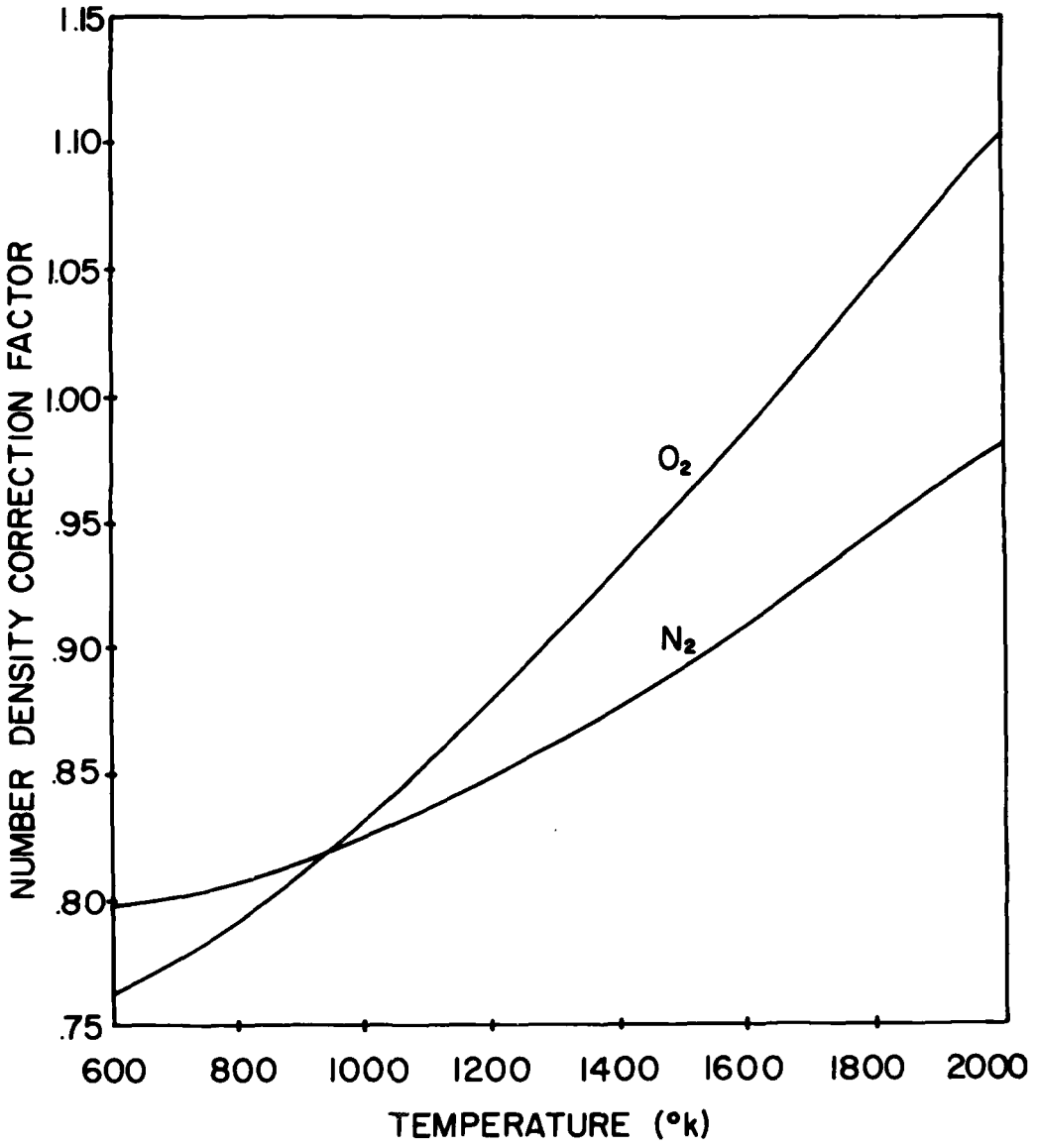

Figure 1. Plot of Number-Density Correction Factors as a Function of Temperature.

Section 3

FUNDAMENTAL LABORATORY WORK

3.1 EXPERIMENTAL APPARATUS

Ruby-Based CARS System

The ruby-based CARS system is shown schematically in Fig. 2. The system consists of a ruby-laser oscillator/amplifier, a ruby-pumped infrared dye laser, monochromator/detector and electronics, and various optics for guiding the beams. In addition, a He-Ne laser beam is used for aligning the entire CARS system. Basically, the system operates as follows: A single-mode (transverse and longitudinal) ruby-laser beam emanating from the ruby oscillator is amplified in the ruby amplifier and split into two parts by means of a beamsplitter (BS1). One part (70%) of the ruby beam is weakly focused and directed into the dye cell slightly off-axis for pumping the dye laser. The dye-laser output is combined collinearly with the other part of the ruby-laser beam and focused into a reference cell containing a non-resonant gas under high pressure (typically 30 atm). This collinear superposition of the pump and the Stokes beams satisfies the phase-matching conditions for coherent generation of anti-Stokes radiation in gases. The anti-Stokes signal generated in the reference cell is removed from the laser beams by means of a dichroic mirror (DM2), and the laser beams are refocused into the sample cell containing the medium under investigation. The ruby-laser power and pulse shape are continuously monitored by means of a PIN diode detector and a transient digitizer (Tektronix R 7912--not shown in the figure). The anti-Stokes signals--one from the reference cell and the other from the sample cell--are detected and processed using either of the detection systems shown in Fig. 3, depending upon the particular experimental requirements. These two detection systems are discussed below along with their respective modes of operation.

The broadband dye mode of operation is used for instantaneous generation of an entire Q-branch spectrum of anti-Stokes radiation in a light molecule such as N_2 and O_2 using a single laser pulse. The dye laser is (typically

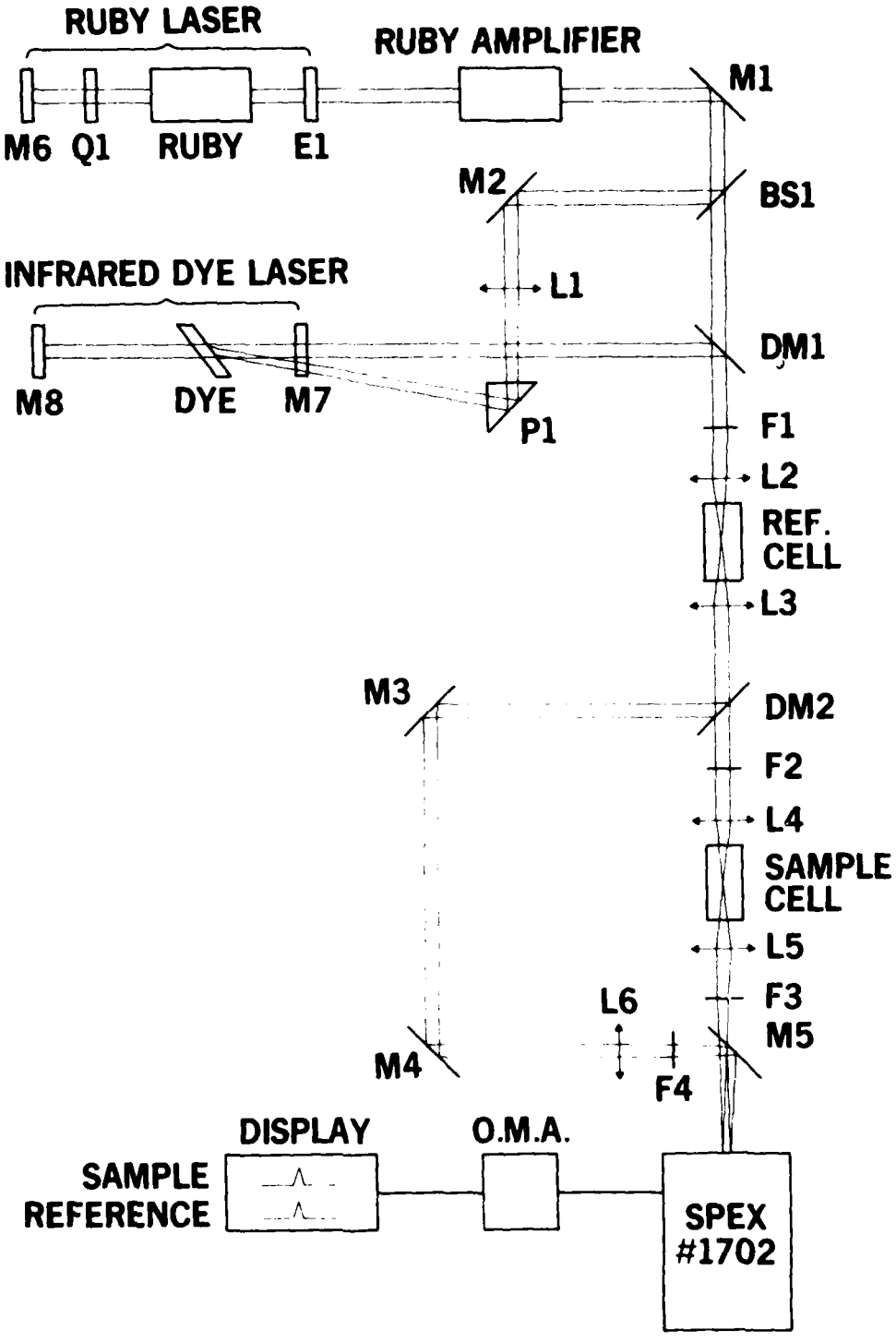

Figure 2. Schematic Diagram of the CARS System. The components are as follows: Mirrors M1-48; achromatic lenses L2-L4; simple lenses L1, L5-L6; filters F1-F4; dichroic mirrors DM1-DM2; beam splitter (70R/30T) BS1; prism P1; Q-switch Q1; output etalon E1; optical multichannel analyzer OMA.

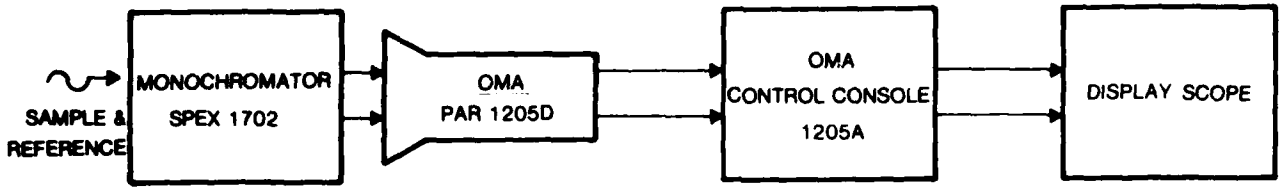

(a) BROAD-BAND (SINGLE-PULSE) MEASUREMENT

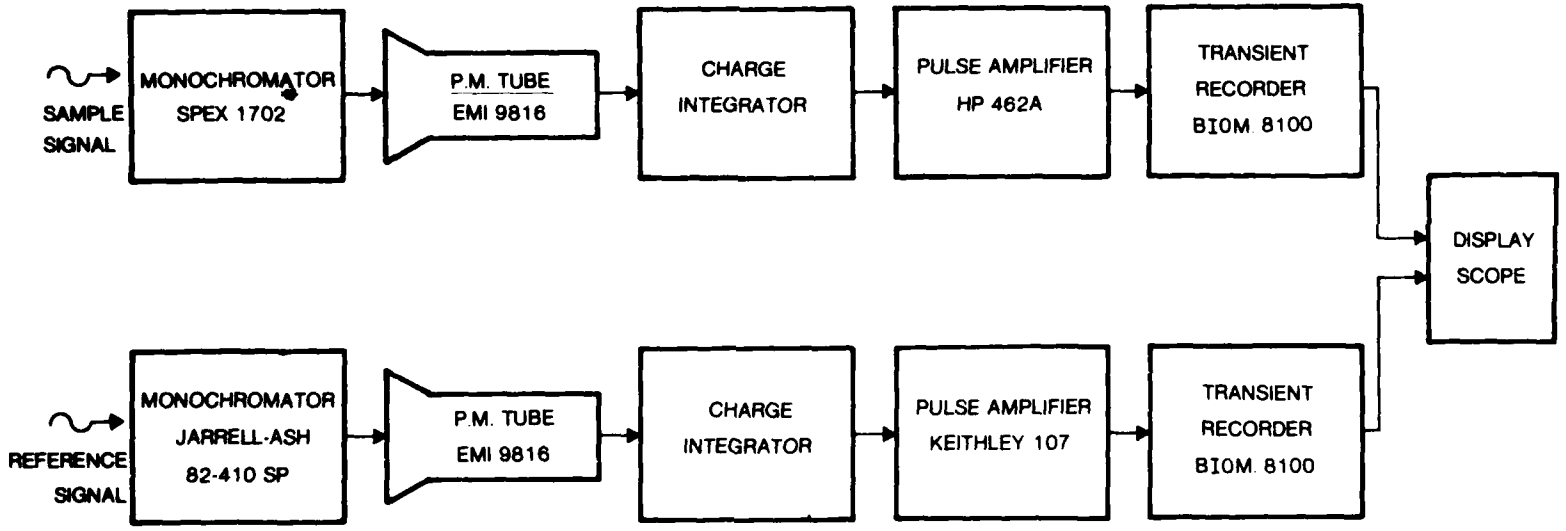

(b) NARROW-BAND SIGNAL MEASUREMENT

Figure 3. Block Diagram of Signal-Processing Electronics for CARS System.

100 wave numbers wide), and the generated anti-Stokes signals from the sample and reference cells are dispersed within a single monochromator and detected by a dual-spectrum optical multichannel analyzer (OMA). Separation of the two optical signals is accomplished by focusing the anti-Stokes beams on two different points on the entrance slit of the monochromator. Because of the instantaneous nature of the generation of the entire spectrum, this mode of operation is more desirable for real-time measurement of gas temperatures.

The narrow-band dye mode of operation is employed for generation of a point in the anti-Stokes spectrum of a gas utilizing a narrow-band dye-laser line (typically $\leq 0.2\ cm^{-1}$). The anti-Stokes signals are dispersed in two separate monochromators and detected by photomultipliers. The photomultiplier-output pulses are integrated in an RC circuit and amplified before being stored in a transient recorder. The stored pulses subsequently are displayed on an oscilloscope for monitoring. Since the spectral power density of the narrow-band dye laser generally is much higher than that of the broadband laser, the anti-Stokes intensity generated is higher with narrow-band operation. Furthermore, since photomultipliers are used in place of the OMA as shown in Fig. 2, the overall sensitivity also is much higher. However, in order to generate the spectrum of an entire band in this mode, hundreds of laser pulses scanning the Stokes region are required. For these reasons, this mode of operation is better suited to species-concentration measurements.

Nd:YAG-Based CARS System

Well into the middle of this program of study, it was decided that the Nd:YAG-based CARS system would be the optimum system for a combustion tool because of its larger power levels and the reliability of the laser. In an effort to reduce mechanical vibrations and beam movement, the laboratory Nd:YAG CARS system was incorporated into a single 4 by 8 ft. NRC floating optical table. Figures 4(a) - 4(c) depict the resulting arrangement. The system consists of a Quanta-Ray Nd:YAG laser whose frequency-doubled output is used to pump a broadband dye laser and subsequently is used in the CARS process. The broadband dye laser consists of an oscillator-amplifier combination with a resulting 30% lasing efficiency. An optical delay line

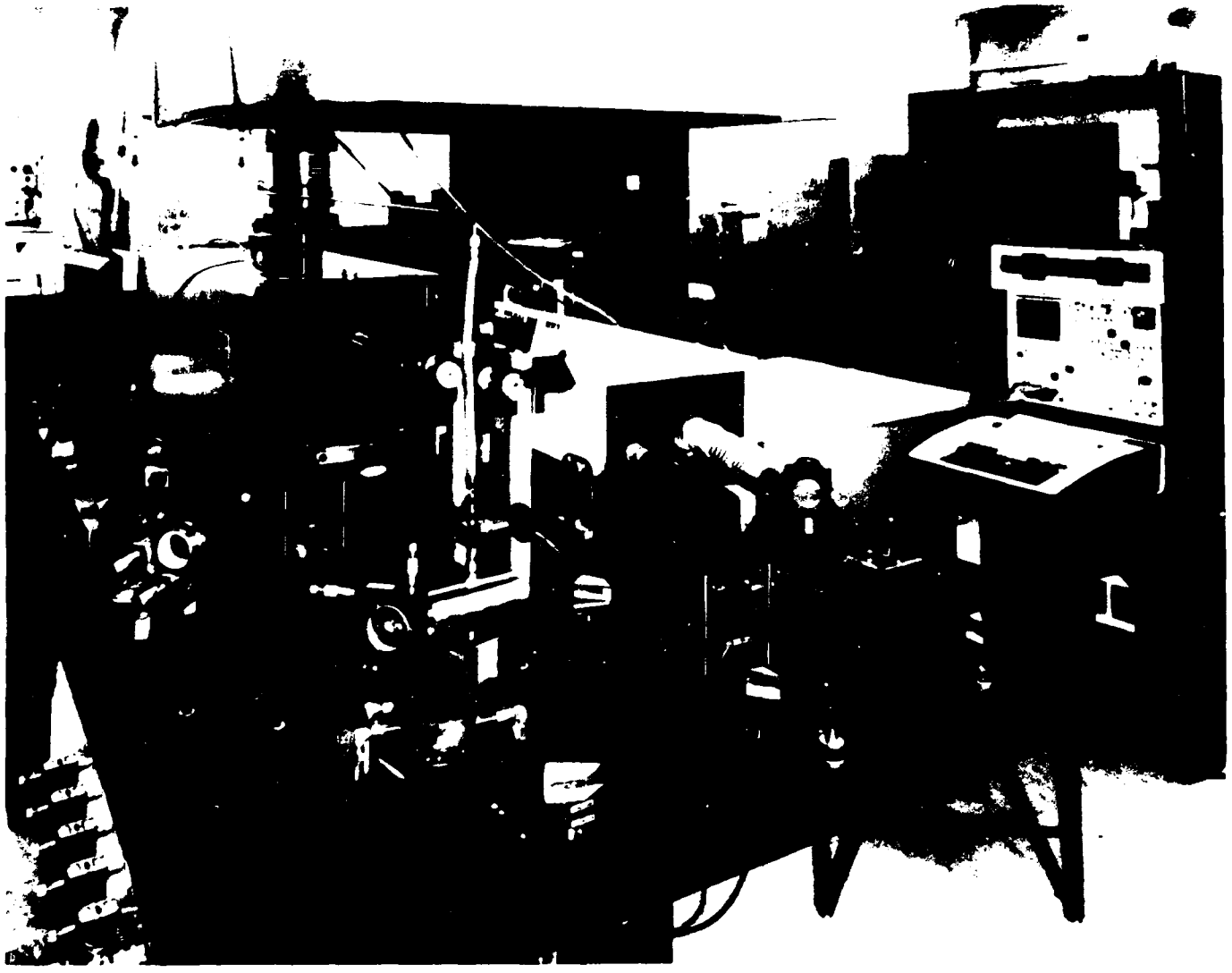

Figure 4(a). Present CARS Experimental Arrangement Depicting the Sample and Reference Paths.

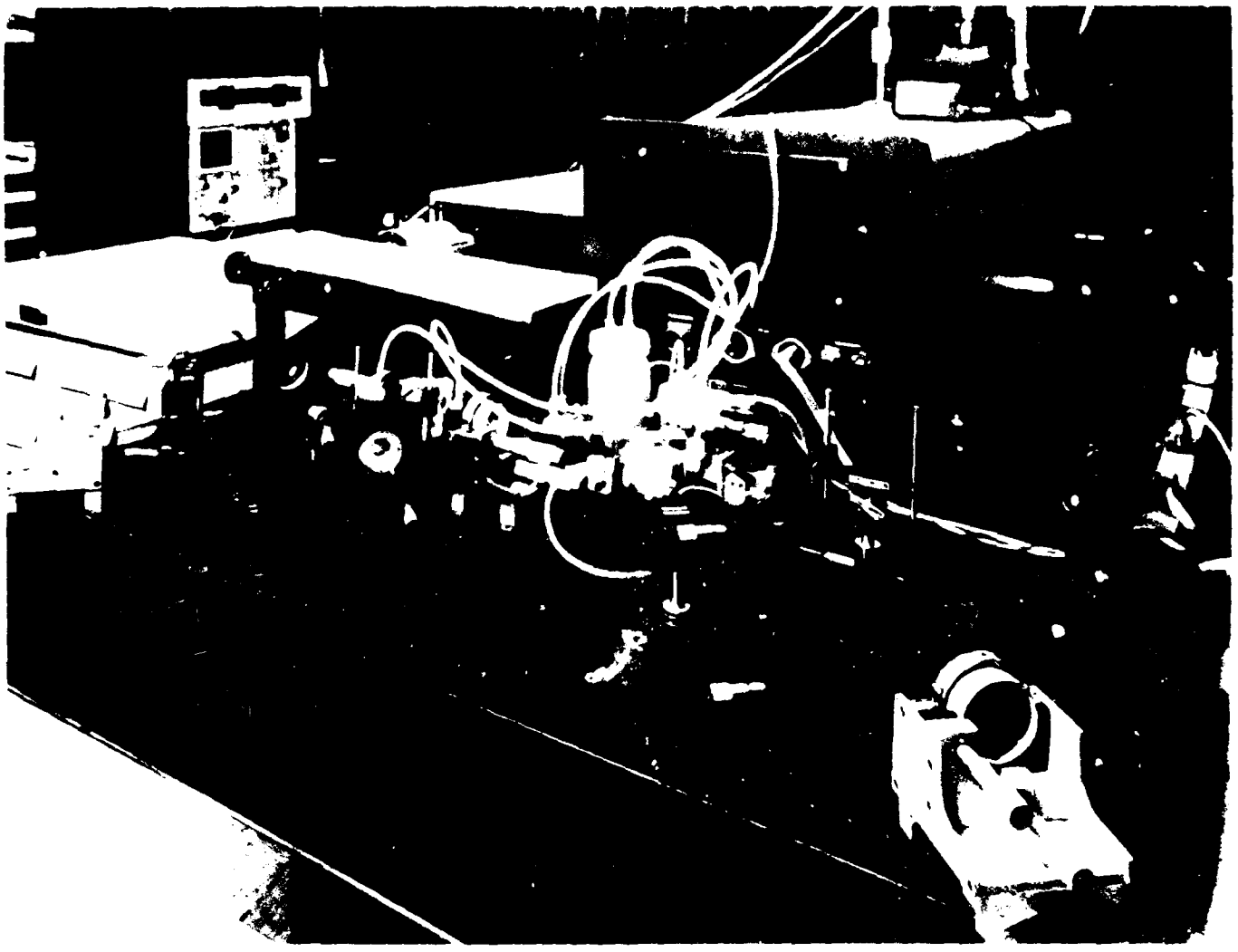

Figure 4(b). Broadband Dye Laser Employed for CARS Production.

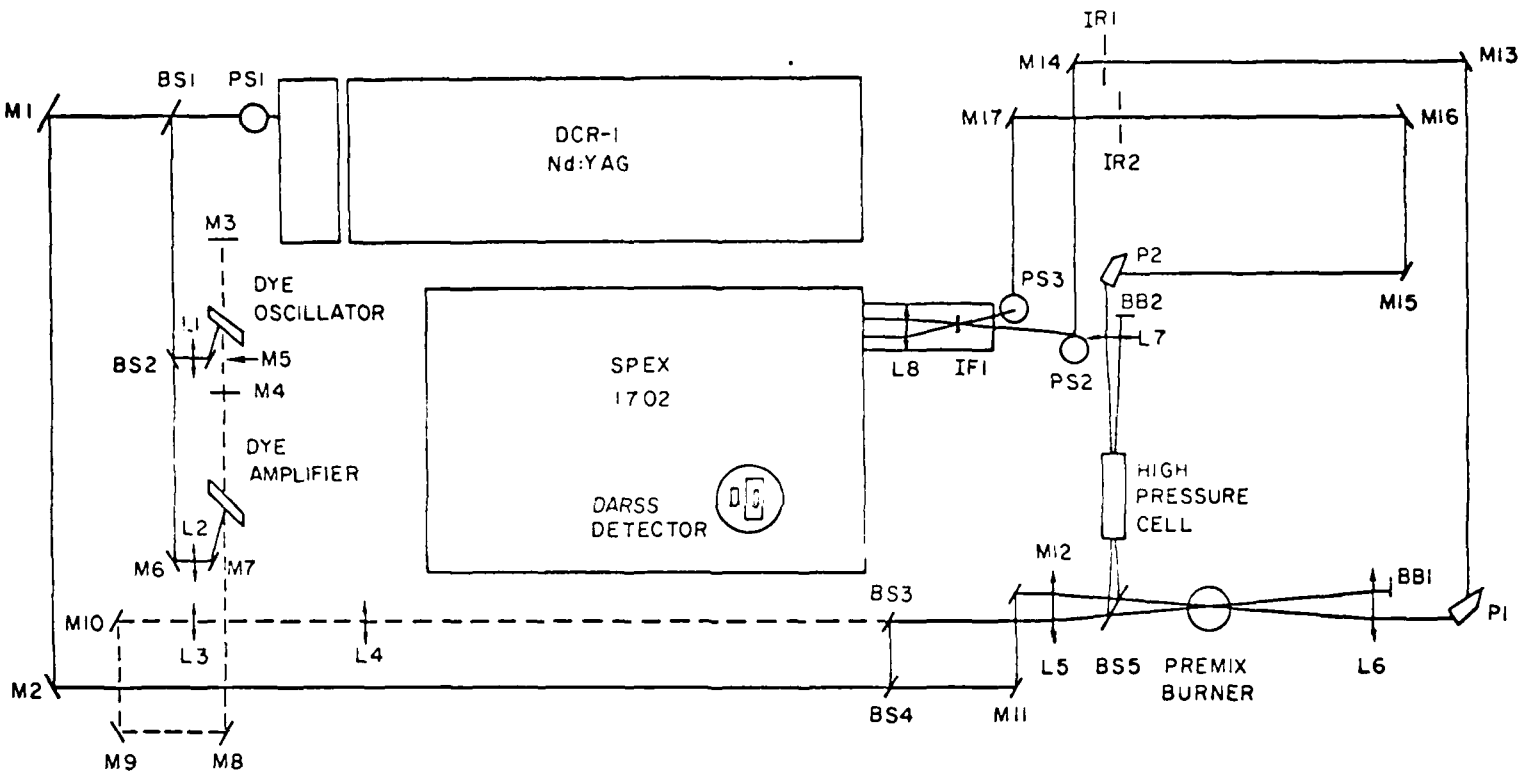

Figure 4(c). Diagram of the Present Laboratory CARS Arrangement.

PS - Periscope	IF - Interference Filter
BS - Beam Splitter	P - Prism
M - Mirror	IR - Iris
L - Lens	BB - Beam Block

(M8, M9, M10) is incorporated into the scheme to provide a temporal match between the Nd:YAG- and dye-laser pulses. The Nd:YAG and dye beams in the BOXCARS orientation are crossed and focused by lens L5 into the premixed burner flame. Beam splitter BS5 splits off ~ 30% of the three beams and forms the reference leg. This path, as discussed later, is used for normalization and species-concentration determinations. The resulting CARS signals in both the sample and reference are then predispersed by the Pellen Broka prisms and coupled into the SPEX 1702 monochromator by periscopes PS2 and PS3.

The second major modification was the replacement of the PAR 1205 OMA (vidicon) with a Tracor-Northern TN1710 DARSS (Diode Array Rapid Scanning Spectrometer) shown in Fig. 5. The DARSS unit consists of a linear (one-dimensional) diode array (reticon) detector element in conjunction with a photo-cathode intensifier. The overall sensitivity of the device is similar to the OMA unit, which is about 50% that of a common S-20 response tube. This was found to be more than adequate for these combustion studies. The major advantages of the DARSS over the OMA are the larger linear-dynamic range, the lack of blooming or cross-talk between channels of the detector, and the better electronic support offered by the TN1710 control unit.

In order to circumvent the single-dimensionality of the Tracor-Northern DARSS detector, the entrance slit of the monochromator was rotated 90° from its usual vertical position into a horizontal position. This allowed the two CARS signals to be aligned on different regions of the DARSS detector. The two CARS signals were then recorded simultaneously by the DARSS and analyzed at a later date. This configuration allows simultaneous determination of temperature and species concentration as discussed later.

Preliminary studies[11] indicated the best possible experimental scheme for normalization of the sample and reference to be that shown in Fig. 4. Temporal studies indicated that single-mode operation of the Nd:YAG and dye lasers was also highly desirable. This requires the use of Quanta-Ray's electronic-line-narrowing device. This device acts to force the electro-optical Q-switch of the Nd:YAG to behave as a lossy Q-switch, which permits a slow build-up of the laser pulse over a relatively long period of time.

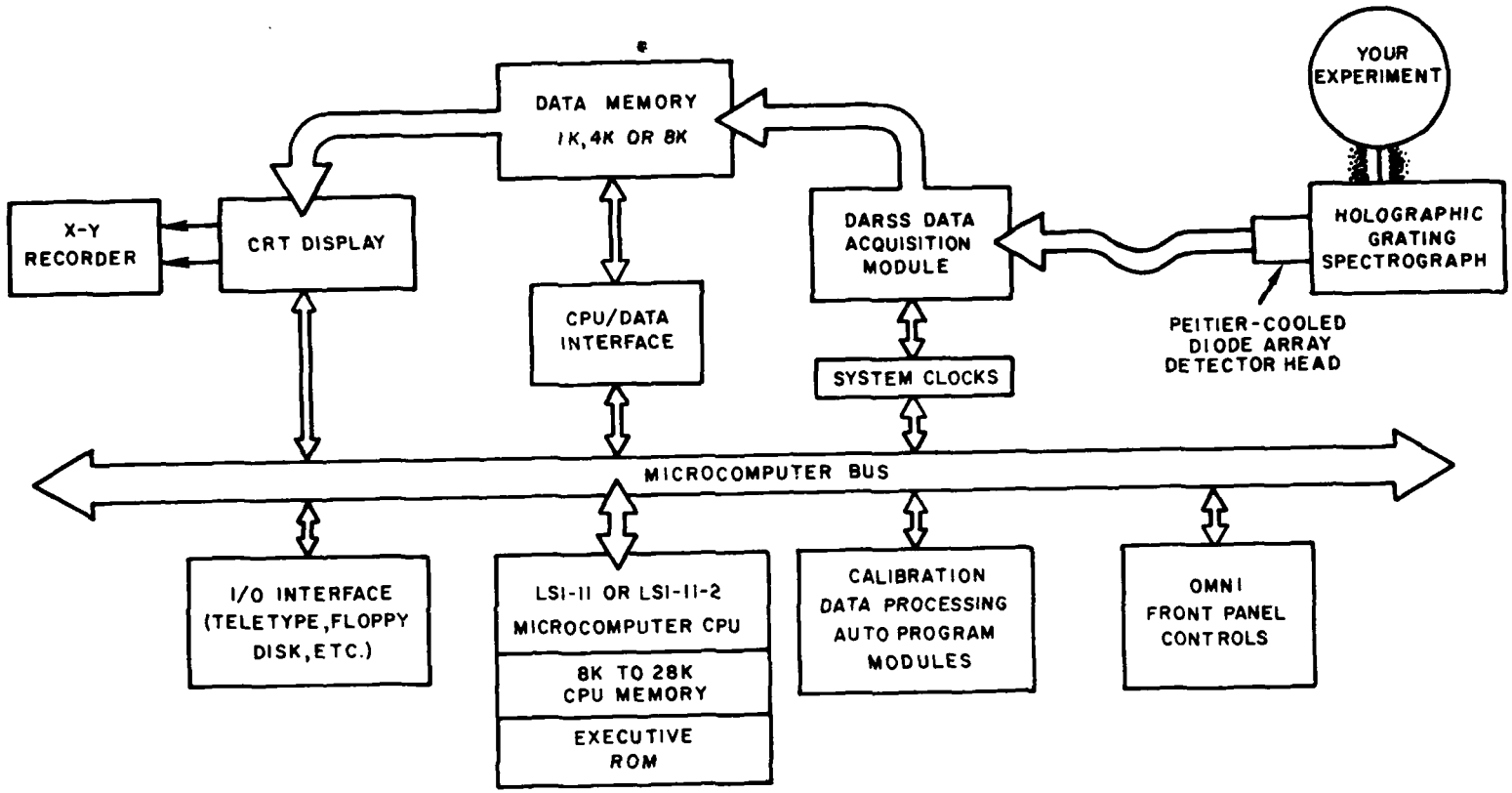

Figure 5. TN-1710 Functional Block Diagram.

This slow build-up allows the intracavity elaton to be more efficient in discriminating against unwanted modes.[12] However, the free-running nature of the cavity-pulse build-up of this device presents a major problem in the timing of the detection electronics.

To circumvent the possible skew and lag problems which this caused, the firing of the lamps of the Nd:YAG was synchronized with the integration/digitization cycle of the TN 1710-DARSS. Figure 6 depicts the time events which occur in the present configuration. The DARSS digitization/integration timing cycle is used to key the firing of the Nd:YAG flashlamps. After a period of 50 - 300 μs, the Q-switch opens and 70 ns later the laser output occurs. This process continues at the hertz rate set by the integration time of the DARSS cycle, which is usually set for 10-Hz operation. When data are to be taken, the DARSS is reset for trigger operation, and the data control, data acquisition, and transient digitizer are triggered. The transient digitizer is used for examining the mode quality of the Nd:YAG to ensure that a single longitudinal mode will be obtained. This is necessary since the ELN device produces single-mode operation only 50% of the time. If the pulse is indeed single mode, the data are accepted and the process continues. This method assures that all data are taken under single-mode operation.

Premixed Burner Arrangement

The burner consists of a premixed Perkin-Elmer assembly No. 290-0107 and an adjustable nebulizer No. 303-0352. The assembly was fitted with a water-cooled argon sheath which was employed for stabilizing the flame. Both acetylene-air and propane-air premixes were used in the burner for flame studies. The operating conditions of the burner for both fuels are listed in Table 1. The assembly was mounted on two translation stages which allowed height and axial profiles of the flame. The observed flame consisted of an inner and an outer portion, both of which could be independently controlled. Figure 7 depicts the flame that was obtained with the burner when acetylene was used as the fuel. The overall height of the flame was greatly reduced in the propane flame due to the slower flame-propagation speed, as shown in Fig. 8.

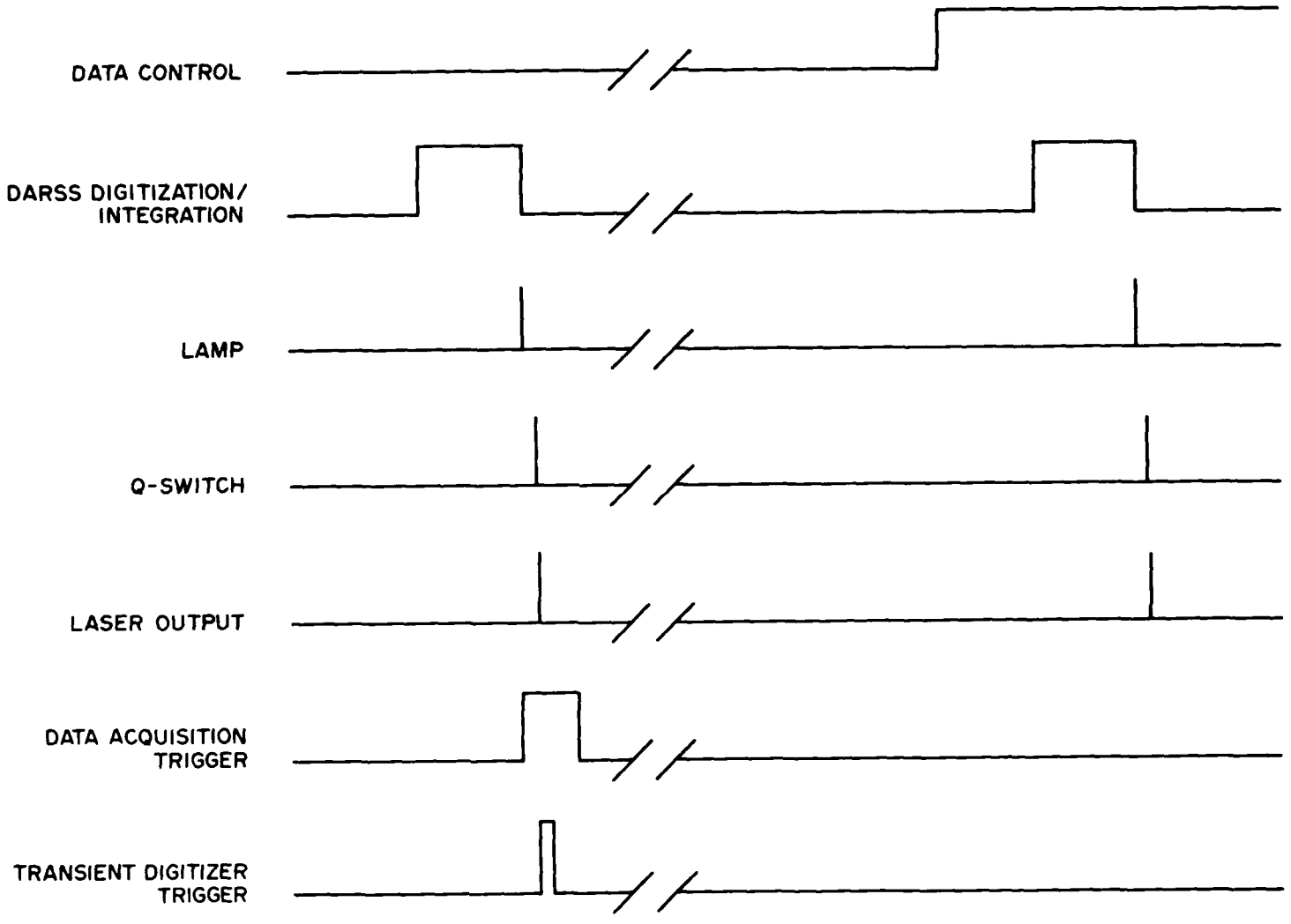

Figure 6. Timing Scheme for DARSS-Nd:YAG Arrangement Used in Concentration Studies.

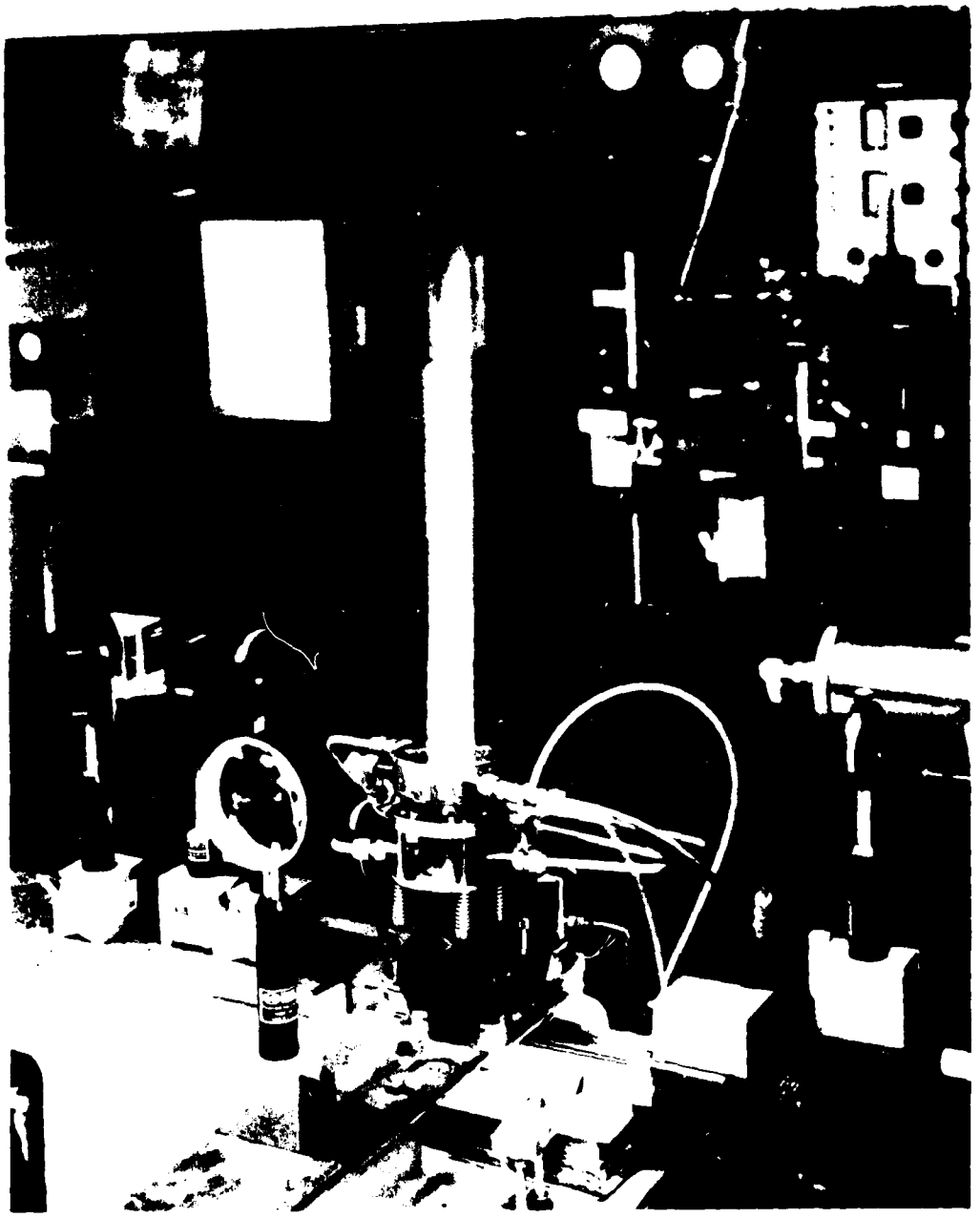

Figure 7. Acetylene-Fueled Flame Produced by the Modified Perkin-Elmer Burner.

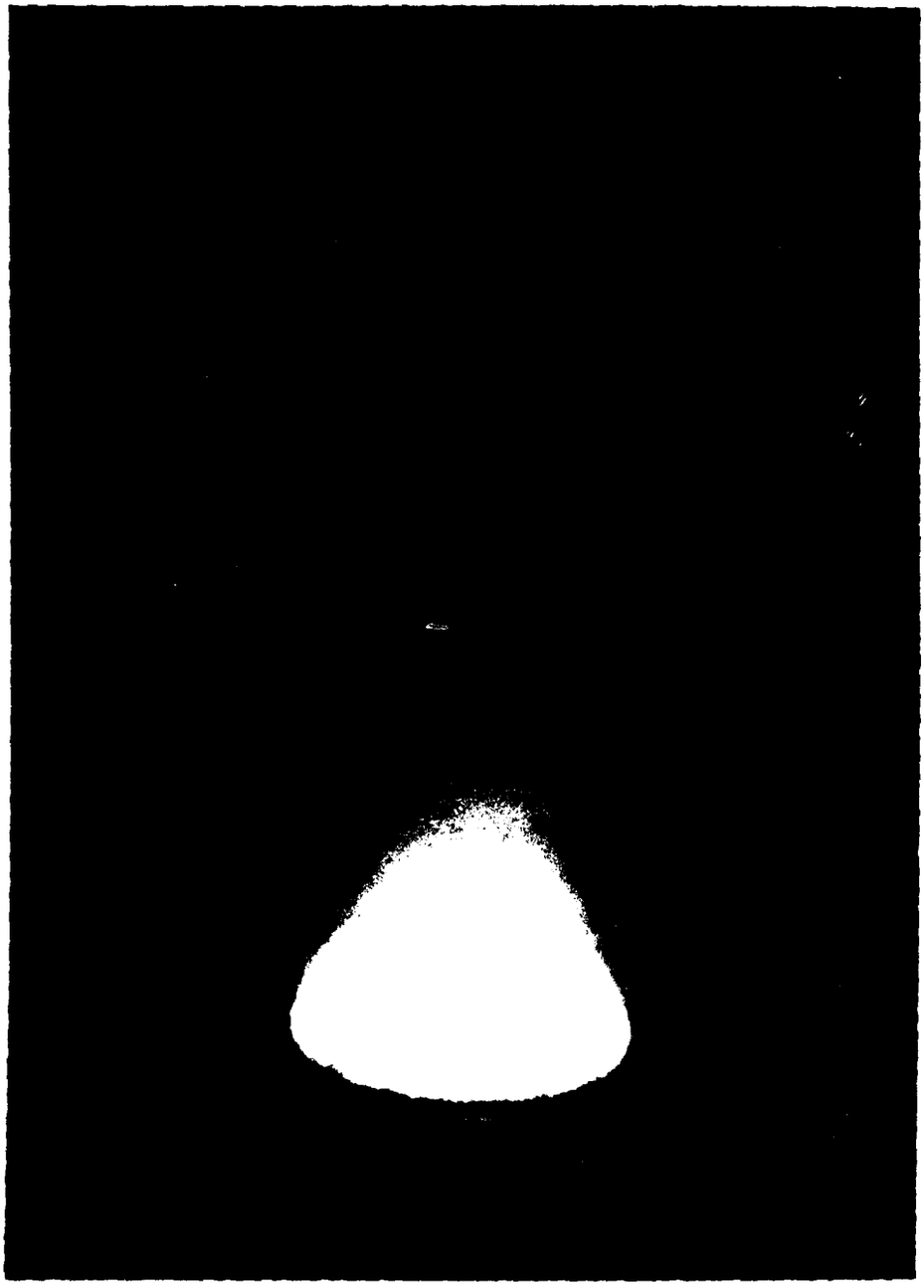

Figure 8. Photograph of Propane-Fueled Flame Obtained with the Perkin-Elmer Burner.

Table 1

FUEL AND AIR SETTINGS* FOR ACETYLENE AND PROPANE FOR THE PREMIXED BURNER

	Acetylene	Propane
Inner Air	9 - 14	4 - 8
Nebulizer	7 - 11	3 - 7
Outer Air	28 - 40	8 - 14
Inner Fuel	2.5 - 5	0.2 - 0.5
Outer Fuel	4 - 9	0.4 - 1
Argon Sheath	15	15

*All rates are in liters/min.

3.2 COMPUTER CODES

In computer codes developed to date, major emphasis has been placed on the determination of temperatures as represented by experimentally obtained spectra. The calculation of the theoretical spectrum is an important part of this process and will be discussed first. To complete the temperature-determination process, a nonlinear Jacobian least-squares routine[13] has been developed for fitting the observed spectrum as a function of temperature.

The third-order susceptibility which governs CARS can be expressed in abbreviated form by

$$\chi^{(3)} = \chi_n + \chi_r \tag{11}$$

where χ_n is the nonresonant contribution and χ_r is the Raman resonant contribution to the third-order susceptibility.

χ_r is given by

$$\chi_r \propto \sum_{v,J} \frac{N\Delta(v,J)\left(\frac{d\sigma}{d\Omega}\right)_{v,J}}{\delta(v,J) - i\Gamma(v,J)} \tag{12}$$

where N is the total number density of the species being probed; $\Delta(v,J)$ is the populational difference between the states involved in the Raman transition; $\delta(v,J)$ is the detuning factor defined by $\delta(v,J) = \omega_r - \Delta$ (ω_r being the frequency of the Raman transition and Δ the frequency difference between the pump, ω_1, and the probe, ω_2); $\Gamma(v,J)$ is the HWHM of the Raman transition; and $(d\sigma/d\Omega)_{v,J}$ is the Raman scattering cross section defined for Q branches as

$$\left(\frac{d\sigma}{d\Omega}\right)_{v,J} = \left(\frac{\omega_2}{c}\right)^4 \frac{\hbar}{2m\omega_o}\left[\alpha^2 + \frac{4}{45} b_J^J \gamma^2\right] (v + 1)$$

where α is the spherical part of the polarizability and $b_J^J\gamma^2$ is the anisotropic part which usually has a weak J dependence.

The CARS power is given by[14]

$$P_3(\omega) = \int P_1(\omega_1)d\omega_1 \int P_1(\omega - \Delta)P_2(\omega_1 - \Delta)|\chi(\Delta)|^2 d\Delta \tag{13}$$

In the normal course of generating a CARS spectrum, the third-order susceptibility is generated according to Eqs. (11) and (12) and then $|\chi^{(3)}|^2$ is convolved over the pump and probe laser linewidths as dictated by Eq. (13). Another convolution over the detector slit, however, must be made before the calculated spectrum can be compared to the experimentally observed one. Under typical experimental conditions when probing N_2, simplification of Eq. (11) and (12) can be accomplished without the introduction of large errors. First, the nonresonant third-order susceptibility, χ_n, can be neglected, except for the cases of minor species concentrations. Secondly, the Raman scattering cross section, $(d\sigma/d\Omega)_{v,J}$ is observed to be a slowly varying function of J level and can be treated as a constant. Thirdly, the Raman linewidths vary slowly with J level and can be treated as constant

for all transitions. Optimum results are achieved by employing a linewidth of 0.1 cm^{-1} for the spectral calculations. As indicated by Eq. (12), the calculation of the third-order susceptibility as a function of frequency involves the summation over all Raman resonances in the spectrum. For typical Q-branch spectra, this entails the summation over three vibrational transitions, each containing 100 rotational transitions. Because of the narrow Raman linewidths, the frequency increment for the calculation is kept at 0.01 cm^{-1}, covering a region from 2265 to 2350 cm^{-1}. The third-order susceptibility must then be squared and convolved over the appropriate experimentally defined slit functions.

Figure 9 shows the $|\chi^{(3)}|^2$ for N_2 at 1700 K before convolution over the detector halfwidth and laser linewidths. The spectral constants employed for this calculation are given in Ref. 15. The present program has the ability to convolve over any of four different functions any number of times. Figures 10 - 13 show the convolved spectrum utilizing the four available functions at a HWHM of 1.67 cm^{-1}. The formulae for the individual functions are:

Gaussian

$$g(\chi) = \frac{\ln 2}{\Gamma\sqrt{\pi}} \exp\left(-\frac{\ln 2\ (\chi)^2}{\Gamma^2}\right) \tag{14}$$

Lorentzian

$$\ell(\chi) = \frac{(\Gamma/\pi)}{\chi^2 + \Gamma^2} \tag{15}$$

Triangular

$$t(\chi) = \frac{2\Gamma - \mathrm{ABS}(\chi)}{4\Gamma} \tag{16}$$

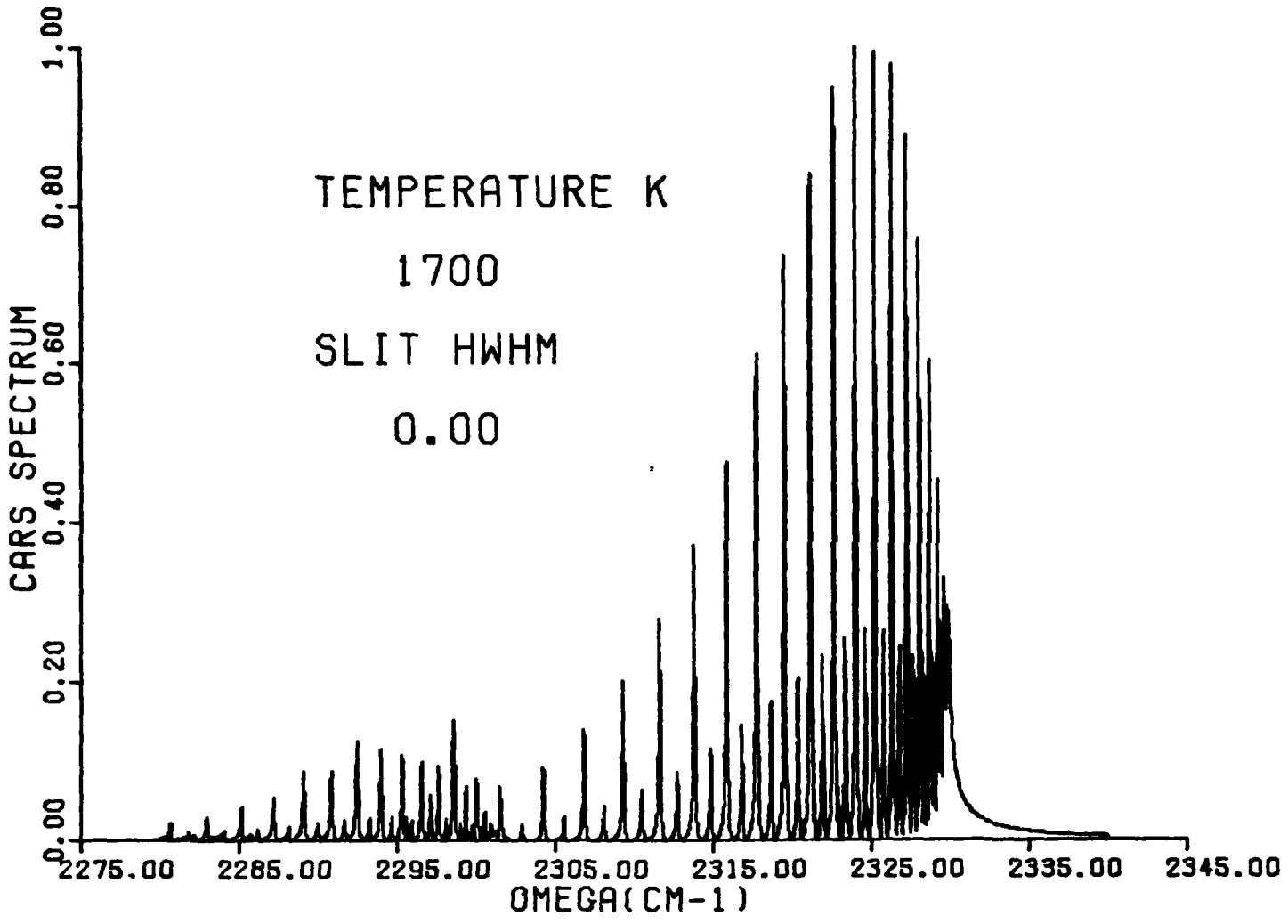

Figure 9. $|\chi^{(3)}|^2$ for a Temperature of 1700 K.

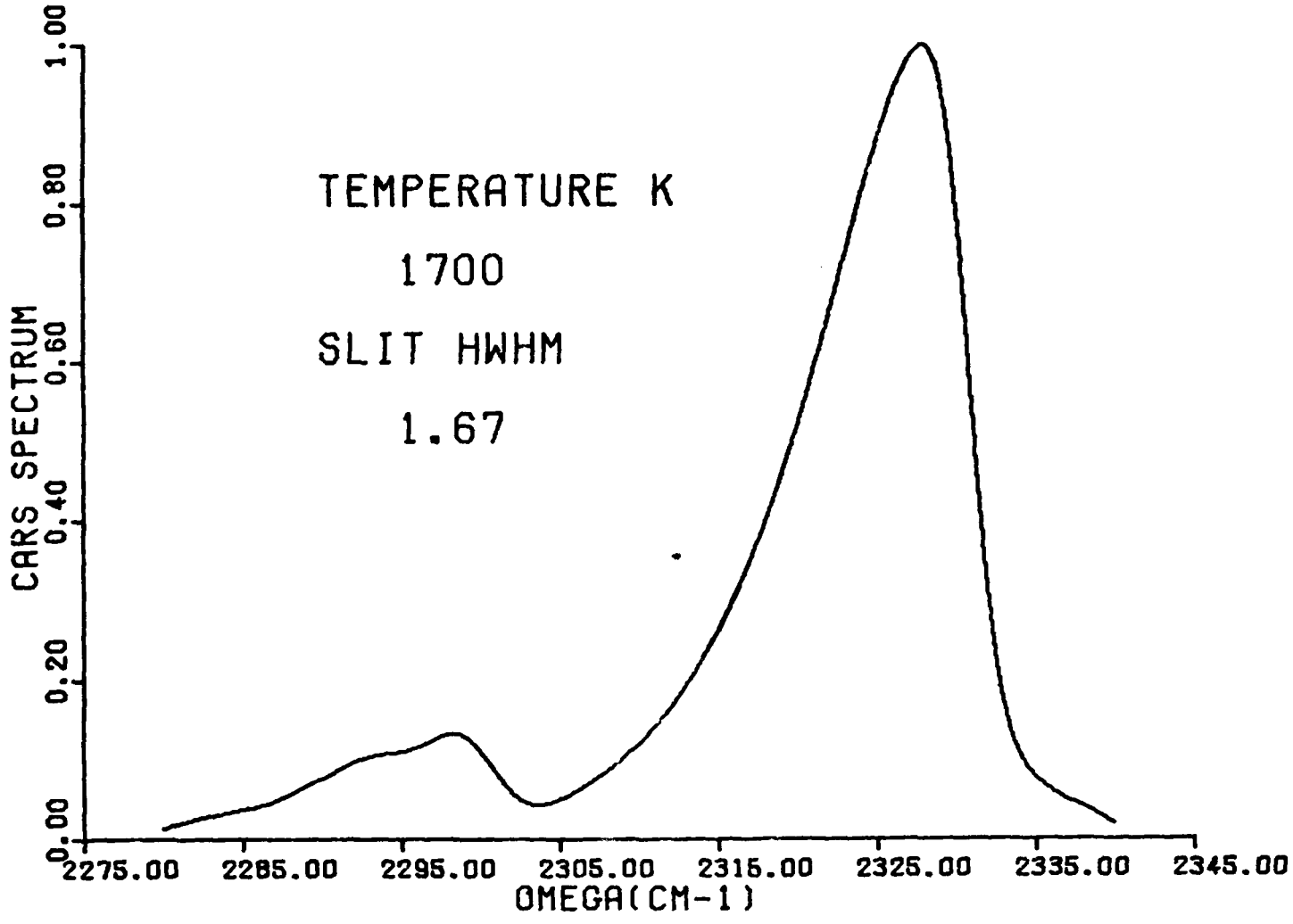

Figure 10. A Gaussian Slit Convolution of $|\chi^{(3)}|^2$ at 1700 K.

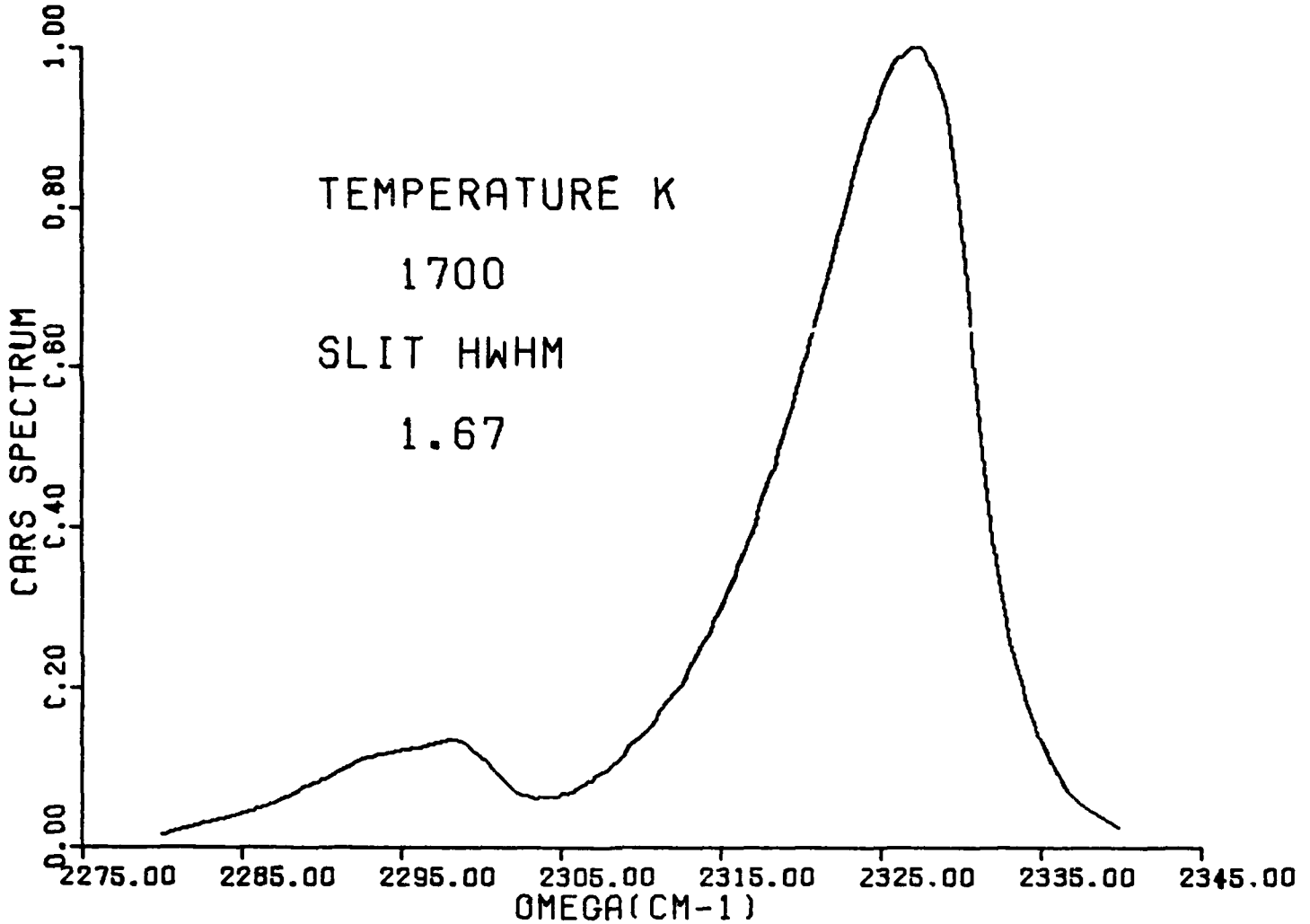

Figure 11. A Lorentzian Slit Convolution of $|\chi^{(3)}|^2$ at 1700 K.

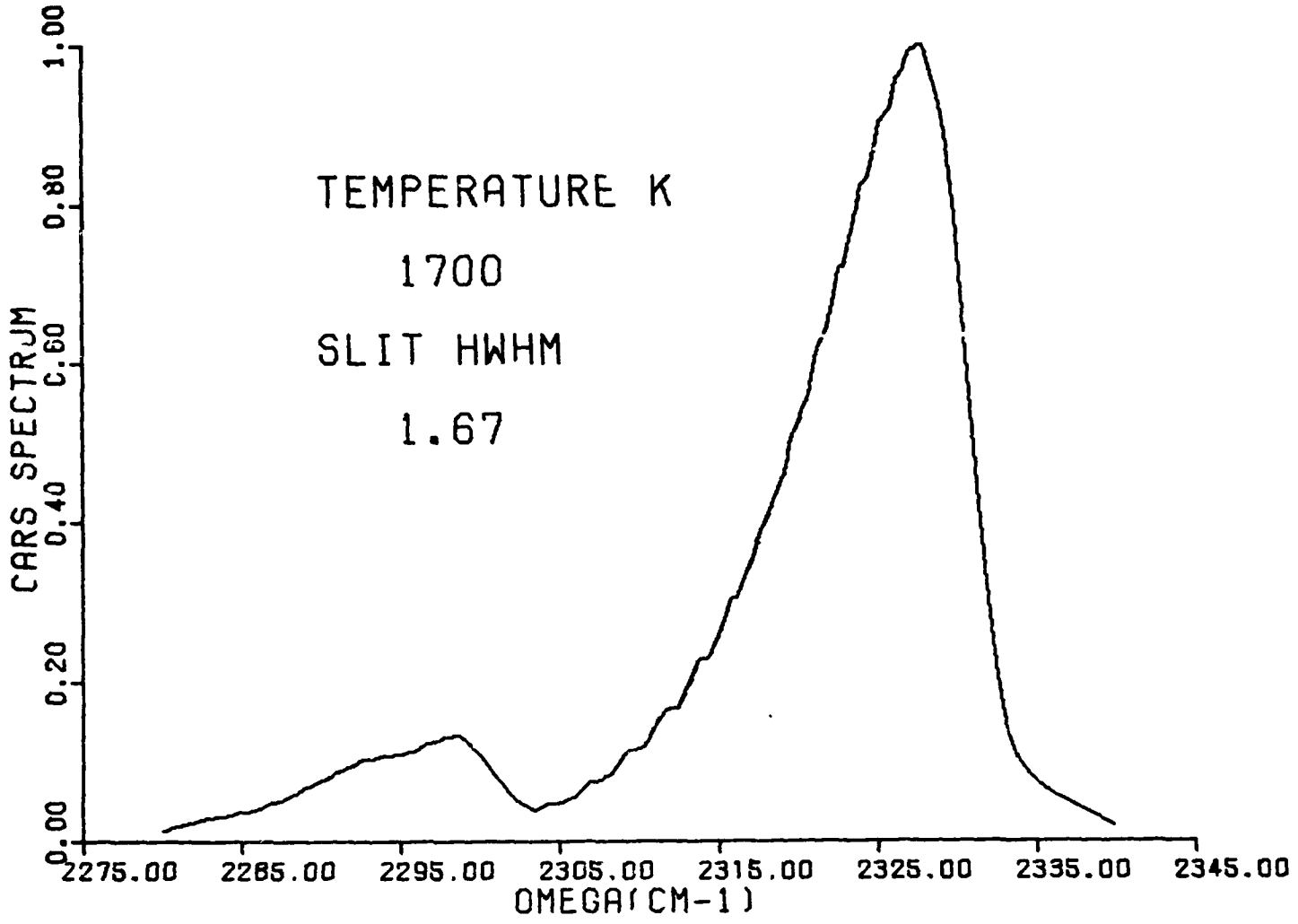

Figure 12. A Triangular Slit Convolution of $|\chi^{(3)}|^2$ at 1700 K.

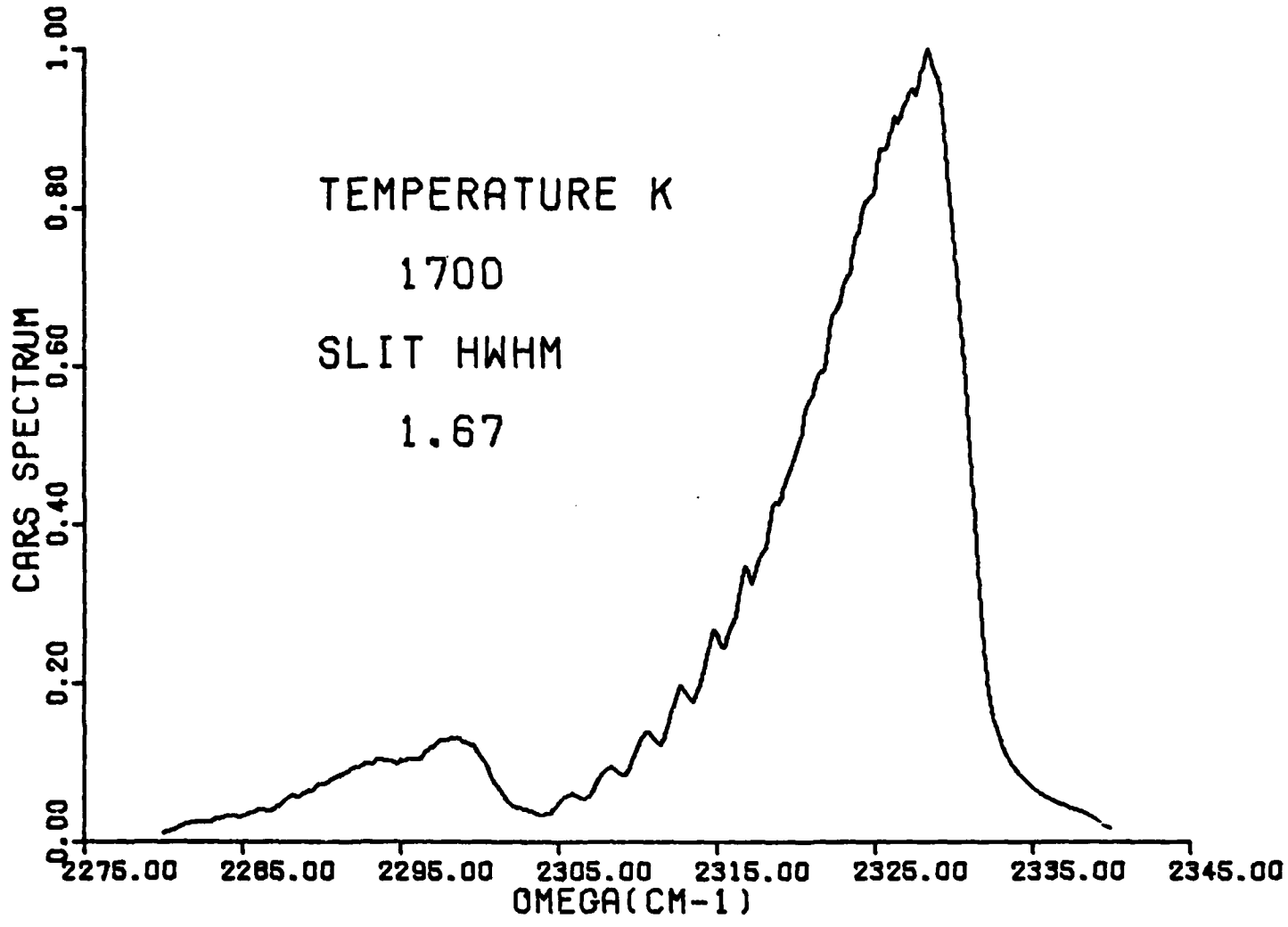

Figure 13. A Trapezoidal Slit Convolution of $|\chi^{(3)}|^2$ at 1700 K.

Trapezoidal

$$t_p(\chi) = \begin{cases} \dfrac{1}{\Gamma - \frac{1}{2} S^{-1}} & \text{if } ABS(\chi) \leq \Gamma - \frac{1}{2} S^{-1} \\ \dfrac{\frac{3}{2} S^{-1} - (ABS(\chi) - \Gamma)}{2\Gamma S^{-1}} & \text{if } ABS(\chi) > \Gamma - \frac{1}{2} S^{-1} \end{cases} \tag{17}$$

where S is the slope of the rising edge of the trapezoid.

The experimental setup dictates the actual form which Eq. (13) must take in order to simulate the obtained spectrum. In the laboratory ruby scheme, the linewidth of the pump is ~ 0.03 cm^{-1}, and the broadband dye has a linewidth of ~ 200 cm^{-1}. The CARS signal is detected by an JMA which, along with the monochromator, contributes to a 1.2 cm^{-1} halfwidth. Under these experimental conditions, the convolutions over the pump and probe lasers can be neglected since in the former case the bandwidth is so small that it has little effect upon the spectrum; and in the latter case the bandwidth is so large that it is in constant over the 60 cm^{-1} region responsible for N_2 CARS production. The detector slit function, however, cannot be neglected and must be convolved over. A triangular slit function is primarily employed for this convolution. In the Nd:YAG scheme the pump has a bandwidth of 0.8 cm^{-1} which must be convolved over; the dye laser has a bandwidth of 130 cm^{-1} as shown in Fig. 14 which, as in the case of the ruby scheme, is not convolved over. With the Nd:YAG system, the detector halfwidth increases to 2.0 cm^{-1} due to the decreased dispersion of the grating in this frequency region. According to Eq. (13) the pump bandwidth must be convolved over twice, but in reality a single Gaussian convolution was found to be adequate.

A nonlinear least-squares program has been developed to fit the observed experimental spectrum as a function of temperature. It is based upon the matrix equation

$$\Delta P = (J^{+}J)^{-1} J^{+} \Delta\phi \tag{18}$$

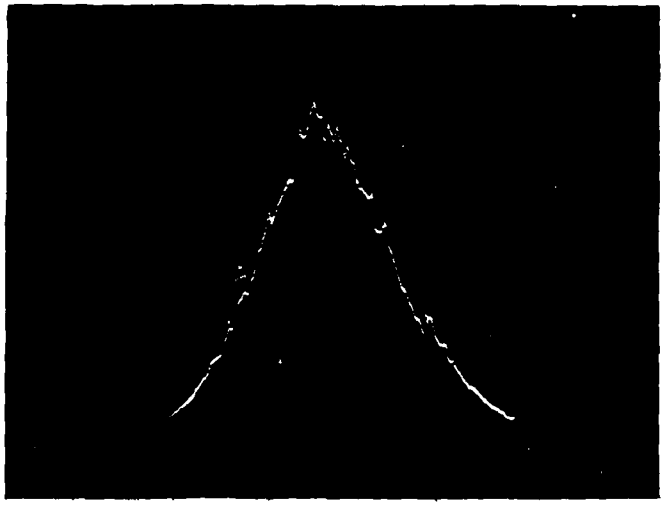

Figure 14. Broadband Dye Output of the Nd:YAG-Pumped Dye Laser.

where J is the Jacobian matrix whose elements are defined by $J_{ik} = dI_i/dP_k$ (J_i being the i^{th} intensity and P_k the k^{th} parameter); J^+ is the transpose of the J matrix; $\Delta\phi$ is the matrix with elements $\Delta\phi_i = I_{iobs} - I_{ical}$ (where I_{iobs} is the i^{th} observed experimental intensity and I_{ical} the i^{th} calculated intensity); and ΔP is the correction matrix whose elements contain the corrections to be made upon the parameters which were varied. Three parameters were chosen for fitting by the program--the temperature, the relative frequency, and the Raman linewidths. The frequency fit was incorporated in order to negate the need for absolute frequency calibration, and the Raman linewidth was used to take into account any dependence of the linewidth upon temperature.

The program works in the following manner. First, the initial guesses as to the parameters to be varied are made and a spectrum calculated. This spectrum is then used to formulate the $\Delta\phi$ matrix. Secondly, the Jacobian matrix is created by a numerical evaluation of the appropriate derivatives. The transpose of the Jacobian and subsequential inverse of the product of the Jacobian with its transpose is formed. The correction matrix can then be constructed according to Eq. (18). The correction to each parameter can then be made and the resulting new parameter used as the initial guess for which cycle to repeat. The iterative process is continued until the variance of the calculated spectrum shows no further improvement. The dispersion--an indicator for the fitting error for each parameter--can be obtained from

$$D_i = \left(\frac{(J^+J)^{-1}_{ii} \sigma^2)}{(NOBS-NPAR)} \right)^{1/2} \tag{19}$$

where $(J^+J)^{-1}_{ii}$ is the i^{th}, i^{th} diagonal element of the $(J^+J)^{-1}$ matrix; σ^2 is the variance obtained between the observed and calculated spectra; NOBS is the total number of data points in the observed spectrum; and NPAR is the total number of parameters varied. The iteration usually requires three cycles for fitting the temperature. (A complete listing of the routine which operates on a CYBER 74 computer can be found in the Appendix.) The first test of the program was made on room-temperature data since, due to the overall lack of structure in the spectra, it is probably the worst possible case to

fit. These fits were routinely within 15 K of room temperature. One such fit is shown in Fig. 15. Figure 16 depicts a fit that was made to single-shot data obtained from the premixed propane burner by the ruby system. The experimental data obtained from the same burner by the Nd:YAG CARS system are shown in Fig. 17.

3.3 EFFECT OF LINEWIDTHS UPON TEMPERATURE MEASUREMENTS

As outlined above, the temperature of a combustion medium can be estimated by obtaining the best fit of a calculated spectrum to an experimentally determined one. To achieve this fit, temperature and linewidth can be used as adjustable parameters if the J dependence upon the linewidth in the Q-branch is neglected. This approach has yielded excellent results for laminar laboratory flames where the temperature has been determined by other methods such as the line-reversal technique.[16] However, it would be advantageous to gain a better understanding of the linewidth problem to improve the reduction of CARS data to temperatures and species concentrations. The latter case presents a much more difficult problem and will be discussed later.

The primary mechanisms for spectral line broadening in a combustion medium are molecular collisions and the Doppler effect. The linewidths depend upon temperature, pressure, and composition of the medium as well as the J value of the line. Collisional effects, as demonstrated for the case of hydrogen, may cause narrowing or broadening of the spectral line.[17] Fortunately, collisional narrowing can be neglected for most species. However, it does present a special problem for the analysis of hydrogen data, and additional work is required for proper analysis of H_2 data in combustion environments. As an approximation, the collisional linewidth can be expressed as a function of the optical collisional frequency,[18] which yields, for the half-intensity breadth,

$$\Gamma = \frac{1}{\tau_o} \tag{20}$$

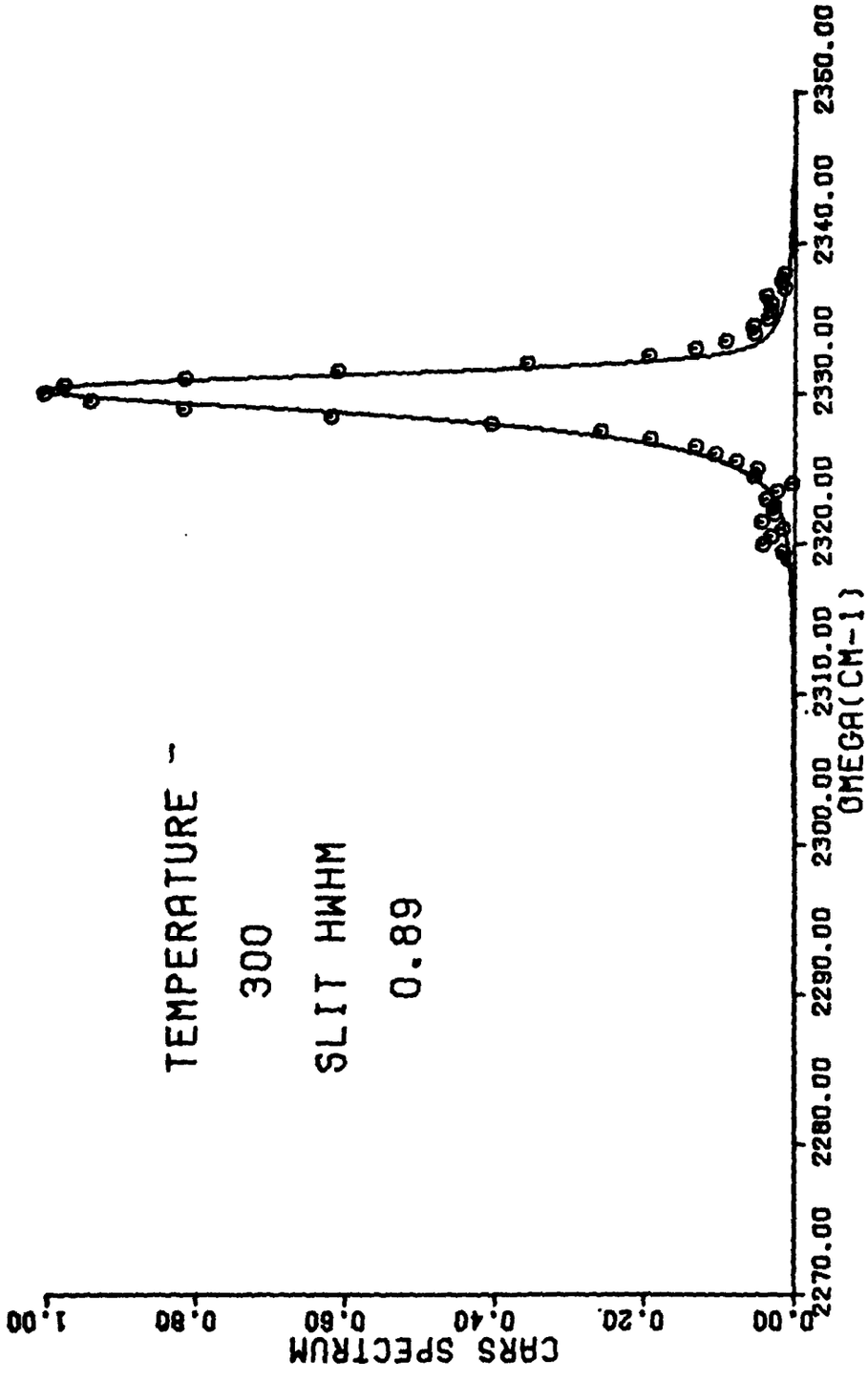

Figure 15. Room-Temperature Fit of OMA Data.

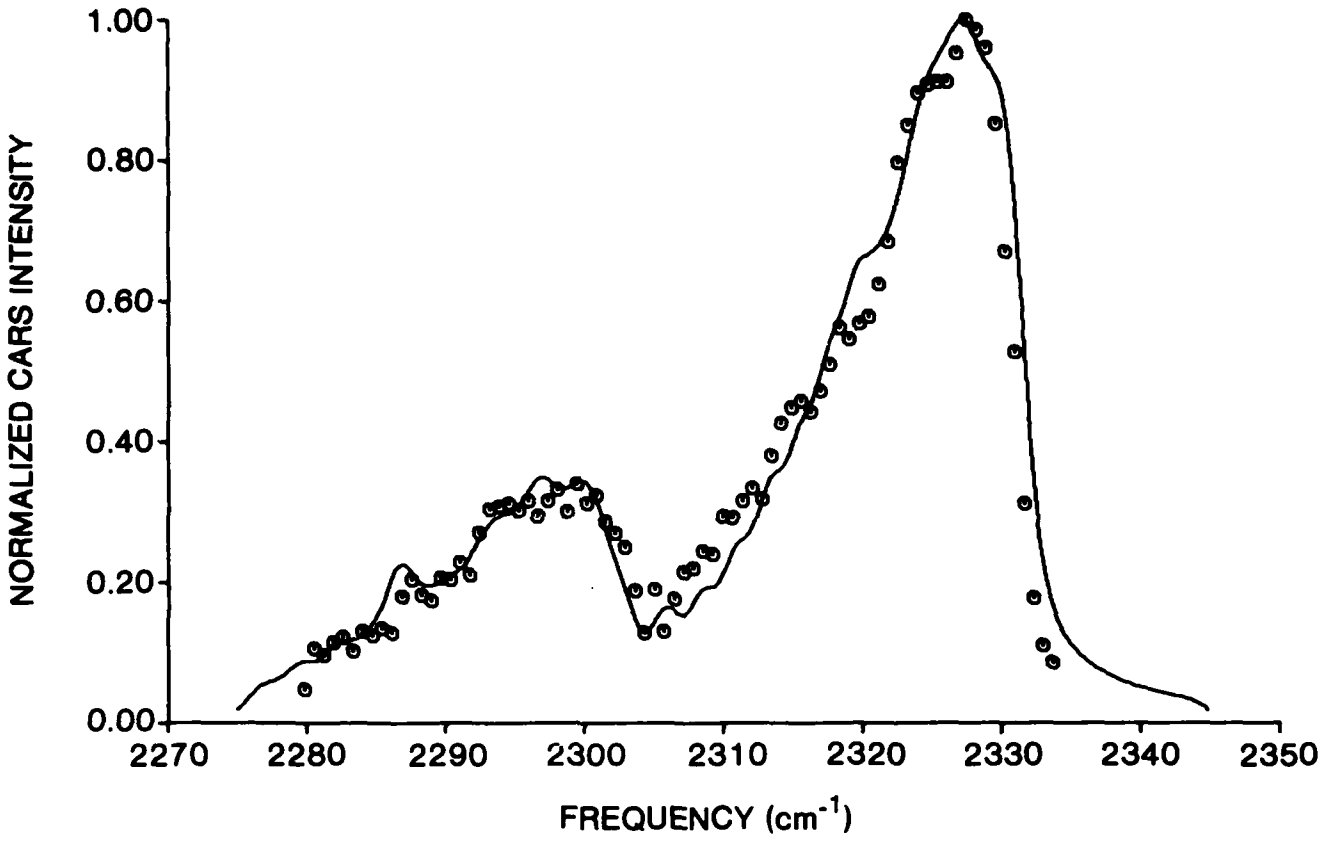

Figure 16. Temperature Fit of a Single-Shot Spectrum Obtained with the Ruby-Based CARS System on the Propane-Fueled Burner. The solid line is the calculated fit, and the dots are the experimentally observed points.

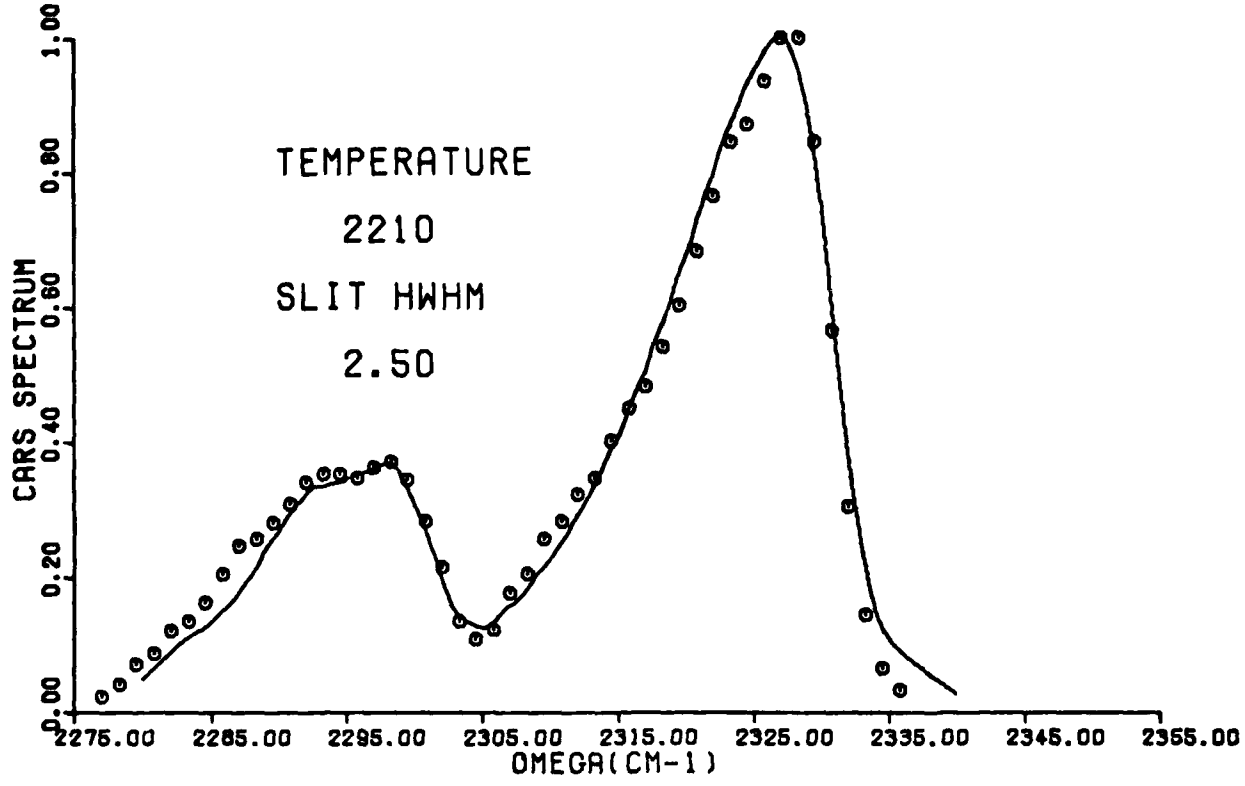

Figure 17. Temperature Fit of the Single-Shot Spectrum Obtained with the Nd:YAG-Based CARS System on the Propane-Fueled Burner.

where τ_o is the time between collisions. From kinetic theory one obtains, for a gas composed of a single species,

$$\Gamma = 4N\sqrt{\frac{\pi kT}{m}}\ \rho^2 \tag{21}$$

where ρ is the optical collisional diameter which may be 10 to 10^3 times greater than the value obtained from kinetic-theory experiments. For N_2 this yields an estimated half-intensity breadth between 2×10^{-3} and 2×10^{-1} cm^{-1} at atmospheric pressure and room temperature. If one assumes that the collisional diameter is independent of the velocity of the molecules, then Γ should depend upon $T^{-1/2}$. This assumption appears to be in reasonable agreement for N_2 linewidth measurements using CARS.[19] A review of recent experiments and theoretical developments in the area of Raman line shapes is given by Srivastava and Zoidi.[20] The theory was compared with experimental CARS data for the N_2 Q-branch by Rahn, Owyoung, Coltrin, and Koszykowski.[21] Although these data indicate that the J dependence is weak, a sufficient change in Γ occurs to warrant the inclusion of this effect in calculated spectra. Additional work is required to investigate the effect of neglecting the J dependence when temperatures are determined by fitting measured Q-branch spectra to calculated spectra.

As the temperature of the combustion gas increases for a given pressure, the effect of Doppler broadening becomes more important. Thus, the linewidth becomes a combination of Doppler and collisional broadening. If collisional narrowing is neglected, it can be shown that the anti-Stokes susceptibility becomes[17]

$$\chi^{(3)}(\omega) = \sum_{v,J} K_{v,J}\left(\frac{(4/\pi)\ln 2}{\Delta\omega_D}\right)^{1/2} \times \int_{-\infty}^{+\infty} \frac{d\xi}{\omega_r(v,J) + \xi - \omega - i\Gamma(v,J)} \exp\left[-4(\ln 2)\xi^2/\Delta\omega_D\right]^2 \tag{22}$$

where

$$K_{v,J} = \frac{N\Delta_J c^4}{3\hbar\omega_s^4}\left(\frac{d\sigma}{d\Omega}\right)_{v,J}$$

and $\Delta\omega_D$ is the Doppler width for forward Raman scattering given by

$$\Delta\omega_D = \omega_J[8(\ln 2)kT/mc^2]^{1/2} \tag{23}$$

If one lets

$$t = \frac{2(\ln 2)^{1/2}\xi}{\Delta\omega_D}$$

the equation for $\chi^{(3)}(\omega)$ becomes

$$\chi^{(3)}(\omega) = \sum_{v,J} -K_{v,J}\left(\frac{(4/\pi)\ln 2}{\Delta\omega_D}\right)^{1/2}\int_{-\infty}^{+\infty}\frac{e^{-t^2}dt}{z - t} \tag{24}$$

where $z = [(\omega - \omega_r + i\Gamma(v,J)]\ 2(\ln 2)^{1/2}/\Delta\omega_D$.

If $\Gamma \to 0$, it can be shown that in this Doppler limit, the expression reduces to

$$\chi^{(3)}(\omega) = \sum_{v,J} K_{v,J}\left(\frac{(4/\pi)\ln 2}{\Delta\omega_D}\right)^{1/2}\left[\pi i e^{-z^2} - 2\sqrt{\pi}\ e^{-z^2}\int_0^{+\infty} e^{t^2}dt\right] \tag{25}$$

where

$$e^{-z^2}\int_0^z e^{t^2}dt$$

(Dawson's integral) is tabulated in Ref. 22 and $z = 2(\ln 2)^{1/2}(\omega - \omega_J)/\Delta\omega_D$. The effect of the real part is to increase the halfwidth of the Doppler line and to increase the wings. At first, the real part was estimated to be

small. With this assumption the width of $|\chi^{(3)}(\omega)|^2$ in the Doppler limit becomes $\Delta\omega_D/\sqrt{2}$. Later it was shown that the real part does contribute significantly and that the halfwidth is ~ 1.22 $\Delta\omega_D$ for a Doppler-broadened CARS line.[23]

If $\Delta\omega_D \to 0$, the Gaussian function in Eq. (22) becomes a δ-function, and one obtains the ordinary collisional broadened line. However, in high-temperature regions of a combustion medium, Doppler broadening can become significant. For example, at 2000 K the Doppler width for N_2 becomes 2.4×10^{-2} which is comparable to the collisional width at atmospheric pressure. The J dependence for the total linewidth would be reduced under these conditions. When it is necessary to include Doppler broadening, $|\chi^{(3)}(\omega)|$ can be estimated by using Eq. (22), if the nonresonant background is not significant. When the J dependence is known, then the temperature can be determined by fitting calculated data to experimental data using temperature and Γ as adjustable parameters.

3.4 LASER-INDUCED GAS-BREAKDOWN-THRESHOLD MEASUREMENT

As with many physical processes initiated by laser radiation, the intensity of the radiation generated in the CARS process by mixing two laser beams depends critically upon the intensity of the incident laser beams in an interaction medium. In general, this means that the more intense the incident beams, the more intense the generated CARS radiation. There is, however, a practical limit beyond which an increase in incident intensity will not result in increased generation of CARS radiation. One of the processes which impose this limit upon the incident laser intensity is the laser-induced gas-breakdown phenomenon. Since the gas breakdown severely disturbs the optical properties of the medium through which the beams propagate, its occurrence cannot be tolerated in optical-measurement processes such as CARS.

In order to determine the upper limit in the laser intensity (or power) which can be safely employed in flame diagnostics without causing gas breakdown, an experiment was carried out to measure the breakdown threshold intensity for the flat flame of the Battelle burner.

The experimental set-up is shown in Fig. 18. A single-mode ruby laser beam is generated in an oscillator cavity and then passed through two amplifiers. A portion (~ 0.1%) of the beam is detected by a PIN photodiode and displayed on a Tektronix R7912 transient digitizer. The majority of the ruby beam continues on through a collection of colored-glass and neutral-density filters and enters a glass cross through a 3-in.-diam. quartz window. Inside the cross the ruby energy is focused by a 55-mm-focal-length quartz lens. The focal point of this lens is near the vertical centerline of a 2.5-in.-diam. low-pressure flat-flame burner developed by Battelle Laboratories. The laser beam exits the cross through another 3-in. quartz window and is detected through a Schott KG1 filter by means of a thermopile detector head which is connected to a Scientech 362 power/energy meter.

Two steps were taken to minimize fluctuations in the energy meter readings caused by environmental conditions and background radiation. The effects of temperature gradients in the surrounding air upon the thermopile were reduced by use of an insulated enclosure which allowed a 1-in.-diam. access to the detector head. This access port was covered with a Schott KG1 filter which was used to absorb the IR radiation produced in the flame. With this filtering background energy affecting the detector was independent of the observed position within the flame.

The experimental procedure used to arrive at the laser energy required for media breakdown consisted of monitoring the laser pulse shape on the transient digitizer, recording the energy-meter reading, and adjusting the laser power to the required levels. The PIN diode/digitizer combination supplied information on the pulsewidth and the relative amplitude of the laser pulse.

The optical breakdown of the gaseous media induced by the laser radiation manifests itself in three ways, the first two being the generation of a visible discharge and an audible "snap" in the focal volume. The third phenomenon, which was most heavily relied upon, was the pronounced reduction in the laser energy transmitted through the affected media, the media breakdown reducing by a factor of two or more the energy throughput.

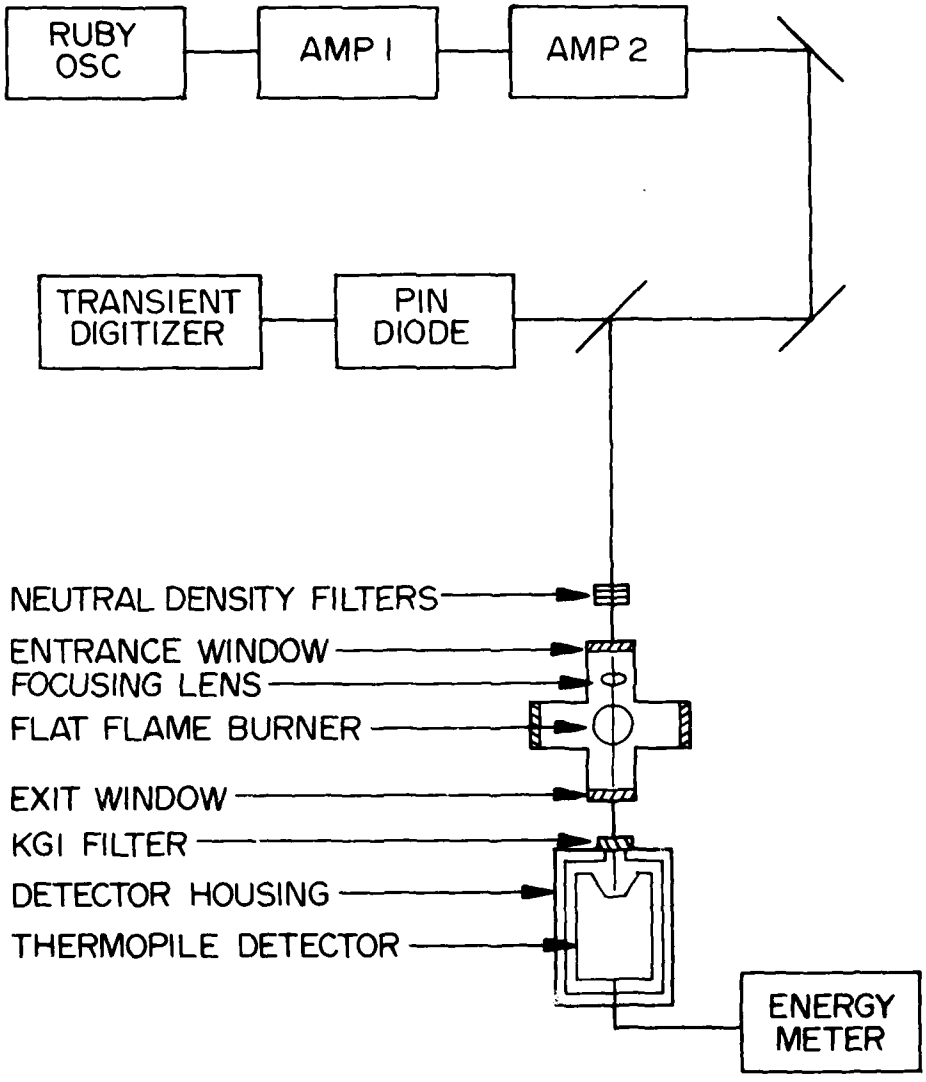

Figure 18. Schematic Diagram of the Experimental System for Breakdown-Threshold Measurement.

Adjustment of the amount of laser energy being focused in the flame cell was accomplished in two ways. Large-scale power changes were accomplished by insertion of various combinations of neutral-density filters into the beam. Fine adjustments in intensity were made by changing the ruby-amplifier flash-lamp voltage. Thus, by increasing the laser-pulse energy to the breakdown limit and measuring the energy transmitted in a "clean" Gaussian beam, the point of optical breakdown was determined.

To arrive at the power density required to cause breakdown in the media, the following expression was employed:

$$P_d = \frac{E_{det}}{\tau_{pw} T_c \frac{\pi}{4} (1.27 \lambda f/D)^2} \tag{26}$$

where P_d = power density; E_{det} = detected laser energy; τ_{pw} = laser pulse-width (FWHM); T_c = combined transmission of exit window and KG1 filter; λ = ruby-laser wavelength; f = focal length of focusing lens; and D = diameter of laser beam at focusing lens. The values of the parameters used in these measurements were: τ_{pw} = 13 ns, T_c = 62.6%, λ = 6943 Å, f = 55 mm, and D = 3.5 mm.

Figure 19 shows the variation of breakdown power densities, as determined through the above procedure, exhibited for five sets of conditions existing at the focal volume. Curves 1 and 2 show the breakdown characteristics at 1 atm of pressure, while 3 and 4 show the effects observed at 130 Torr. Data Point 5 indicates the trend of the breakdown threshold in a fuel-rich (dirty) flame.

One general conclusion that is supported by the data in Fig. 19 is that the power density required for media breakdown is inversely proportional to the number density of the molecules available in the focal volume and that this number density can be varied by changing either the pressure or temperature. A comparison of Curves 2 and 4 lends credence to this conclusion and reflects known characteristics of flame composition and geometry. Specifically, the leading edges of these two curves tend to describe a mixing zone for the

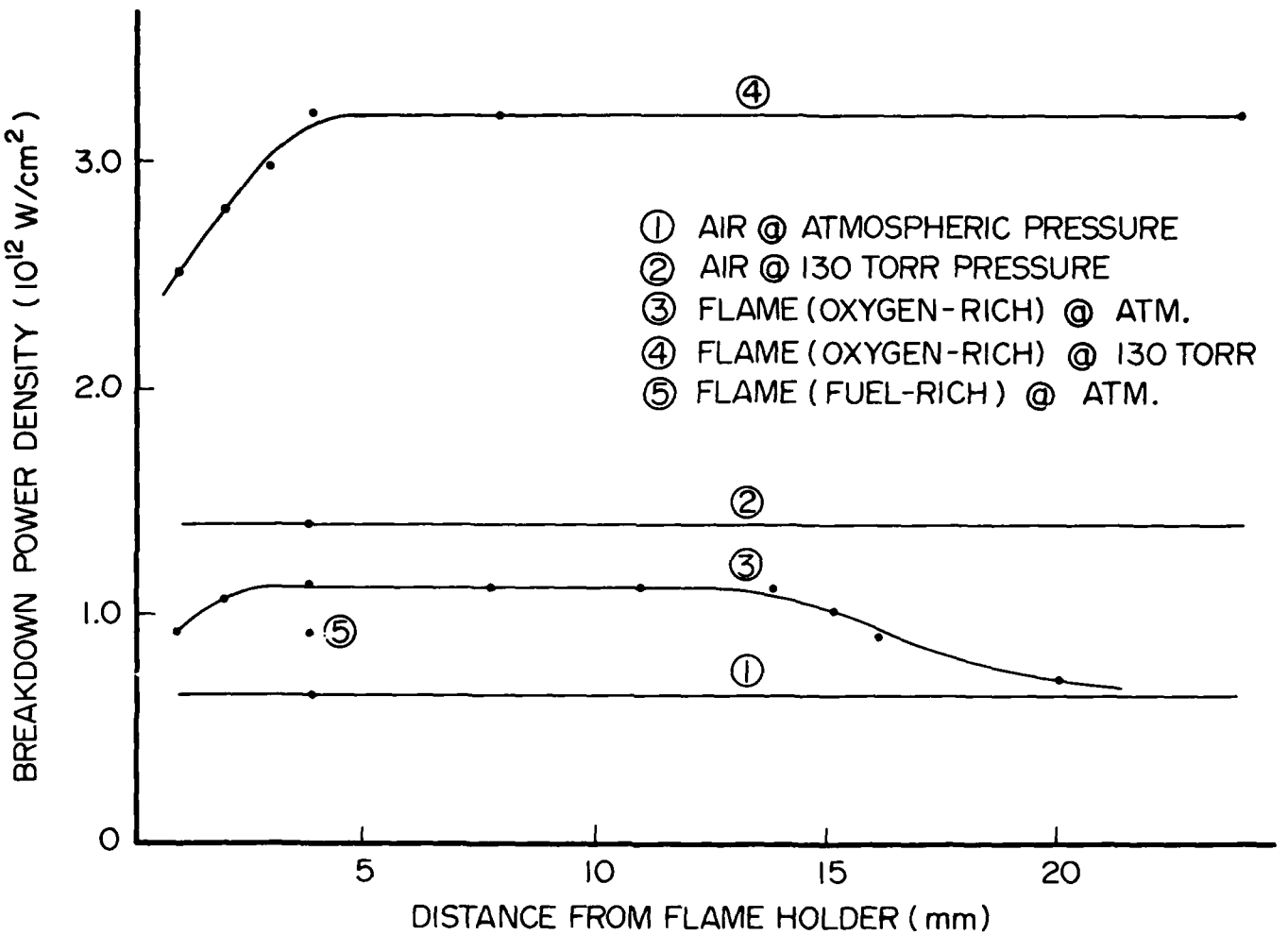

Figure 19. Laser-Induced Breakdown-Threshold Profile of the Battelle-Burner Flame.

relatively cool combustion gases. Also, the trailing edge of these curves describes the effect of pressure upon a flame operating in a lower-pressure environment causing a lengthening of the flame reaction zone. To our relief, the reduction in breakdown threshold due to high temperature in flames which had been anticipated did not materialize in our experiments.

During the course of this experiment, one heretofore unnoticed physical characteristic of the Battelle burner was observed. The surface of the burner consists of a 2.5-in.-diam. wire mesh which, when heated, buckles slightly. When breakdown measurements were attempted at altitudes less than 1 mm above the burner, the wire screen intercepted the laser radiation, resulting in undersirable scattering and absorption. This characteristic, in effect, limits the usable measurement zone of this burner to a minimum of 1 mm.

3.5 POSSIBILITY OF USING THE CO_2 RAMAN BANDS FOR REAL-TIME TEMPERATURE MEASUREMENT IN FLAMES

Efforts on developing a temperature-measurement technique for application to flame diagnostics using the CARS process have thus far been limited to the analysis of the N_2 band spectrum in one manner or another. This analysis may involve either evaluation of the slope of the linear portion of the Q-branch spectrum as outlined previously,[24] or contour matching of an experimental spectrum with those generated by a computer. An alternate approach to obtaining temperatures from combustive environments is to use the vibrational structure of the CARS spectrum of the CO_2 molecule present in flames. This method is based upon the comparison of integrated intensities for one of the Raman-active fundamentals and its associated hot bands. This method, if it proves to be practical, will have a number of advantages over use of the N_2 spectrum. First, because this method is insensitive to fluctuations in the CO_2 concentration in flames, it would permit real-time as well as time-averaged temperature measurement. Secondly, the method would require a relatively simple data-processing system and instrumentation for operation. The disadvantages are that the temperature measured is vibrational temperature

of a combustion product and thus may be reaction-dependent and that the relative concentration of CO_2 available in flames typically at ~ 10% is lower than that of N_2, and thus may be difficult to detect.

Although the CO_2 molecule has only one Raman-active fundamental band, due to Fermi resonance[25], there are in reality two strong, fundamental-like bands at 1388.2 cm^{-1} and 1285.4 cm^{-1} which correspond, respectively, to ($10^00 - 00^00$) and ($02^00 - 00^00$) transitions. Although the assignment used here is the traditional assignment of these bands, it has been shown in recent years that this traditional assignment should, in fact, be reversed (see Refs. 26 and 27). Each of these bands has its own hot-band structure which becomes more prominent as the gas temperature is increased. The pertinent energy levels and the Raman bands of interest are diagramatically shown in Fig. 20. For diagnostic purposes, either of the two bands can be used. However, the one labeled 1388 cm^{-1} group is about twice as strong as the other, and naturally it is a better choice. Also, the 1388 cm^{-1} group does not suffer from interference of the other blending bands as does the 1285 cm^{-1} group. For example, the Raman transition ($04^00 - 02^00$) at 1263.0 cm^{-1} (although not shown in the diagram) is very near the ($03^10 - 01^10$) band at 1265.1 cm^{-1}. Since the relative intensity of these lines is a function of the population-density difference between levels involved in the CARS process and since the population density is, in turn, a function of temperature, measurement of the relative intensity of two or more lines can be used for determining the gas temperature.

The integrated power of the first hot band at 1409.5 cm^{-1} relative to that of the fundamental band at 1388.2 cm^{-1} can be expressed by:

$$\frac{P_{INT,1}}{P_{INT,0}} = \left(\frac{N_{d1}}{N_{d0}}\right)^2 \frac{F_1(T)}{F_0(T)} \frac{\Gamma_{eff,0}}{\Gamma_{eff,1}} \left(\frac{\left(\frac{d\sigma}{d\Omega}\right)_1}{\left(\frac{d\sigma}{d\Omega}\right)_0}\right)^2 \qquad (27)$$

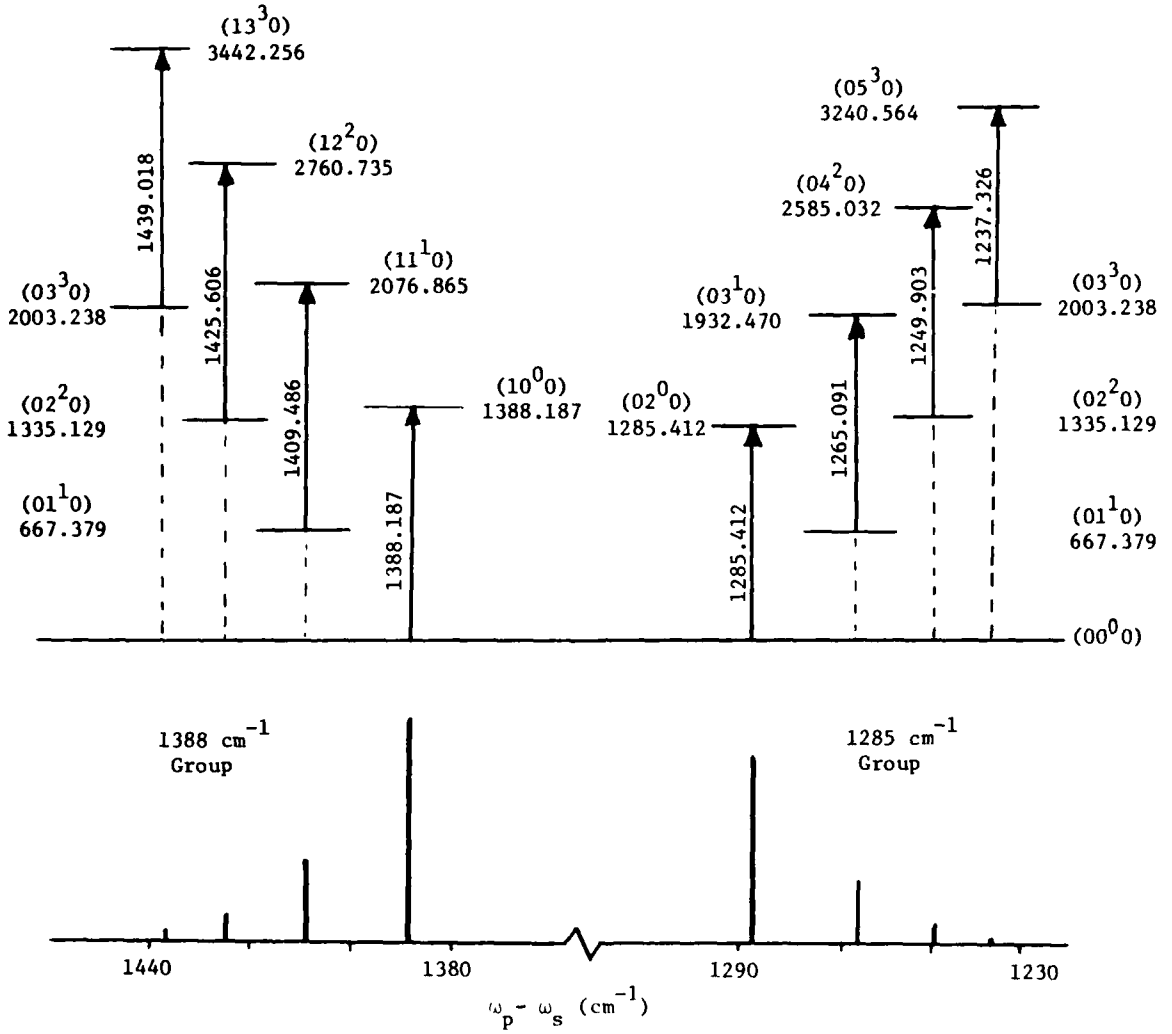

Figure 20. Pertinent Energy Levels and Raman Bands of Interest to Combustion Diagnostics. Energy levels (in cm^{-1} units) were obtained from Ref. 28.

where P_{INT} is the integrated CARS power of a band, N_d is the number-density difference between the lower and upper levels involved in the CARS process, $d\sigma/d\Omega$ is the differential spontaneous Raman cross section, and F(T) and Γ_{eff} are the previously defined parameters[4] representing the effect of rotational distribution and the interference among various rotational lines, respectively. In the following paragraphs, the factors which appear in Eq.(27) will be examined individually.

In general, the population density of a vibrational level of a linear triatomic molecule (ignoring the vibrational angular momentum and Fermi resonance for the moment) is given by:

$$N(v_1,v_2,v_3) = \frac{(v_2 + 1)}{Q_v} \quad \exp\left[\frac{-E(v_1,v_2,v_3)}{kT}\right] \tag{28}$$

where v_1,v_2, and v_3 are the three vibrational quantum numbers of the CO_2 molecule; $E(v_1,v_2,v_3)$ is the energy of the level (v_1,v_2,v_3); and Q_v is the vibrational partition function given by:

$$Q_v(T) = \sum_{v_1,v_2,v_3} \sum \sum (v_2 + 1) \quad \exp\left[\frac{-E(v_1,v_2,v_3)}{kT}\right] \tag{29}$$

where the temperature dependence of the partition function is explicitly indicated.

Vibrational levels with $v_2 \geq 2$ are split according to their vibrational angular momentum which takes on a value $\ell_2 = v_2, v_2-2, \ldots 1$ or 0. The statistical weight of these sublevels is a function of ℓ_2 and is tabulated below for the first three excited levels of v_2.

v_2	ℓ_2	Degeneracy
0	0	1
1	1	2
2	2	2
	0	1
3	3	2
	1	2

A real CARS spectrum of the 1388 cm^{-1} group is shown in Fig. 21. This spectrum having a spectral resolution of 2 cm^{-1} was recorded with an OMA from the flat flame of the Battelle burner operated with the N_2 buffer gas replaced by CO_2 gas. Note that the lines at 1388.2 and 1409.5 cm^{-1} were attenuated by a factor of 10 (ND 1) and 4 (ND 0.6), respectively. Even at room temperature, the first hot band ($11^10 - 01^10$) can be easily observed since about 7% of the CO_2 population occupies the (01^10) state.

The ratio of the number-density difference of the first excited state (01^10) to that of the ground state (00^00) is given by:

$$\frac{N_{d1}}{N_{d0}} \equiv \frac{N(01^10) - N(11^10)}{N(00^00) - N(10^00)} = \frac{N(01^10)\left[1 - \exp\left(-\frac{E(11^10) - E(01^10)}{kT}\right)\right]}{N(00^00)\left[1 - \exp\left(-\frac{E(10^00) - E(00^00)}{kT}\right)\right]}$$

$$\approx \frac{N(01^10)}{N(00^00)} \approx 2 \exp\left[-960.0/T\right] \qquad (30)$$

where $N(00^00)$ is the ground-state number density and the others are similarly defined. The second equality is justified in view of the nearly equal energy differences in the exponents. This approximation entails less than 0.3% error at 2000°K, although at that temperature the upper-level population is more than 30% that of the lower level. Similarly for the second excited state, the ratio can be written as:

$$\frac{N_{d2}}{N_{d0}} \equiv \frac{N(02^20) - N(12^20)}{N(00^00) - N(10^00)} \approx \frac{N(02^20)}{N(00^00)} \approx 2 \exp\left[-1920.5/T\right] \qquad (31)$$

These ratios are plotted in Figure 22 as a function of temperature. One measure of the sensitivity of the temperature measurement is given by the derivative of these ratios with respect to temperature. However, the accuracy with which the population ratio can be determined in a CARS experiment is usually given in terms of a percentage error. Therefore, it is more meaningful in practice to consider the percentage change in the population density ratio with temperature than the simple derivative in this regard. This

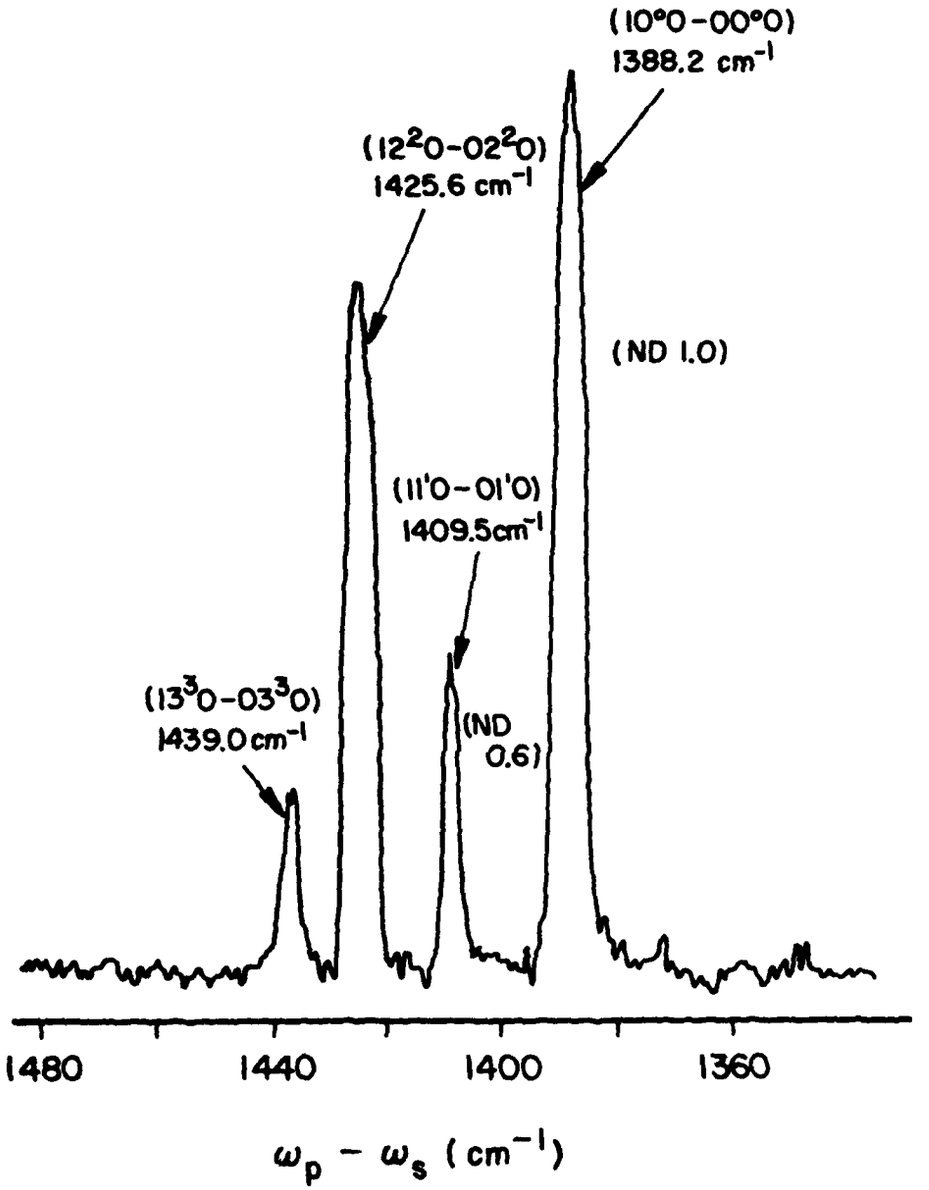

Figure 21. CARS Spectrum of CO_2 in a Flame in the Vicinity of 1400 cm^{-1}.

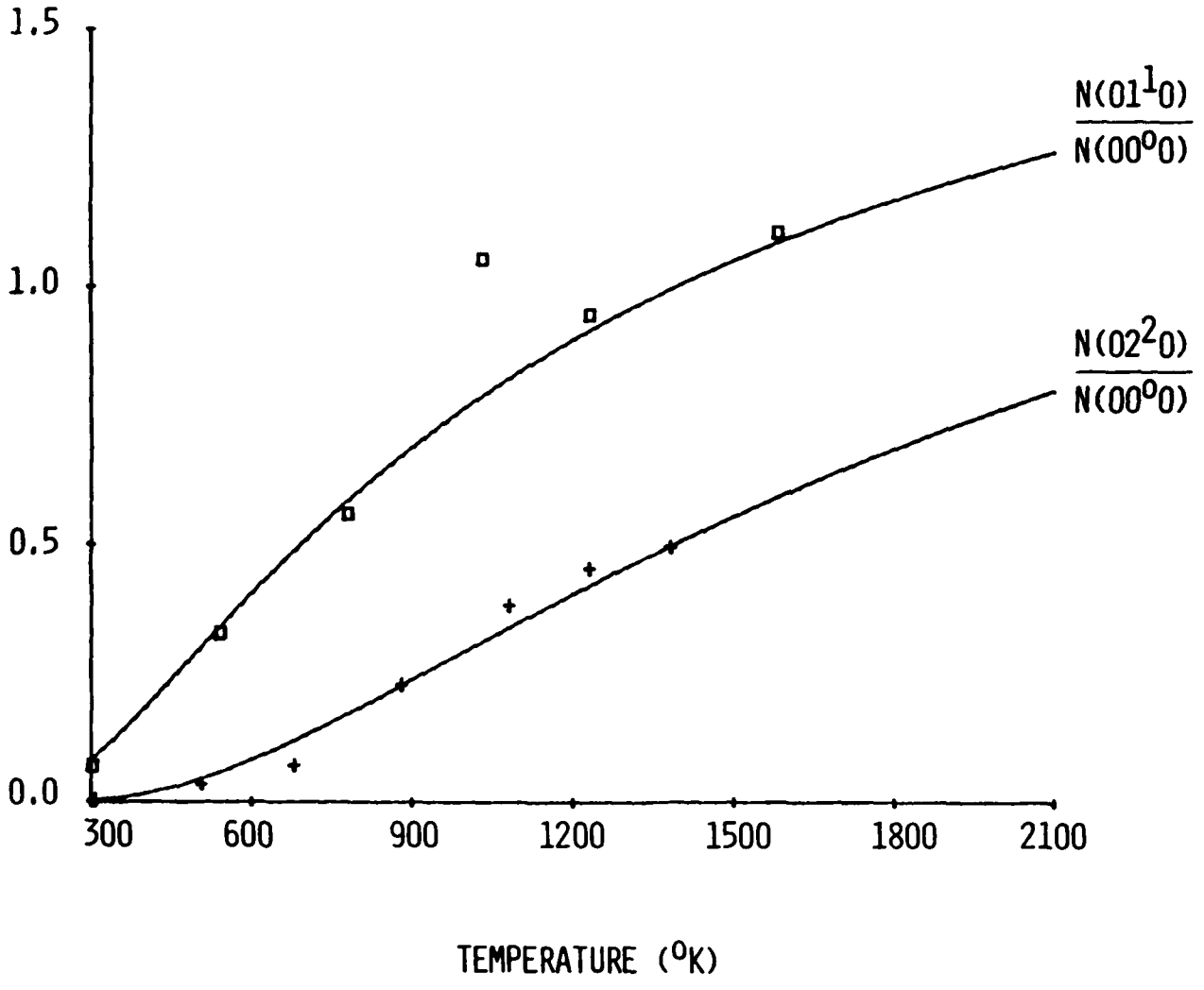

Figure 22. Ratio of the Population Densities of (01^10) and (02^20) States of the CO_2 Molecule to that of the Ground State (00^00). Preliminary experimental results are also shown.

percentage change is given by

$$\frac{d}{dT}\left(\frac{N_{d1}}{N_{d0}}\right)\Big/\left(\frac{N_{di}}{N_{d0}}\right) = 960.0/T^2 \qquad (32)$$

for the first hot band and

$$\frac{d}{dT}\left(\frac{N_{d2}}{N_{d0}}\right)\Big/\left(\frac{N_{d2}}{N_{d0}}\right) = 1920.5/T^2 \qquad (33)$$

for the second hot band. This indicates that the sensitivity of the second hot band is greater than that of the first. In fact, the sensitivity is directly proportional to the energy spacing of the levels being compared. Of course, this criterion of the sensitivity is valid only as long as the population densities can be determined with the same accuracy for both levels.

Equation (33), for instance, can be used to estimate the accuracy of the temperature measurement made using the second hot band and the fundamental band. For this estimation it is more convenient to rewrite the equation as follows:

$$\frac{dT}{T} = \frac{T}{1920.5}\, d\left(\frac{N_{d2}}{N_{d0}}\right)\Big/\left(\frac{N_{d2}}{N_{d0}}\right) . \qquad (34)$$

The above equation states that the estimate of the error in the temperature measurement is T/1920.5 times the relative error in the ratio of the number densities. Thus, a 5% error in the determination of the ratio of the number densities would result in a 4.7% and 2.6% error at 1800 K and 1000 K, respectively. In comparison, the use of the first hot band in conjunction with the fundamental would yield 9.4% and 5.2%, respectively, for the same temperatures.

Function F(T), which accounts for the effect of changing rotational distribution with temperature, has been calculated for the first two excited states (01^10 and 02^20) as well as the ground state, and the results are

tabulated in Table 2. Neglecting to include this factor in the evaluation of the number density from CARS intensity data would introduce an error of up to 3% and 6% for the $(01^{1}0)$ and $(02^{2}0)$ levels, respectively.

Information on the effective linewidth (Γ_{eff}) and the differential Raman cross section for the Raman bands under consideration is not available at this time. Pressure-broadened Raman linewidth data are needed to calculate Γ_{eff}. However, because of the small difference in the rotational constants of the states involved in the CARS process, the Q-branch lines are not resolved at all, and thus it would be impossible to measure linewidth. It would be highly desirable to measure the Raman cross section of the hot bands relative to that of the fundamental band.

Preliminary results of experiments designed to test the feasibility of this idea were also presented in Fig. 22. The CO_2 gas was heated in an oven and the temperature monitored with a thermocouple. The integrated CARS power was measured using a Stokes beam having a linewidth of ~ 2 cm^{-1}. This linewidth is sufficiently wide to excite all the rotational lines that are thermally populated since calculation shows that the widths of the Q-branches are in fact 0.10, 0.75, and 0.88 cm^{-1} for the $(10^{0}0 - 00^{0}0)$, $(11^{1}0 - 01^{1}0)$ and $(12^{2}0 - 02^{2}0)$ bands, respectively. In making these measurements, the Stokes beam was tuned from band to band at each temperature setting. A least-squares fit of the experimental data to the theoretical curve yielded a value of 0.31 for the ratio of the factor $(d\sigma/d\Omega)/\sqrt{\Gamma_{eff}}$ for the first hot band to that of the fundamental and similarly 0.49 for the second hot band. Although the present experiment is not being carried out in real time, the extension of this scheme to real-time measurement should not be very difficult.

Table 2

CALCULATED VALUES OF F(T) FOR CO_2 NORMALIZED TO THE VALUE FOR T = 300 K

T (K)	$\frac{F_o(T)}{F_o(300)}$	$\frac{F_1(T)}{F_1(300)}$	$\frac{F_2(T)}{F_2(300)}$
300	1.000	1.000	1.000
450	0.819	0.815	0.815
600	0.711	0.706	0.707
750	0.635	0.630	0.630
900	0.579	0.575	0.575
1050	0.536	0.529	0.529
1200	0.503	0.493	0.494
1350	0.479	0.464	0.464
1500	0.462	0.441	0.441
1650	0.449	0.424	0.419
1800	0.440	0.411	0.398
1950	0.432	0.403	0.381
2100	0.428	0.397	0.366

3.6 COMPARISONS OF SINGLE-SHOT THERMOMETRY OF CARS WITH OTHER OPTICAL THERMOMETRIC TECHNIQUES

Two-Line Fluorescence

A fluorescence system was developed in order to implement the two-line fluorescence techniques[29] for measuring flame temperature. The development of this system was motivated by the desire for a means of determining temperature in flames, independent of the CARS technique. An independent measurement of flame temperature would constitute a firm basis for evaluating the validity and accuracy of the CARS process as a thermometric tool for flames.

Winefordner[30] has shown that the temperature in a flame can be measured by means of a two-line fluorescence method. The advantage which this method has over other spectroscopic methods that have been used is spatial resolution, i.e., "local" temperatures in various parts of the flame can be measured directly rather than inferred from average temperature measurements across the flame. The method involves seeding the flame with atoms whose energy-level structure is similar to that shown in Fig. 23 (for example, In, Ga, or Tl). Level 2 is connected via electric dipole transition to both Levels 0 and 1. It is assumed that thermal equilibrium exists and the ratio of the populations of Levels 1 and 0 is given by

$$\frac{N_1}{N_0} = \frac{g_1}{g_0} \exp(-E_1/kT) \tag{35}$$

where g_1 and g_0 are the statistical weights of Levels 1 and 0, respectively; E_1 is the energy difference between Levels 1 and 0; k is the Boltzmann constant; and T is the local temperature of the flame. E_1 is generally known. Therefore, determination of the ratio N_1/N_0 would yield a value for T. A simple analysis shows that N_1/N_0 may be measured in the following way: The transition $0 \rightarrow 2$ at wavelength λ_{02} is excited by a broadband light source of known energy density ρ_{02} (erg cm^{-3} Hz^{-1}) centered at λ_{02}, and F_{21} fluorescent photons/sec are observed at wavelength λ_{12}. Then under steady-state conditions

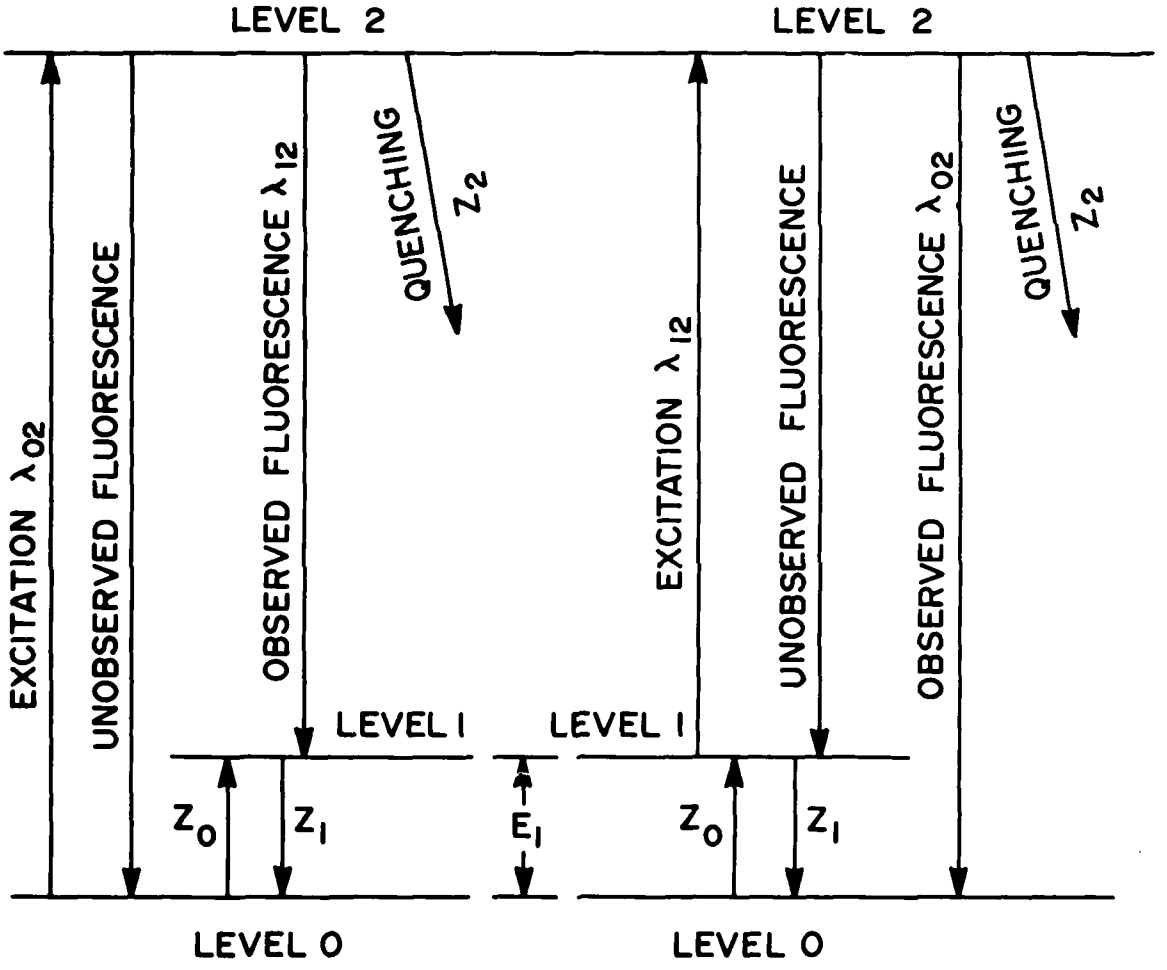

Figure 23. Level Diagram for Two-Line Fluorescence.

$$\frac{dN_2}{dt} = \rho_{02}B_{02}N_0 - (A_{21} + A_{20} + Z_2)N_2 = 0 \qquad (36)$$

and

$$F_{21} = CN_2 A_{21} \qquad (37)$$

where C is a constant which depends upon a geometrical factor, and Z_2 is the total non-radiative quenching rate of Level 2. The stimulated-emission term ($\rho_{02}B_{20}N_2$) which is very small has been neglected. Also the transition 1 → 2 is excited by a broadband light source of energy density ρ_{12} centered at wavelength λ_{12}, and F_{20} fluorescent photons are observed at wavelength λ_{02}. Under steady-state conditions one may write two equations which are similar to Eqs. (36) and (37). A simple manipulation of these four equations, along with the use of the well-known relationship between Einstein A and B coefficients, yields

$$\frac{N_1}{N_0} = \frac{F_{20}}{F_{21}} \frac{g_1}{g_0} \frac{\rho_{02}}{\rho_{12}} \left[\frac{\lambda_{02}}{\lambda_{12}}\right]^3 \qquad (38)$$

Note that the ratio N_1/N_0 is independent of the quenching rate Z_2, even under nonsaturating conditions. Using the measured values of ρ_{02}, ρ_{12}, F_{20}, and F_{21}, the temperature T may be determined using Eqs. (35) and (38). Winefordner has measured the temperature profiles of several kinds of flames using this method.

The experimental system is shown schematically in Fig. 24. The broadband light output from an Eimac lamp is chopped (~ 145 Hz), line-selected for either 410.2 or 451.1 nm by means of a pair of interference filters, and focused (L1) into an argon-shielded, premixed acetylene flame which is seeded with indium atoms (in reality, $InCl_3$ dissolved in distilled water is nebulized into the flame). In the two-line fluorescence method, the fluorescent signal is measured at one wavelength--say 410.2 nm--while the fluorescing medium is excited at the other wavelenght--451.1 nm--and vice versa. The nonresonant

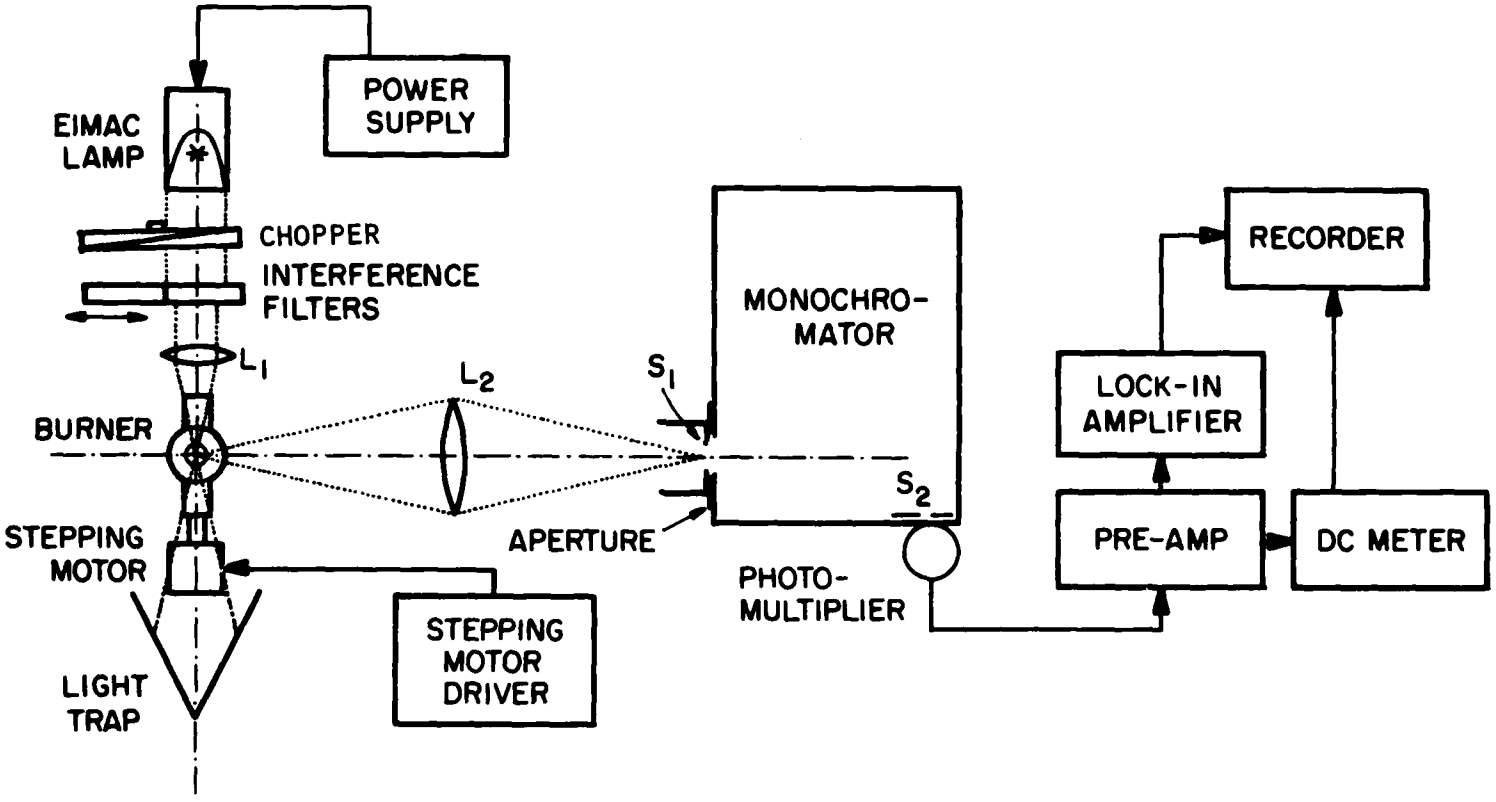

Figure 24. Schematic Diagram of a Two-Line-Fluorescence System.

fluorescence signal from the excited indium atoms is collected (L2), analyzed (monochromator), and synchronously detected (photomultiplier plus lock-in amplifier), and recorded. At the same time, the dc component of the photomultiplier current is monitored and recorded in order to ascertain the constancy of the level of seeding throughout a measurement.

In making the two-line fluorescence measurement, it is necessary that the relative transfer function (defined here as the ratio of the photomultiplier output to the incident-light intensity) be known. This was accomplished using an NBS-calibrated standard tungsten filament lamp. Figure 25 gives an example of such a transfer function for the detection system used in the experiment which consists of a Spex 1702 monochromator having a 1200-gr/mm grating and an EMI 9816 photomultiplier. The values of the transfer function for the two fluorescence lines i.e., 410.2 and 451.1 nm, were calculated to be 2.4169 and 2.9134, respectively, and their ratio was 0.8296. A spectral scan of the transfer function with a different standard lamp yielded a similar result for the relative transfer function at the two wavelengths.

In order to determine the optimum seeding level for the measurement, a set of stock solutions having various concentrations of $InCl_3$ was prepared; the fluorescent intensity was measured for the two wavelengths as a function of $InCl_3$ concentration. The results which are shown in Fig. 26 indicate that the fluorescence is a linear function of the $InCl_3$ concentration up to 200 mg/l. At higher concentrations, the self-absorption of the medium can no longer be neglected, i.e., the medium cannot be treated as though it were optically "thin." Based upon these observations, an optimum concentration of 150 mg/l was used for all experiments.

Data obtained from the two-line atomic fluorescence system are presented in Fig. 27. This profile was obtained by stepping the approximate 6-mm-diam. focused pump beam through the 10-mm-diam. indium-seeded flame at a height of 4 cm above the burner. The profile indicates that the temperature is constant over a large section of the burner. The measurement resulted in a temperature of 2650 $\pm$ 50 K. Several difficulties were encountered in performing the two-line fluorescence experiments. Of most concern was the

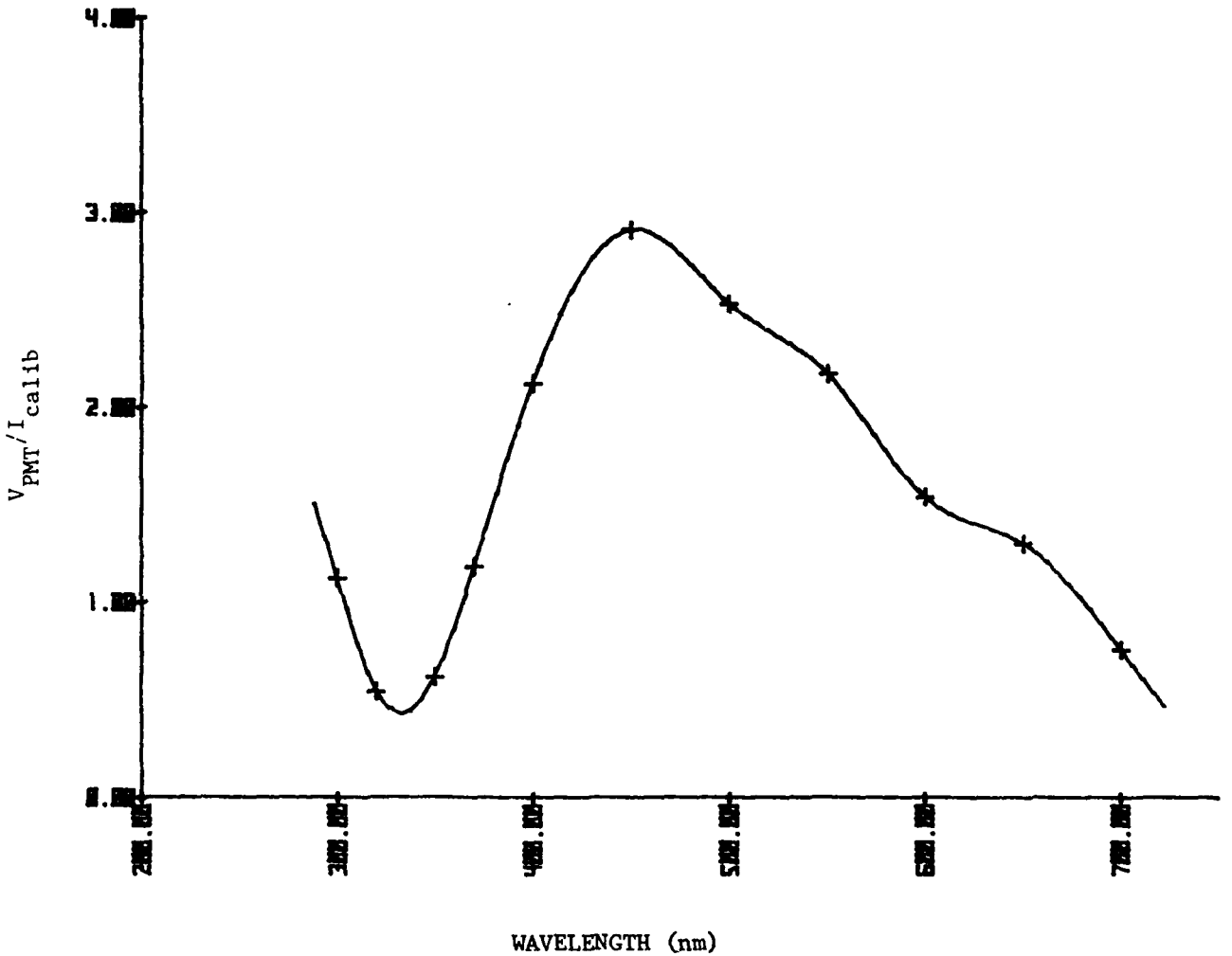

Figure 25. Relative Transfer Function of the Detection System (Monochromator and Photomultiplier).

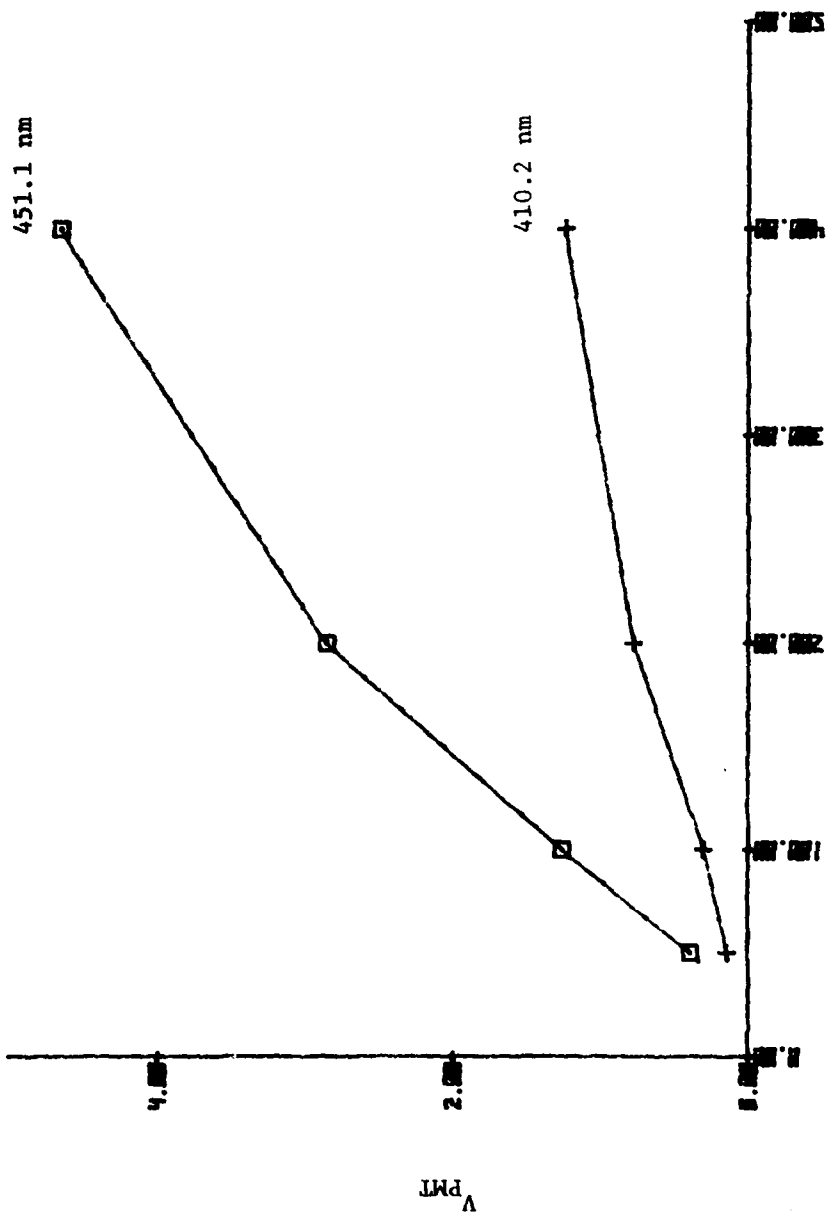

Figure 26. Dependence of Fluorescence Intensity upon Concentration.

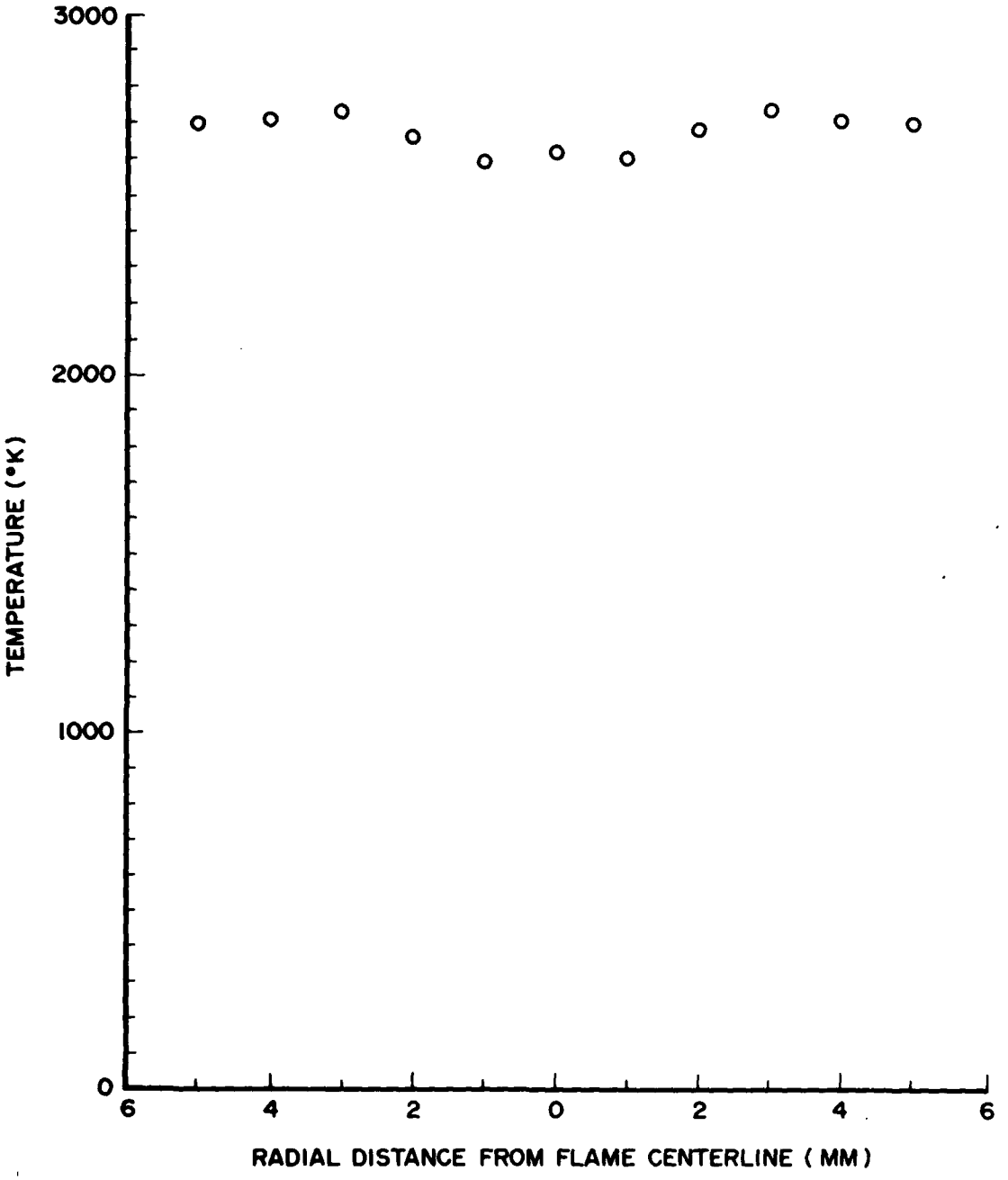

Figure 27. Temperature Profile 4 cm above Burner.

relatively low signal-to-noise ratio (3:1) obtainable. This required the use of long lock-in-amplifier filter time constants (30 sec), which resulted in slow system response.

In order to compare the results to CARS measurements, a similar profile of the acetylene-fueled flame was obtained with the Nd:YAG-based CARS system. This profile (shown in Fig. 28), like the two-line fluorescence results, indicated that the temperature was essentially constant over a large region of the flame and dropped sharply at the edges. The average temperature from these sets of measurements was 2600 K $\pm$ 50 K. This was generally in good agreement with the fluorescence measurement, considering the larger uncertainty of those data. Figure 29 shows a computer fit which was made to the data, indicating that the program and input parameters were indeed replicating the true CARS spectra.

Sodium-Line Reversal

A system for performing temperature determinations by the sodium line-reversal technique[31] was assembled, as shown in Fig. 30. This technique utilizes the emission characteristics of (in this case) the sodium molecules in ordinary tap water nebulized into the flame to determine a blackbody radiance function from which the flame temperature is extracted. An average temperature of 2560 K was measured for the 6-mm-diam. sample volume through the acetylene-fueled flame at the test height of 4 cm. This is in excellent agreement with the CARS measurements discussed previously in this section.

Applications of the above technique to a propane-fueled flame indicated a temperature of 2241 $\pm$ 30 K. The results of CARS measurements made with the ruby-based CARS system are listed in Table 3. The CARS data in this case indicated a temperature of 2143.5 $\pm$ 140 K. The large variation and lower temperature of the CARS measurement indicated that the position of the flame was somewhat off center and toward the more turbulent edges. Another measurement was conducted on the burner with the Nd:YAG-based CARS system which gave a temperature of 2220 K $\pm$ 50 K for the same flame conditions and position as the sodium-line reversal. These results were in good agreement with the

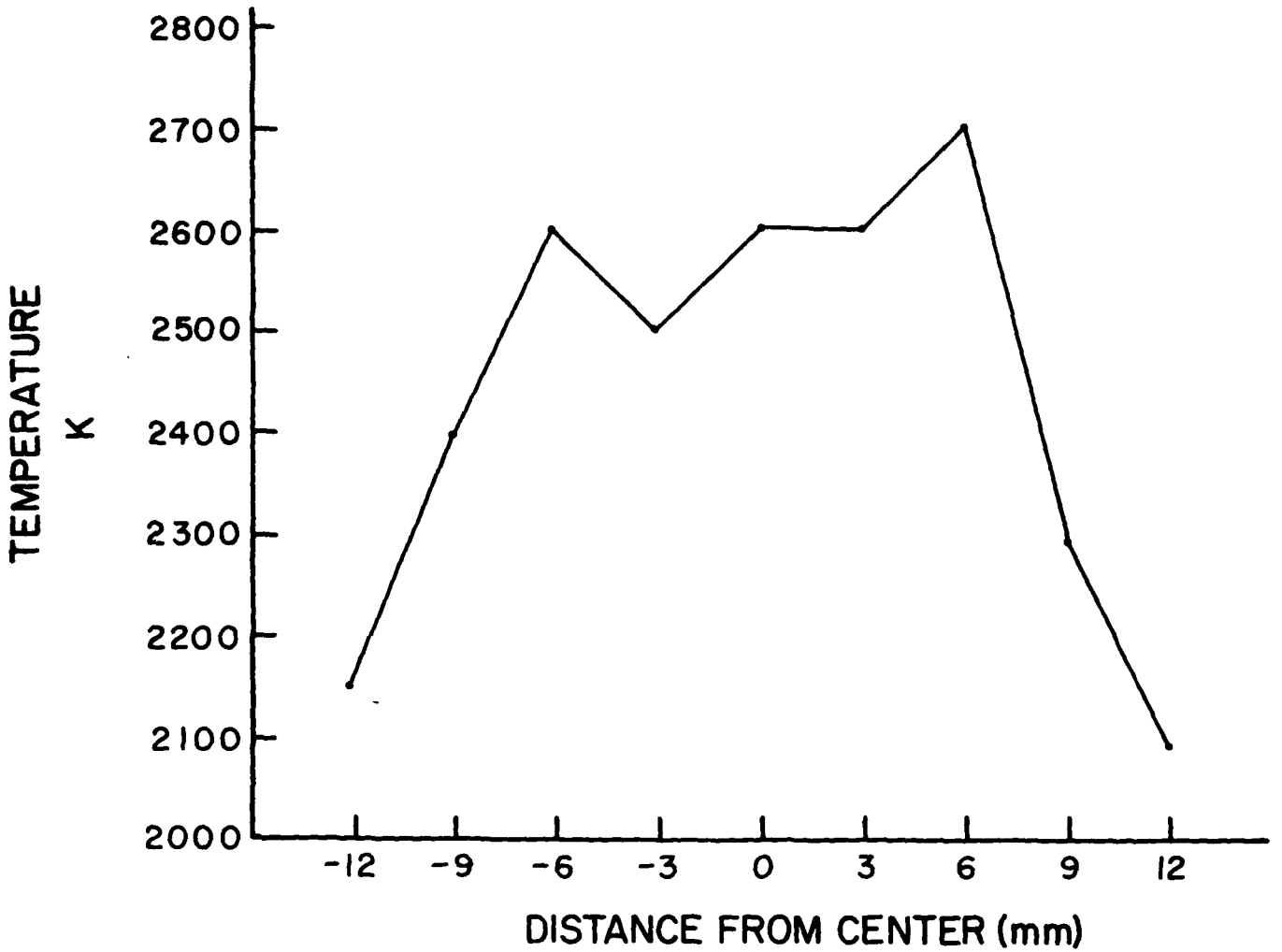

Figure 28. Horizontal Temperature Profile of the Acetylene-Fueled Flame 16 mm above Base of Premixed Burner.

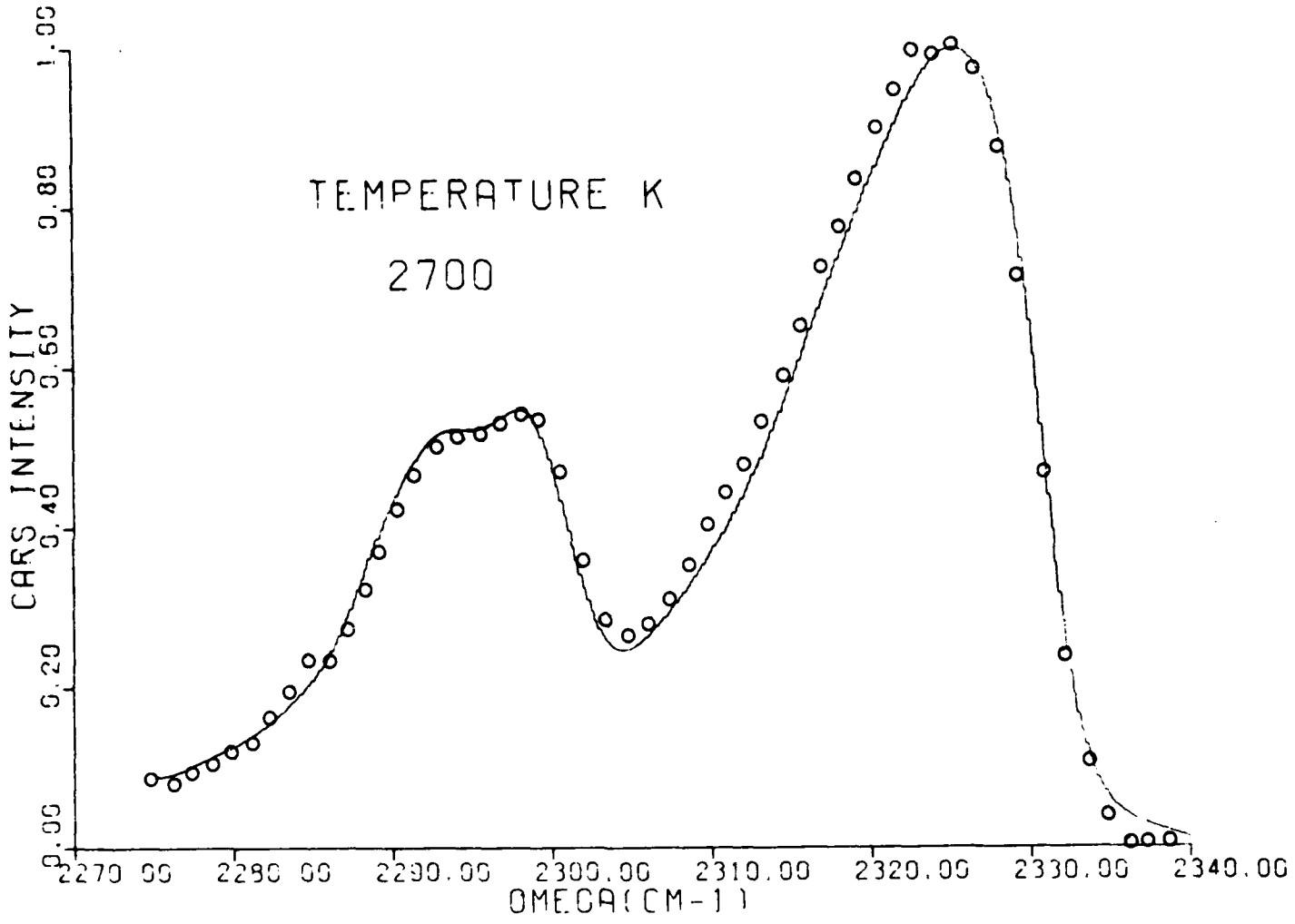

Figure 29. Temperature Fit of CARS Spectrum Obtained from an Acetylene-Fueled Flame.

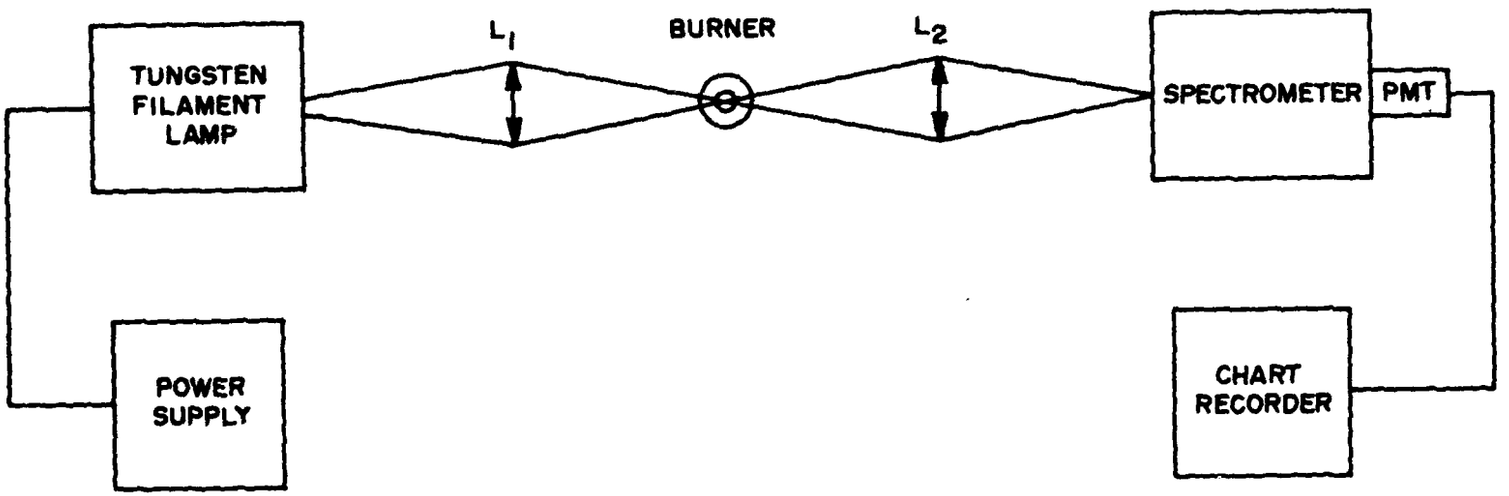

Figure 30. Line-Reversal Temperature-Measurement System.

Table 3

TEMPERATURE FITS TO THE PROPANE-FLAME DATA

Spectra No.	Temperature (K)	Dispersion (±K)
1	2009.7	31.86
2	1853.7	30.21
3	2389.9	30.67
4	2252.9	26.70
5	2177.4	26.95
6	2208.2	48.01
7	2125.8	24.07
8	2059.9	27.56
9	2010.6	34.81
10	2086.4	26.43
11	2185.4	41.78
12	2315.9	25.28
13	2167.3	30.72
14	2117.0	24.03
15	2215.5	25.99
16	2309.8	37.83
17	1876.4	41.43
18	2220.5	20.43

Avg. Temperature = 2143.5 K + 140 K

reversal measurements. Temperature profiles which were obtained on the flame are shown in Fig. 31. The propane-fueled flame showed the same basic trends as the acetylene-fueled flame--primarily that the temperature is essentially flat over a large region and drops off sharply at the edges. Figure 31 shows a typical spectrum and temperature fit of the spectrum for these data.

3.7 REFERENCE-SCHEME STUDIES

In order to obtain single-shot number densities, either an absolute or a relative measurement of the integrated intensity of the Raman transition must be made. The former is extremely difficult--if not impossible--in most cases. The latter is performed through use of a ratioing technique in which the majority of the experimental parameters are canceled. In an effort to discover the optimum ratioing arrangement, a preliminary study was conducted on various signal-detection schemes. The basic experiment consisted of a ruby CARS setup in which the sample and reference legs were in series with each other. In order to insure that the CARS signal from one leg would not interfer with the other, special blocking filters were employed which passed the ruby and dye signals but blocked the CARS signal. Room air was chosen as the gas to be probed for both the reference and sample paths. Various detectors were utilized during the experiment in order to determine the best possible arrangement.

Results of this experiment are given in Table 4. A ratioed variation of 10 - 18% was encountered depending upon the particular detectors and/or signals ratioed. This would contribute a 5 - 9% error in the measured concentration. While this error was considered to be relatively small, it was decided that further studies into lowering these errors would be necessary. An important observation was made during the incorporation of the Nd:YAG laser into the CARS system--the CARS signal fluctuations increased dramatically. This observation sparked a major investigation in order to understand this phenomenum. Figure 32 depicts some of the various arrangements that were employed during the testing. In Fig. 32(a) a parallel-path configuration was used in which a small percentage of the BOXCARS beams was split to form two separate paths in which the CARS signals were formed by two independent lenses. This

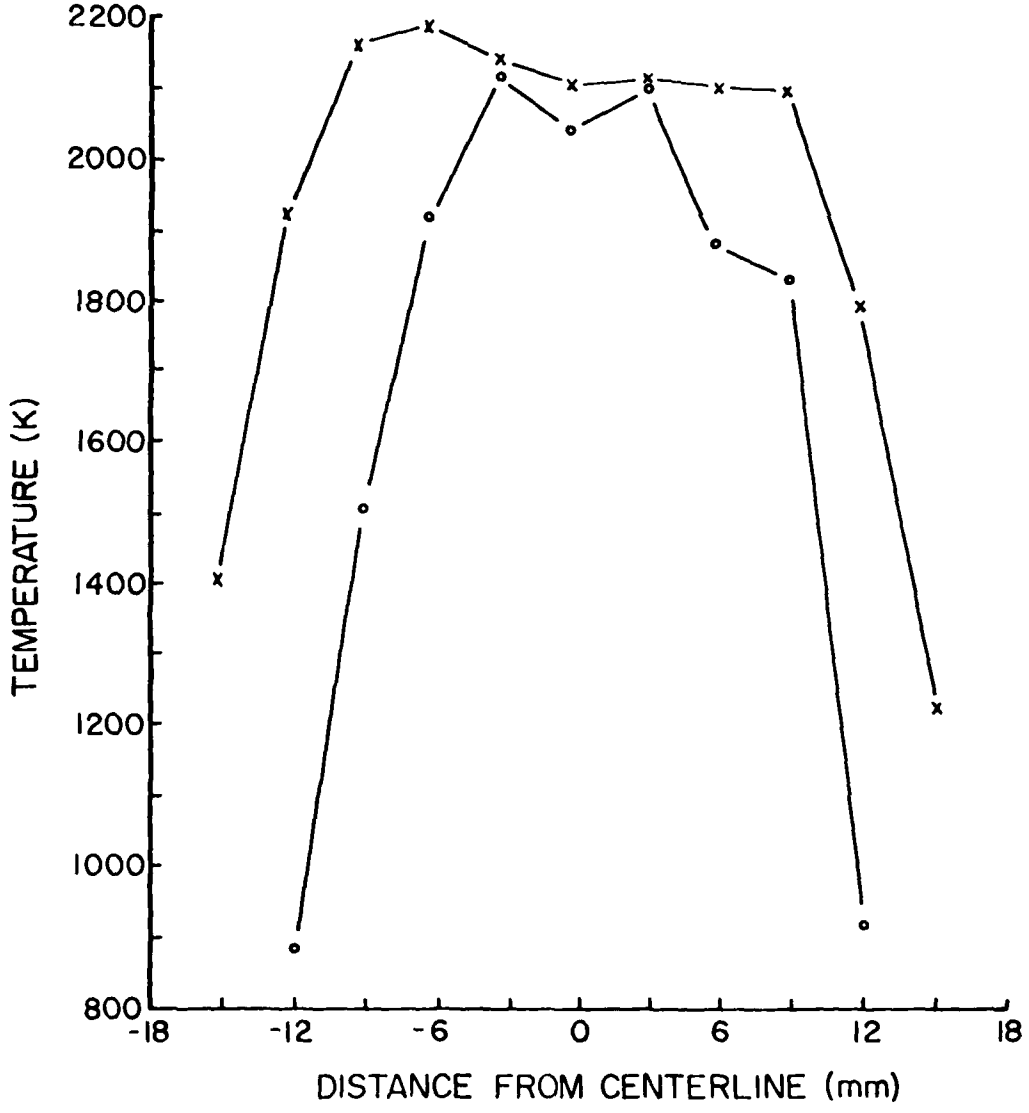

Figure 31. Temperature Profiles Obtained on a Propane-Fueled Flame. x——x Y = 16 mm; o——o Y = 55 mm.

Table 4

RATIOING ARRANGEMENT AND STANDARD DEVIATIONS OF RATIOS OBTAINED WITH THE RUBY CARS SYSTEM

Ratio Technique	Standard Deviation of Ratio
OMA/OMA	11%
OMA/Photomultiplier	16%
OMA/PIN-Diode*	14%
OMA/(PIN-Diode)^2	13%
OMA/(PIN-Diode)^3	12%
Photomultiplier/Photomultiplier	10%
Photomultiplier/PIN-Diode	18%
Photomultiplier/(PIN-Diode)^2	17%
Photomultiplier/(PIN-Diode)^3	17%

*The PIN-Diode monitored the pump beam during the experiment.

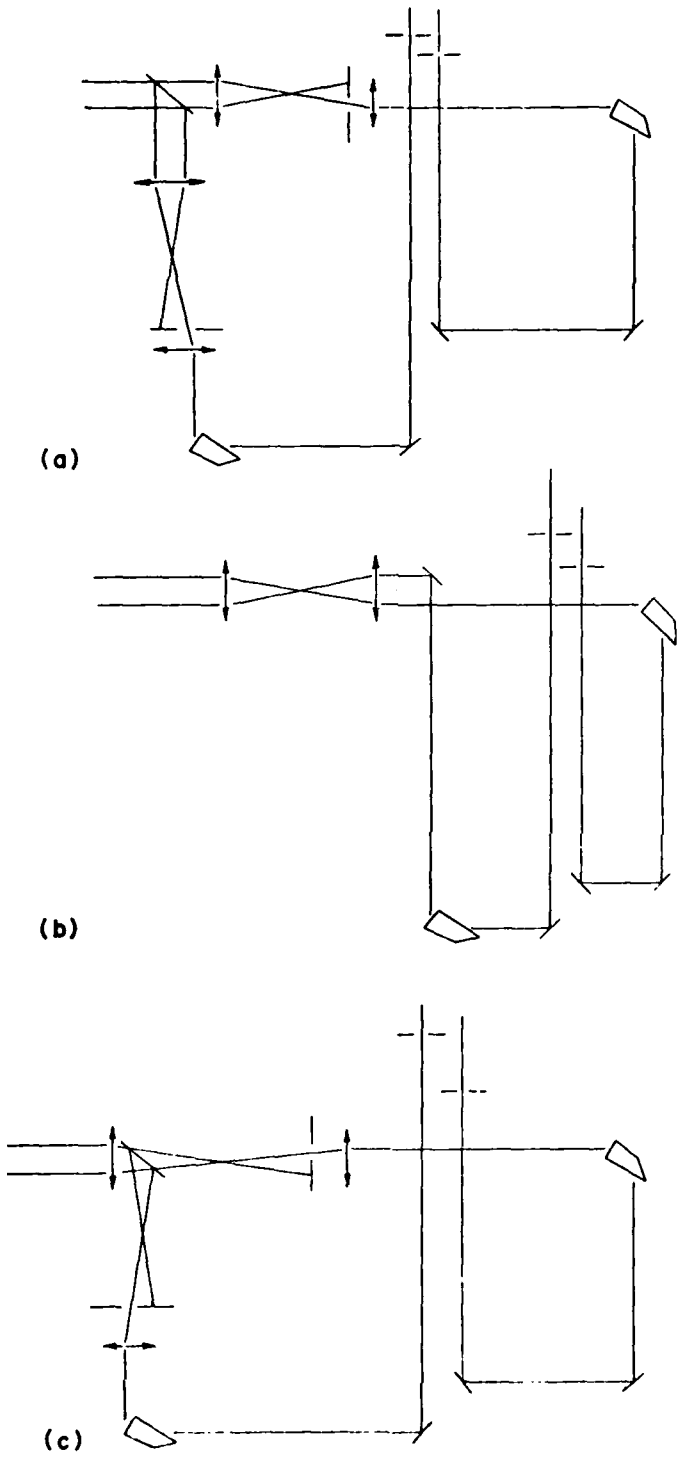

Figure 32. Various Referencing Arrangements Tested.

scheme typically showed intensity fluctuations of 40 - 60% in each leg. Ratioing improved the variations only slightly. The slight improvement in the signal upon ratioing indicated that while the signals were correlated, the degree of correlation was small. The small degree of correlation is believed to be caused by the inequality of the sample and reference paths. This was expected to be true especially in a BOXCARS arrangement, primarily due to the smaller overlap of the beams. This overlap resulted in a smaller region for CARS production in which small path differences could overlap different regions of each beam.

The basic difference between the Nd:YAG and the ruby laser systems which were employed for these studies was the transverse and longitudinal modes of the lasers. The ruby laser was operated under single transverse (TEM_{00}) and longitudinal modes (linewidth of 0.035 cm^{-1}), while the Nd:YAG had a linewidth of 0.8 cm^{-1} (~ 160 longitudinal modes) and operated in the familiar donut transverse mode typical of these unstable resonators. Figure 33 depicts the relative mode beating of the longitudinal modes of the Nd:YAG and dye laser as recorded with a 100-ps rise time photodiode. The modulation of the temporal shape of the Nd:YAG is quite extensive. The modulation shown in the dye laser is due to the off-axis pumping geometry employed with the Nd:YAG. The modulation is somewhat smoothed due to the averaging effect (finite response time) of the dye.

The CARS intensity which is governed by the Fourier transform of such waveforms as shown in Fig. 33 is given by[32]

$$I_{jk\ell} = CI_j I_k I_\ell \int d\alpha\, F(\alpha - \omega_j) \int d\beta \int d\gamma |\chi(\beta - \gamma)|^2 F(\beta - \omega_k) f(\gamma - \omega_\ell) \quad (39)$$

where $I_{jk\ell}$ is the integrated intensity of a CARS mode generated by the interaction of two pump modes with spectra $I_j F(\alpha - \omega_j)$ and $I_k F(\beta - \omega_k)$ and one Stokes mode $I_\ell f(\gamma - \omega_\ell)$.

The quadratic dependence on the pump-mode structure and linear dependence on probe-mode structure could lead to small changes in mode structure resulting in large changes in intensity. Figure 34 demonstrates the effect of temporal

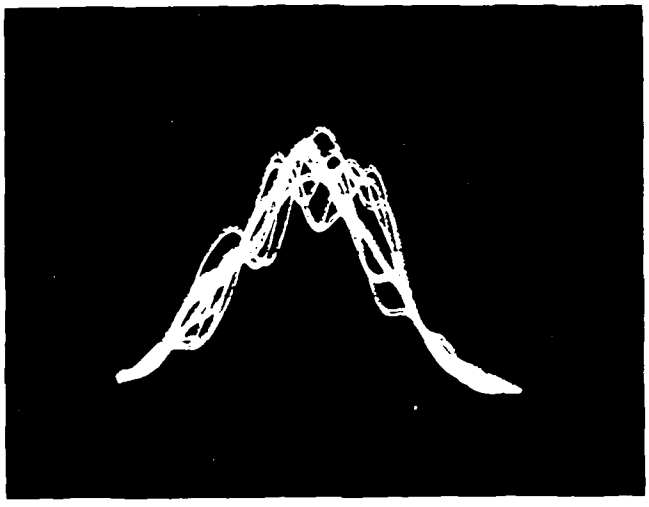

(a)

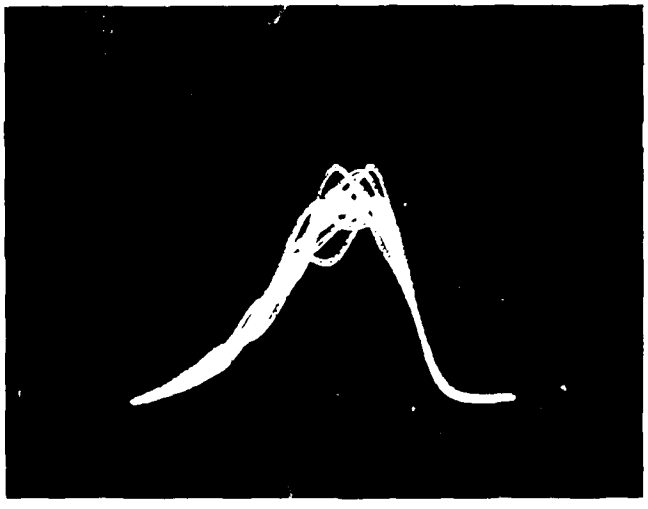

(b)

Figure 33. (a) Temporal Response of Ten Shots of the Nd:YAG Laser.
(b) Temporal Response of Ten Shots of the Dye Laser.

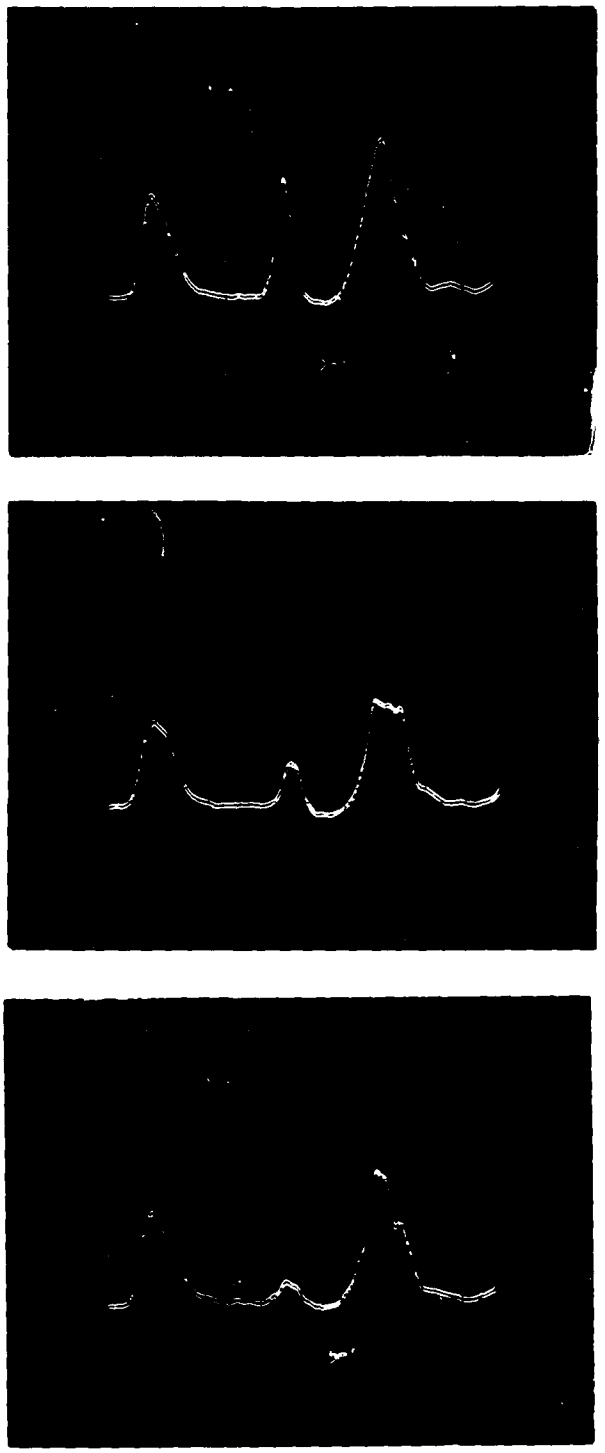

Figure 34. Temporal Responses of the Dye (Left), CARS (Center), and Nd:YAG (Right) Pulses.

shape (and thus mode structure) on the CARS intensity; it also indicates that while the overall intensities of the pump and probe lasers remained approximately the same for three shots, the CARS signal fluctuated tremendously. This was due primarily to the interaction of the pump and probe mode structure.

A comparison of BOXCARS and collinear CARS temporal responses was conducted using the arrangement depicted in Fig. 32(b). In this arrangement the two CARS signals are produced by the same lens and except for the interaction zones being different, the two paths can be considered to be identical. But as indicated by Fig. 35, the variation in the temporal responses of the BOXCARS and collinear CARS indicates that even though the same lens was used to produce both signals, the difference in interaction zones was enough to cause a large variation in temporal response and signal levels. This further indicates that the sample and reference paths should be constructed in a manner to obtain minimum path difference.

With this in mind, the setup in Fig. 32(c) was devised as a viable arrangement. The BOXCARS signals produced by this arrangement were formed by the same lens, dispersed by the same monochromator, and detected by matching photomultipliers. Typical results achieved using this arrangement indicated variations in both legs on the order of 50 - 70%, but with a reduction in the overall modulation by ratioing of at least a factor of 3. While this is a significant reduction in the variation, it still represented a large uncertainty in a concentration measurement. The paths still were not exact enough for operation of a laser with multi-model structure. One possibility for further reducing this variation was operating the Nd:YAG in a single mode, which had been used with good results in the ruby system.

An Electronic Line-Narrowing (ELN) device was used for operating the Nd:YAG in single mode. This device acts to force the electro-optical Q-switch to behave as a lossy Q-switch, which allows build-up of the laser pulse to occur over a long period of time. This slow build-up allows the intracavity etalon to be more efficient in discriminating against unwanted modes.[12] With the ELN, deviations of the CARS signal of ~ 7% were obtained when ratioing resonant N_2 and utilizing the configuration of Fig. 32(c). This experimental technique reduced to less than ~ 5% the uncertainties of concentration measurements due to laser-power and mode-structure fluctuations.

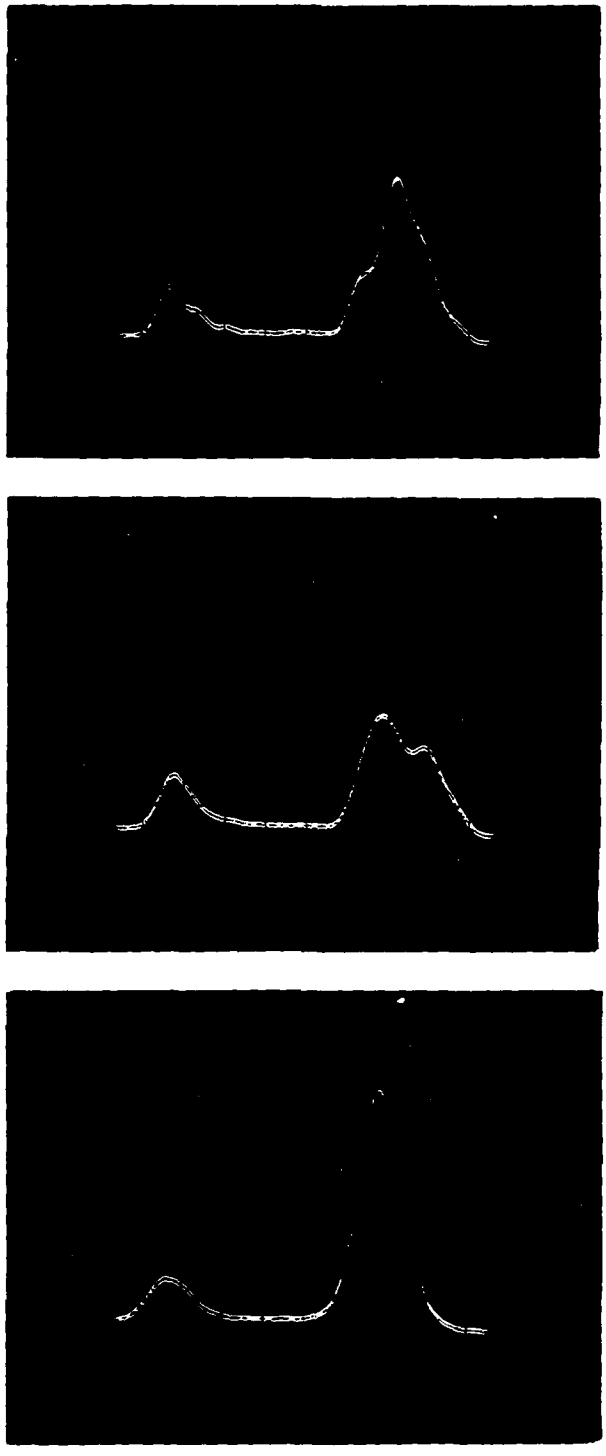

Figure 35. Comparisons of the Temporal Responses of BOXCARS (Left) and Collinear CARS (Right).

3.8 SIMULTANEOUS MEASUREMENTS

In the past, concentration measurements have been made by first determining the temperature at a given location either by scanning or by a single shot and then determining the concentration by integration using a photomultiplier.[33] The net effect has been that temperature and concentration determinations were made at different times. The magnitude of the error in the concentration measurement due to the variation of the temperature can be assessed by the following: The mole fraction on nitrogen (χ_{N_2}), as determined by a CARS measurement, is given by

$$\chi_{N_2} = 0.7808 \frac{T_2 F_{N_2}}{T_1} \left(\frac{I_2}{I_1}\right)^{1/2} \tag{40}$$

where $T_2 = T_{flame}$

I_2 = intensity at T_2

T_1 = calibration temperature

I_1 = intensity at T_1

F_{N_2} = temperature-dependent correlation factor

The term F_{N_2} is a temperature-dependent quantum-mechanical function which considers the ideal gas law, number densities, electron-spin degeneracies, and number of rotational levels.[34] F_{N_2} ranges from 1.0 at T_2 = 300 K to 2.0 at T_2 = 2100 K. Thus, for small variances in T_2

$$\left(\frac{\partial F_{N_2}}{\partial T_2}\right)_{T_1} \cong 0 \tag{41}$$

From Eq. (40) the probable error in χ_{N_2} from probable errors in T_2, T_1, I_2, and I_1 (assuming no intensity losses due to turbulence effects) is given by

$$\Delta\chi_{N_2} = \left[\left(\frac{\partial\chi_{N_2}}{\partial T_2}\right)^2_{T_1,I_2,I_1} \Delta T_2^2 + \left(\frac{\partial\chi_{N_2}}{\partial T_1}\right)^2_{T_2,I_2,I_1} T_1^2 + \left(\frac{\partial\chi_{N_2}}{\partial I_2}\right)^2_{T_1,T_2,I_1} \Delta I_2^2 + \left(\frac{\partial\chi_{N_2}}{\partial I_1}\right)^2_{T_1,T_2,I_2} \Delta I_1^2\right]^{1/2} \tag{42}$$

Combining Eqs. (40) and (42), performing the differentiation, and simplifying yields

$$E\chi_{N_2} = \left[E_{T_1}^2 + E_{T_2}^2 + 1/4\ E_{I_2}^2 + 1/4\ E_{I_1}^2\right]^{1/2} \tag{43}$$

where E is the relative error of the specific parameter.

From this relationship, it can be seen that the major contributors to $E\chi_{N_2}$ are E_{T_1} and E_{T_2}. Thus, the associated error in the temperature determination due to instrumental factors as well as measurement uncertainties has a tremendous effect upon the precision of the concentration measurement. Simultaneous determination of temperature and number density assures that the relative error introduced due to turbulence during time-averaged measurements will not enter into the concentration measurement. Simultaneous measurements are possible because the general shape of the Q-branch profile can be used to determine the temperature, while the integrated area of the Q-branch can be used to determine the concentration.

In order to make simultaneous measurements, the sample and reference signals which are produced must be simultaneously recorded by either a photomultiplier-OMA combination or by a TN1710-DARSS detector. The DARSS detector was primarily used for these measurements due to the simple detection and electronics scheme it offers.

The major problem encountered with the DARSS unit was the single dimensionality of the reticon detector. Previously the simultaneous recording of a sample and reference signal required that each signal be placed on a separate half of a two-dimensional detector such as the PAR 1205 OMA. However, in the case of the DARSS, a different arrangement (shown in Fig. 36) had to be employed. The two beams to be input into the spectrometer were crossed slightly more than one focal length in front of the collection lens. This allowed the two signals to run parallel and also focus at the required position on the entrance slits. The slits were then rotated 90° from their customary vertical position into a horizontal position so that the signals could be placed side by side and simultaneously recorded by the linear reticon detector. A typical display taken during the simultaneous measurements is shown in Fig. 37. Data were gathered and stored in the Spectral Data Memory (SDM) of the DARSS unit. Once filled, the SDM was dumped onto a floppy disk and accumulation continued. All data were taken under ELN operation. The timing diagram for this mode of operation is discussed in Section 3.1.

Simultaneous measurements of temperature and concentration were obtained on a premixed propane fueled flame, and the results are shown in Figs. 38 and 39. N_2 in the air was used as the reference medium in these concentration studies. Figure 38 is a horizontal profile of the flame starting from the center position (0 mm) and moving outward. The figure indicates that toward the edge of the flame the temperature decreased while the N_2 concentration increased. The concentration at the maximum temperature 2255 K of both profiles was found to be ~ 70%, which is comparable to a calculated temperature under stoichiometric conditions for a propane-air premixed flame of 2275 K and a concentration of 71.5% N_2.

Two extremely important parameters used in combustion research are fuel-to-air ratio and combustion efficiency.[35] Fuel-to-air ratios are typically determined by gas-sampling measurements of CO_2, CO, NO_2, and the total hydrocarbon concentration (THC), subject to the procedures set forth in Aerospace Recommended Practice 1256.[36] Combustion efficiencies can be determined in a number of ways. In ramjet combustor development, combustion efficiencies are calculated from thrust or temperature measurements. For

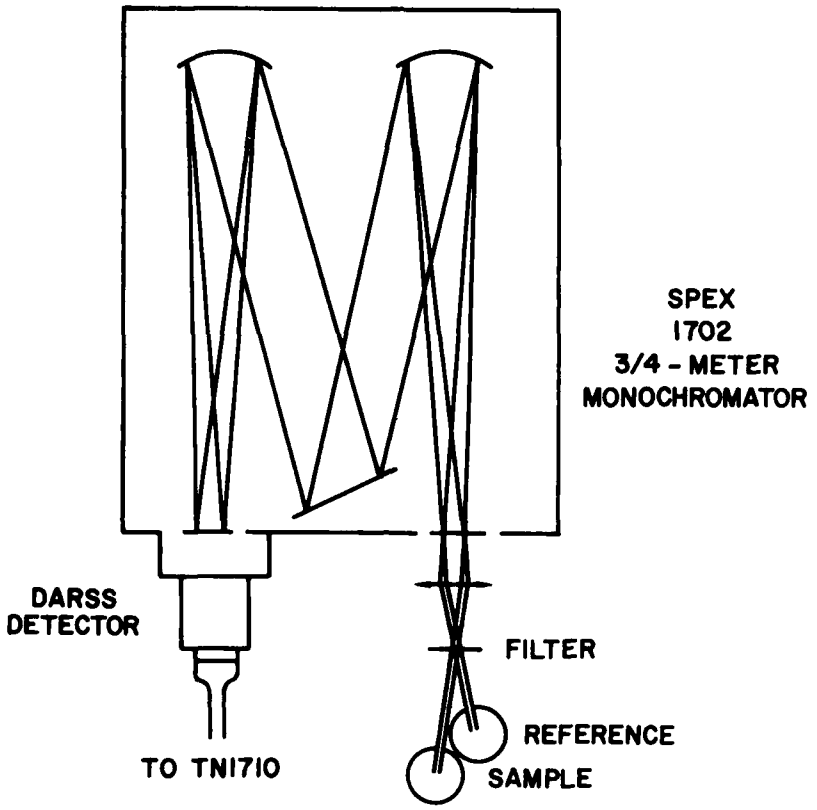

Figure 36. Optical Arrangement for Simultaneous Recording of a Sample and Reference Signal.

Figure 37 Simultaneous Measurement of Sample and Reference Signals by the Tracor-Northern DARSS.

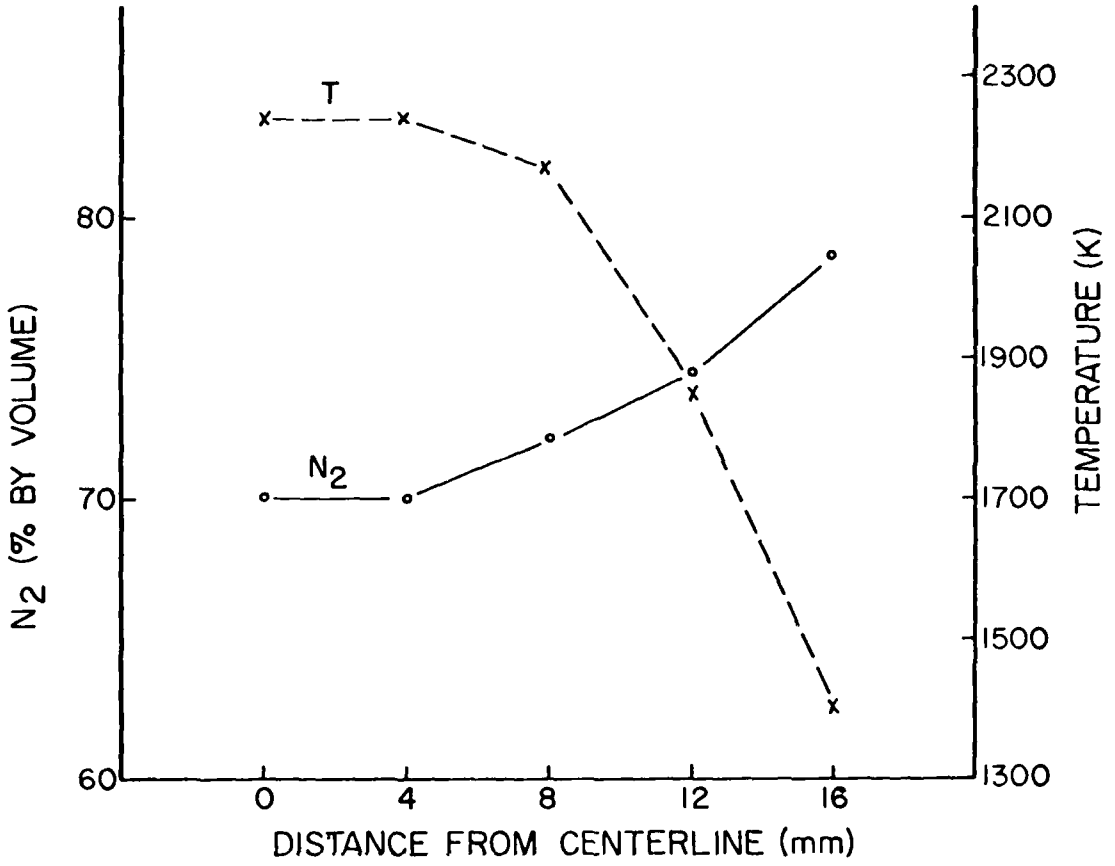

Figure 38. Horizontal Profiles of the Propane-Fueled Flame from the Centerline (0 mm) of the Flame.

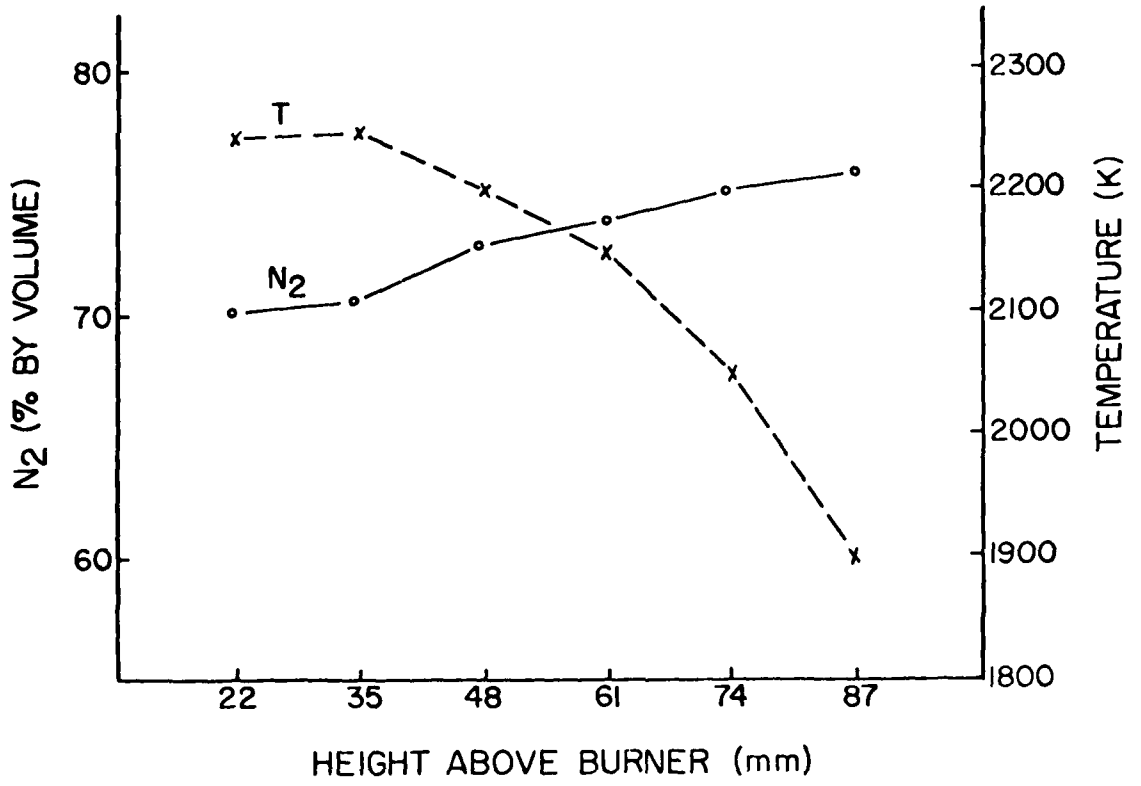

Figure 39. Vertical Profiles of the Propane-Fueled Flame.

gas-turbine development, combustion efficiencies normally are determined from emission measurements of CO, H_2, and THC.[37]

The CARS technique is capable of making N_2 and O_2 concentration measurements along with temperature determinations in combusting environments. Assuming that the THC levels are very low, the following equations have been derived for the determination of fuel-to-air ratios and combustion efficiencies:[36]

$$FA = \frac{0.79\ M_f}{(1 + 1/2\ \alpha)M_a} \left(\frac{1 - \chi_{O_2} - \chi_{N_2}}{\chi_{N_2}} \right) \tag{44}$$

where α = hydrogen-atom-to-carbon-atom ratios in the fuel

M_f = molecular weight of fuel = $12 + \alpha$

M_a = molecular weight of air = 28.9

FA = fuel-to-air ratio

χ_{O_2} = mole fraction of O_2

χ_{N_2} = mole fraction of N_2

The combustion efficiency is given by

$$\eta = \frac{T_{flame} - T_{inlet}}{\Delta T_{comb,\ ideal}} \tag{45}$$

where $\Delta T_{comb,\ ideal}$ = ideal gas temperature calculated from the fuel-to-air ratio

T_{flame} = measured local flame temperature

T_{inlet} = temperature of the inlet gases.

As indicated, the above equations dictate that N_2 and O_2 measurements and flame-temperature determinations be made simultaneously at a given location. However, in the case of a premixed flame in which the concentration of O_2 is extremely low due to combustion, only the N_2 concentration and temperature must be known in order to determine the fuel-to-air ratios. A study was conducted using the premixed burner whose profiles were reported above. The propane fuel flow was varied and the simultaneous temperatures and concentrations determined by the simultaneous CARS technique. The results of this study are shown in Fig. 40. As indicated, the temperature initially is low, maximizes, and then gradually decreases. The nitrogen concentration, however, shows a steady decline as the fuel is increased. Given the temperature and concentration, the fuel-to-air ratios can be determined from Eq. (44). A direct comparison of the calculated fuel-to-air ratios could not be made with the existing flow meters since they were calibrated only for acetylene flow and not propane. However, an indirect comparison can be made with calculated results from the modified version of the NASA ODE program[38] for calculating ideal flame temperatures, fuel-to-air ratios, equivalence ratios, average molecular weights of the combustion products, and equilibrium concentrations of CO_2, CO, H_2O, H_2, O_2 and N_2 for constant pressure combustion for a specific fuel. The experimental data presented in Fig. 40 were used to calculate the fuel-to-air ratio, which then was used in the ODE program to calculate the ideal flame temperature and nitrogen concentration. The results of this comparison are listed in Table 5. The results agree quite well with the calculated results, which indicates that this is a viable method of determining the fuel-to-air ratios.

3.9 BACKGROUND-SUPPRESSION MEASUREMENTS IN PREMIXED PROPANE FLAME

The major limitation to the sensitivity of the CARS technique is the interference effects between the resonant and nonresonant contributions to the third-order susceptibility. Several methods have been proposed for reduction of this background.[39-42] Most are experimentally complex because of the need for three lasers or the need for excellent polarization characteristics; and, in some cases, only one-order-of-magnitude rejection of the background is produced. Of the present techniques proposed, polarization cancellation is considered to be the best method for background suppression because of its relative ease of application and complete rejection of the background. The

AD-A103 932 SYSTEMS RESEARCH LABS INC DAYTON OH RESEARCH APPLICA--ETC F/G 21/2
APPLICATION OF COHERENT ANTI-STOKES RAMAN SCATTERING TO COMBUST--ETC(U)
FEB 81 L P GOSS, G L SWITZER F33615-77-C-2019
UNCLASSIFIED SRL-6948 AFWAL-TR-80-2122 NL

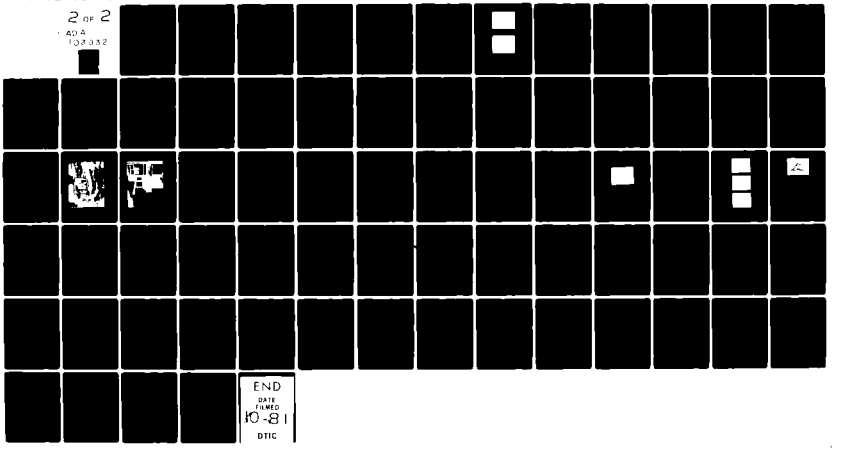

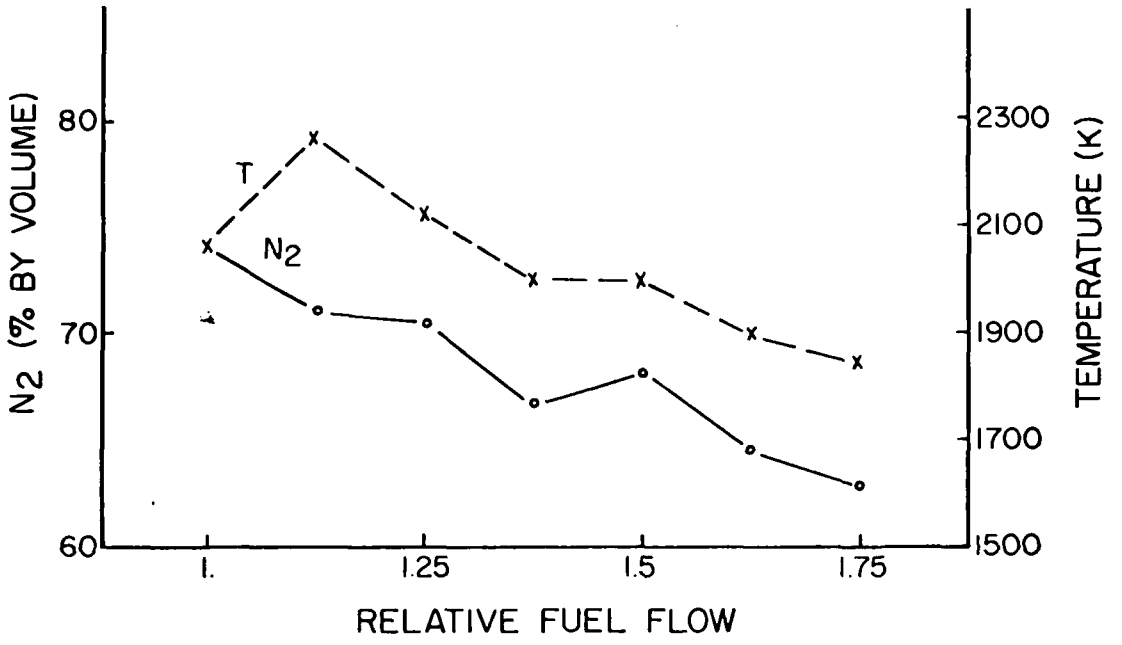

Figure 40. Plot of Variation of Nitrogen Concentration and Temperature of the Propane-Fueled Flame as a Function of Relative Fuel Flow with Constant Air.

Table 5

COMPARISON OF TEMPERATURES AND NUMBER DENSITIES OBTAINED FROM CARS MEASUREMENTS WITH THOSE PREDICTED BY IDEAL FLAME CALCULATIONS FROM THE MEASURED FUEL-TO-AIR RATIOS
(M - MEASURED, C - CALCULATED)

T_m	$(\%N_2)_m$	$(F/A)_m$	T_c	$(\%N_2)_c$
2065	74.0 $\pm$ 4.3	0.0595	2209	72.8
2300	71.0 $\pm$ 6.5	0.0701	2265.7	70.9
2122	70.5 $\pm$ 7	0.0718	2250.7	70.4
2000	66.7 $\pm$ 10	0.0858	2087.4	66.7
2000	68.3 $\pm$ 5	0.0796	2165.0	68.4
1900	64.4 $\pm$ 4	0.095	1981.2	64.3
1850	62.7 $\pm$ 9	0.1022	1901.0	62.8

basic polarization technique for a two-laser collinear CARS system was reported by Rahn, et al.[43] In this setup the polarization of the analyzer and that of the probe beams was ~ 60° with respect to the pump, as shown in Fig. 41(a). This arrangement allowed for complete cancellation of the background with a maximum of resonant signal production.

In BOXCARS, some flexibility is afforded by the availability of two spatially distinct laser beams at ω_1, which can have different polarizations. Figure 41(b) shows the polarization scheme for BOXCARS. In this instance the analyzer angle β is given by

$$\beta = \tan^{-1}\left(\frac{3\cos\theta\cos\phi + \sin\phi\sin\theta}{\cos\theta\sin\phi + \sin\theta\cos\phi}\right) \tag{46}$$

where the CARS intensity is proportional to

$$I \propto \left|4\cos\theta\cos\phi\cos\beta + 2\sin\theta\sin\phi\cos\beta - 2\sin\theta\cos\phi\sin\beta\right|^2 \tag{47}$$

Computer solutions of Eqs. (46) and (47) as a function of θ for the maximum intensity are given in Table 6 and plotted in Fig. 42. As indicated, a minimum loss of 16 is observed with background suppression as compared to that of the parallel-polarization arrangement for all beams which is normally used.

It was assumed that since the fuel mixture employed by the burner was premixed, the concentration of oxygen inside the flame was very low. In an effort to examine oxygen, rhodamine 610 was incorporated and the concentration tuned to the correct region. Inside the propane-fueled flame, only a nonresonant background could be seen; but as the burner was translated to the edge of the flame, the interference of resonant oxygen and nonresonant background was encountered. Figure 43(a) shows the spectrum obtained on the outer edge of the flame. In order to clean up the spectrum and to permit temperature determination, background cancellation employing the technique of Rahn, et al.,[43] was utilized. The results are shown in Fig. 43(b). A temperature of 1500 K was fit to this spectrum. While no attempt was made to obtain the

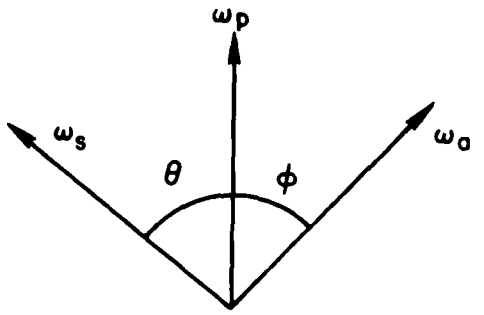

(a)

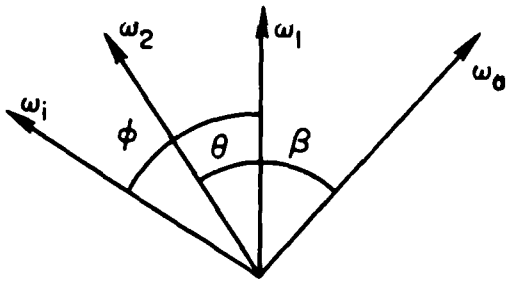

(b)

Figure 41. Polarization Angles for Background Cancellation in (a) Collinear CARS and (b) BOXCARS.

Table 6

COMPUTER DETERMINATIONS OF BOXCARS INTENSITY
AND ANGLES OF POLARIZATION FOR
BACKGROUND SUPPRESSION

θ	ϕ	β	I
0	0.0	0.0	16.00*
0	60.0	60.0	1.00
5	62.5	57.5	1.00
10	65.0	55.0	1.00
15	70.0	51.0	0.995
20	70.0	52.0	0.999
25	75.0	48.5	0.999
30	77.5	47.5	0.999
35	80.0	47.6	0.998
40	85.0	45.7	0.999
45	90.0	45.0	1.00
50	95.0	46.05	0.999
55	105.0	45.32	0.993
60	115.0	60.0	0.992
65	105.0	72.39	0.713
70	100.0	76.91	0.467
75	100.0	83.9	0.267
80	95.0	84.67	0.124
85	90.0	85.0	0.03
90	--	--	0.00

*Parallel polarization employed in normal CARS.

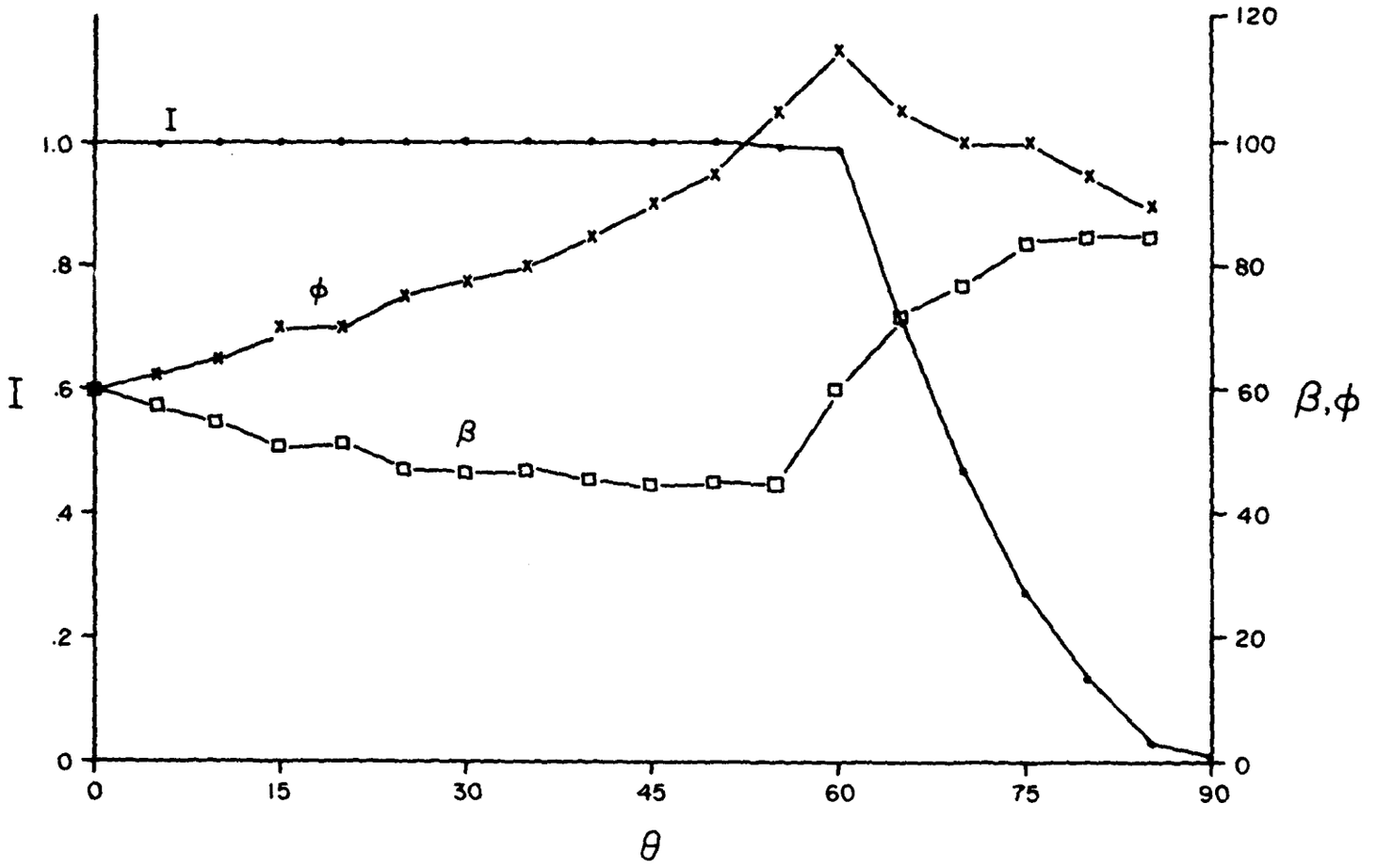

Figure 42. Computer Calculations for the Maximum Intensity, I, for a Given θ as a Function of β and ϕ.

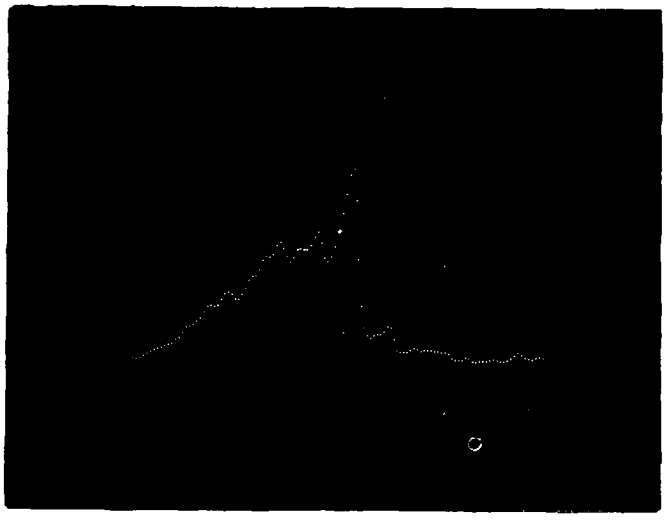

(a)

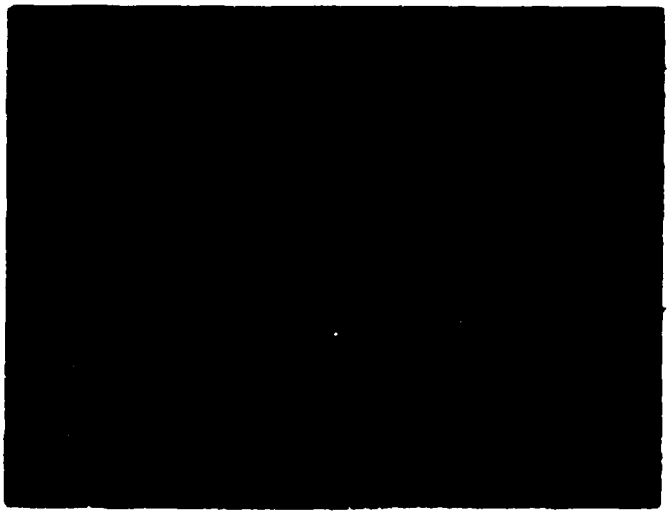

(b)

Figure 43. Oxygen with (a) Nonresonant Background and (b) Background Suppression.

concentration profile, future emphasis should be placed upon mapping the flame in the lower-concentration regions in order to acquire the lower limit of single-shot detectivity.

3.10 TURBULENCE EFFECTS ON CARS INTENSITIES AND A SCHEME FOR THEIR COMPENSATION

The CARS intensity depends upon tight focusing of the pump and Stokes beams at the same point in the medium under investigation. The effect of turbulence upon the propagation of these beams is to cause the focal volume to increase with a corresponding decrease in the CARS signal.[44] Density fluctuations of the measured species concentration in a turbulent medium also cause variation in the CARS intensity due to the dependence of the CARS signal upon the square of the number density. The latter variation, which is the desired parameter of the measurement, may be adversely affected by the effects of turbulence upon the beams. Since combustion media are highly turbulent, it is important that the effects of turbulence upon the operation of the CARS signal be critically evaluated if accurate number densities are to be measured.

The generation of CARS occurs in a gaseous medium when two intense collinear electromagnetic waves interact with a molecular species. The higher-frequency wave, $E_p(\omega_p)$, which is called the pump wave and the lower-frequency wave, $E_s(\omega_s - \delta)$, generate an anti-Stokes spectrum at $2\omega_p - \omega_s + \delta$ when E_s is tuned through the Stokes spectrum of the molecular species under investigation. The anti-Stokes spectrum can also be generated by employing a broadband source for E_s in conjunction with the narrow-band pump wave.[4] The appropriate term in the third-order polarization which is responsible for this effect is[45]

$$P_a^{(3)}(\omega_a + \delta) = 3\chi^{(3)}(\omega_p, \omega_p, \omega_s + \delta) E_p^2 E_s(\omega_s - \delta) \qquad (48)$$

where $\chi^{(3)}$ is the corresponding third-order susceptibility, ω_s is the center frequency of the Stokes line, δ is the deviation from ω_s, and ω_a is the center frequency of the anti-Stokes line given by $2\omega_p - \omega_s$.[45] Similar third-order polarizations can be written at the pump and Stokes frequencies. However, for

weak interactions the amplitude of the pump and Stokes waves are not significantly affected by the medium. Thus, only the electromagnetic-wave equation at the anti-Stokes frequency must be considered in the analysis. This wave equation is

$$\nabla^2 E_a = \frac{1}{c^2} \frac{\partial}{\partial t^2} \left[E_a + 4\pi \left(P_a^{(1)} + P_a^{(3)} \right) \right] \tag{49}$$

where E_a is the anti-Stokes field and $P_a^{(1)}$ is the linear polarization. For plane waves, the solution of the above equation yields for the anti-Stokes intensity

$$I_a(\omega_a + \delta, Z) = \left(\frac{4\pi^2 \omega_a}{c^2} \right)^2 |3\chi^{(3)}|^2 \; I_p^2 I_s(\omega_s - \delta) \; \frac{\sin^2 (Z\Delta k/2)}{(\Delta k/2)^2} \tag{50}$$

where

$$\Delta k = \frac{2\omega_p \eta_p}{c} - \frac{\omega_s \eta_s}{c} - \frac{\omega_a \eta_a}{c}$$

and η_a and η_s are the indices of refraction. For most applications $Z\Delta k/2$ is small; thus, Eq. (50) reduces to

$$I_a(\omega_a + \delta, Z) = \left(\frac{4\pi^2 \omega_a}{c^2} \right)^2 |3\chi^{(3)}|^2 \; Z^2 I_p^2 I_s(\omega_s - \delta) \tag{51}$$

To obtain spatial resolution, focused beams are used and most of the CARS intensity is generated near the focal volume. For this case, the solution for E_a may be placed in the integral form[46]

$$E_a(\vec{r}, t) = 1/c \int \frac{P_a^{(3)}(\vec{r}', t') \, d^3\vec{r}'}{|\vec{r} - \vec{r}'|} \tag{52}$$

where $t' = t - |\vec{r} - \vec{r}'|/c$. As can be seen from Eq. (48), the evaluation of this integral requires an explicit expression for the focused pump and Stokes waves. Although approximate analytical expressions for E_p and E_a are available,[47] it is not possible to carry out the integration to yield a closed

form. An easier approach to the problem utilizes the plane-wave solution for $I_a(\omega_a + \delta)$ at the focal volume and simple diffraction theory to estimate the diameter of the focal spot.[48] This approach yields the approximate solution

$$P_a(\omega_a + \delta) = \left(\frac{4\pi\omega_a\omega_p}{c^3}\right)^2 |3\chi^{(3)}|^2 P_p^2 P_s (\omega_s - \delta) \tag{53}$$

where P_a and P_s are the corresponding spectral power densities and P_p is the power of the monochromatic pump.

In this study, number-density measurements are made by using a Nd:YAG laser and a broadband Stokes wave from a broadband dye laser which permits the simultaneous generation of the entire Q-branch of the molecular species under investigation. The duration of these waves is approximately 10 nsec, and a photomultiplier is used to integrate the total anti-Stokes power in the Q-branch for each pulse. The energy in a pulse may be expressed as[45]

$$P_a]_{int} = \frac{KN^2F(T)\ P_p^2\ P_s}{\Gamma_{eff}\ (p,T)} \tag{54}$$

if the contributions due to nonresonant species are negligible and $P_s(\omega_s + \delta)$ is constant over the Q-branch. In Eq. (54), N is the number density, p is the total pressure, K is a constant, Γ_{eff} is an effective linewidth and F(T) is a function of the thermal distribution of the molecules of the medium.

A complete analysis of the effect of turbulence on the generation of CARS requires a solution of Eq. (52), which is a very difficult task. However, in a turbulent medium the focal spot increases in size and is also displaced from the nonturbulent position in a statistical way from pulse to pulse. The change in the spot size should have the greatest effect on the CARS signal since this reduces the intensities in the focal volume. For this case, the plane-wave solution yields

$$P_{at} = A_t I_a = \left(\frac{4\pi^2\omega_a}{c^2}\right)^2 |3\chi^{(3)}|^2 z^2 \left(\frac{P_p}{A_t}\right)^2 P_J (\omega_s - \delta) \tag{55}$$

where A_e is the effective area of the focal spot and Z_e is the corresponding distance over which the major portion of the CARS signal is generated. From geometrical considerations, it is reasonable to postulate that the value of Z_e increases with A_e such that

$$Z_e^2 = kA_e \tag{55}$$

where k is a constant. Thus, the ratio of the anti-Stokes energy for a nonturbulent medium to that for a corresponding turbulent medium can be estimated from Eqs. (55) and (56). This gives

$$\frac{P_a}{P_{at}} = \frac{P_a]_{int}}{P_{at}]_{int}} = \frac{A_{et}}{A_e} = \left[\frac{D_{et}}{D_e}\right]^2 \tag{57}$$

where the subscript t is used for parameters corresponding to the turbulent medium.

Since turbulence affects beam propagation by inducing random fluctuations in the index of refraction within the medium, two gases having a large difference in their refractive indices can be mixed in a turbulent jet to produce a small turbulent field. Thus, to investigate the effects of turbulence upon beam propagation and the generation of CARS signals, the turbulent generator shown in Fig. 44 was employed. To make the turbulence field produced by the generator as uniform as possible, the nozzles of the generator were made by photographically producing an etching pattern on copper-clad epoxy plates. The copper was etched away in a pattern which formed six nozzles on each plate when the plate was sandwiched between separating plates. The nozzles were fed from the large openings in the plate which, in turn, were fed from the header. Alternating the orientations of the plates allowed for feeding even- and odd-numbered nozzle rows with two different gases to generate a turbulent mixing medium.

The CARS experimental setup for studying the turbulence effects shown in Fig. 45(a) was the same as that employed for the simultaneous temperature-species concentration measurements discussed in Section 3.8, with the

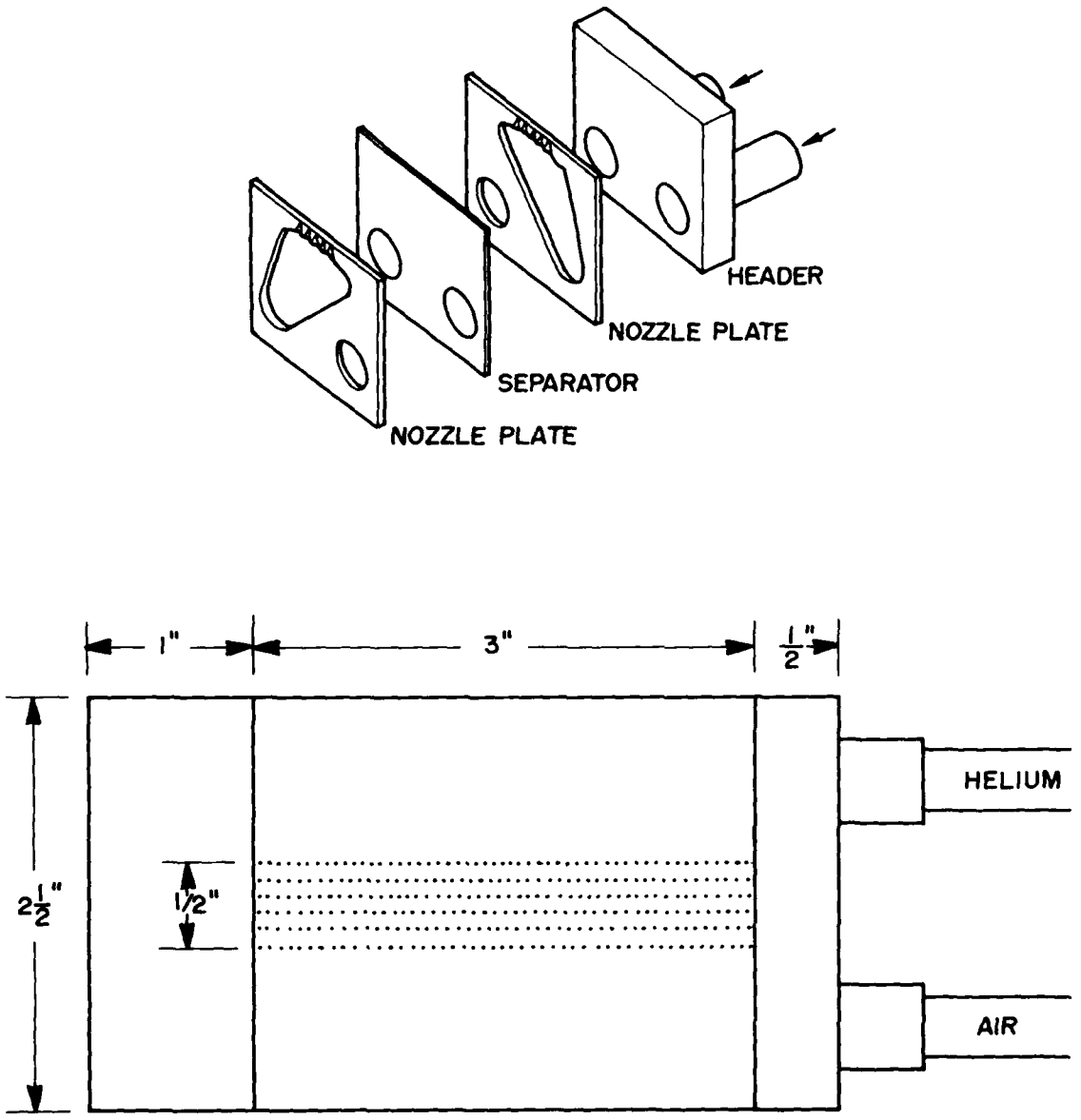

Figure 44. Diagram of Turbulent Generator Used for Experiments.

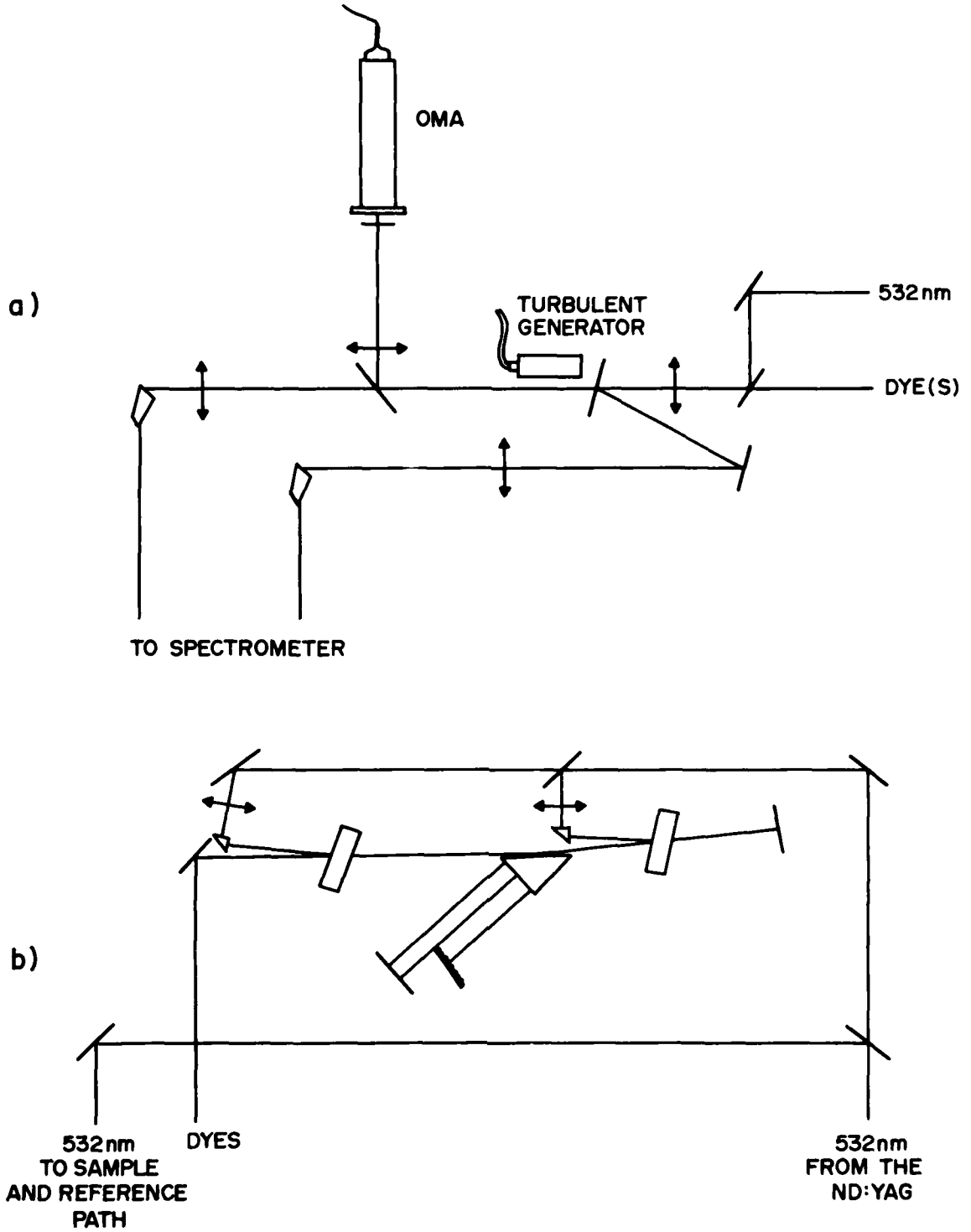

Figure 45. a) Experimental Setup of Turbulent Studies
b) Setup Employed for Broadband and Narrow-Band Dye Laser.

exception that a collinear rather than a BOXCARS arrangement was employed for the turbulence studies. The turbulent generator in these studies was placed between the focusing lens and its focus in the sample leg and kept well away from the focal region where the majority of the CARS signal is produced. This procedure ensured that any loss in the CARS signal would be due primarily to turbulence effects and not to number-density changes resulting from helium being introduced into the focal volume.

In order to study the variation in spot size after propagation through turbulence, a small portion of the pump and Stokes beams was split off from the sample path just after focus. The split beams were then coupled onto a PAR 1205 OMA detector which allowed recording of the spread of the focal spot. Figure 46 shows the effects of turbulence upon the spot size and upon the CARS intensity as recorded by the setup described above. As can be seen from Fig. 46(a), with the use of air only (and no helium flow), the focal spot is sharp and well defined; the resulting CARS signal from the sample path is strong. However, when the helium is allowed to flow (forming a refractive-index gradient), the focal spot expands drastically with a corresponding decrease in the CARS intensity in the sample leg. The effect of introducing this type of turbulence in the beam path, in this case, resulted in a factor-of-eleven reduction in intensity, with a corresponding 330% error in the concentration measurement.

Figure 47 shows the results of a detailed study of the variation of the CARS intensity as a function of turbulent generator position. Along with the relative CARS signal, the relative beam spread as measured by the OMA setup is also displayed. The x-axis represents the distance of the generator from the lens for a 16.5-in.-focal-length lens. As indicated by the experimental curves, the relative CARS signal decreases as the distance from the generator to the focal region of the beam increases. Inversely, the beam spread increases. A quick calculation of the natural log of the relative intensity as a function of the natural log of the inverse of the relative beam spread indicates, however, that the intensity varies not as the square of the inverse of the beam spread [see Eq. (59)] but simply as the inverse of the beam spread. Figure 48 is a plot of the experimentally obtained intensities as a function of the intensities predicted by

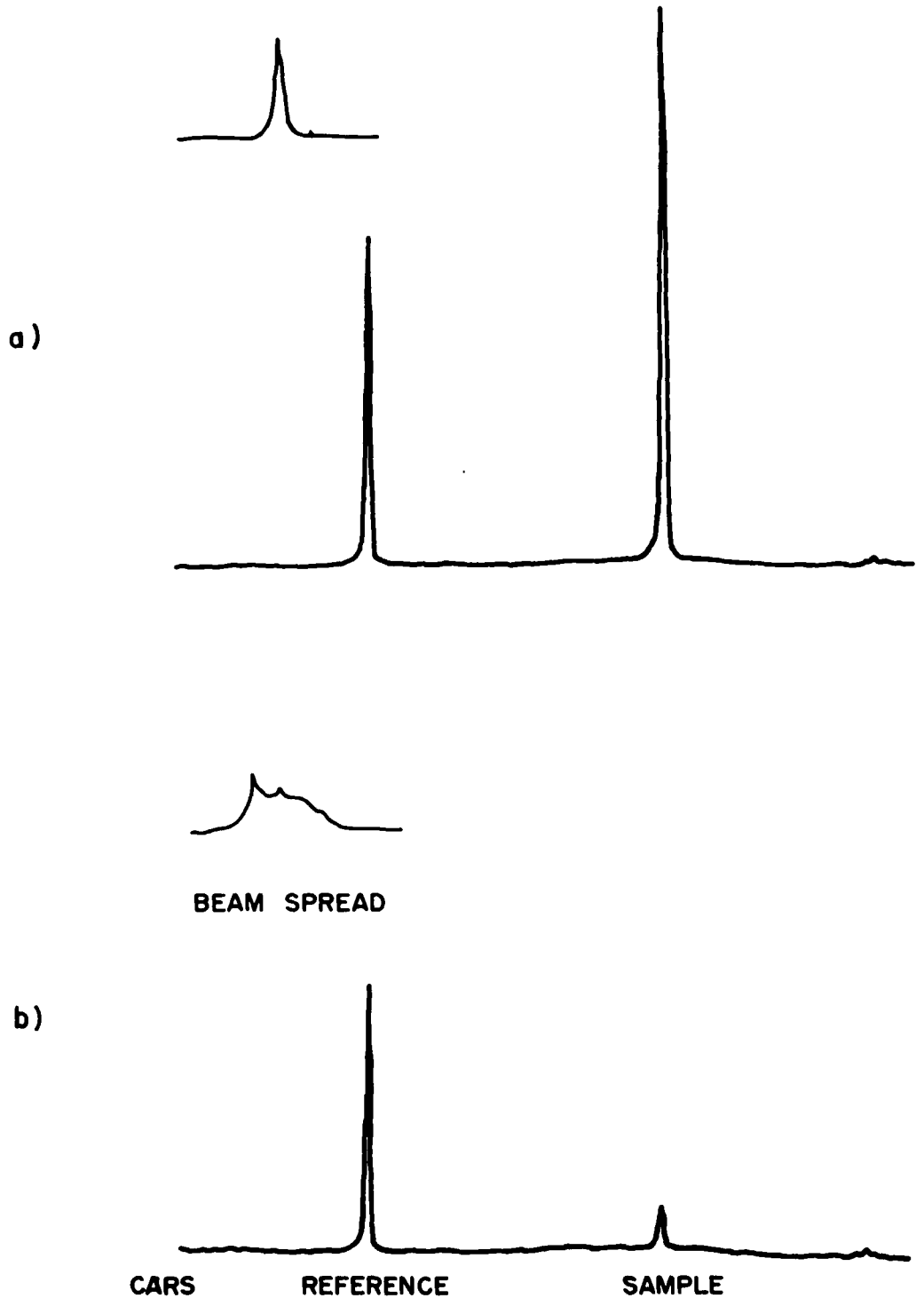

Figure 46. Beam Spread and Resulting CARS Intensity
a) Without Turbulence
b) With Turbulence.

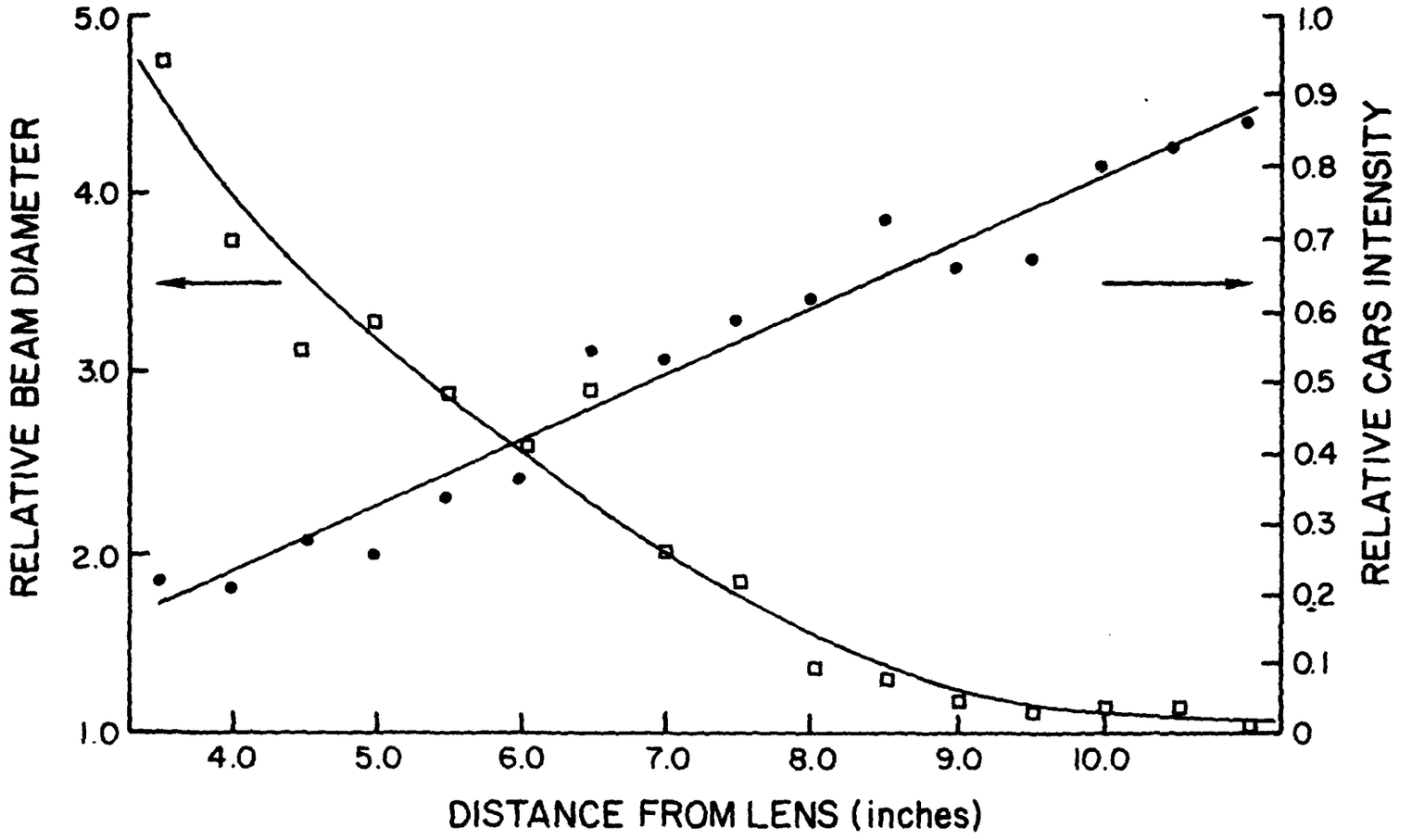

Figure 47. Variation of CARS Intensity and Beam Diameter with Horizontal Scan of Turbulent Generator.

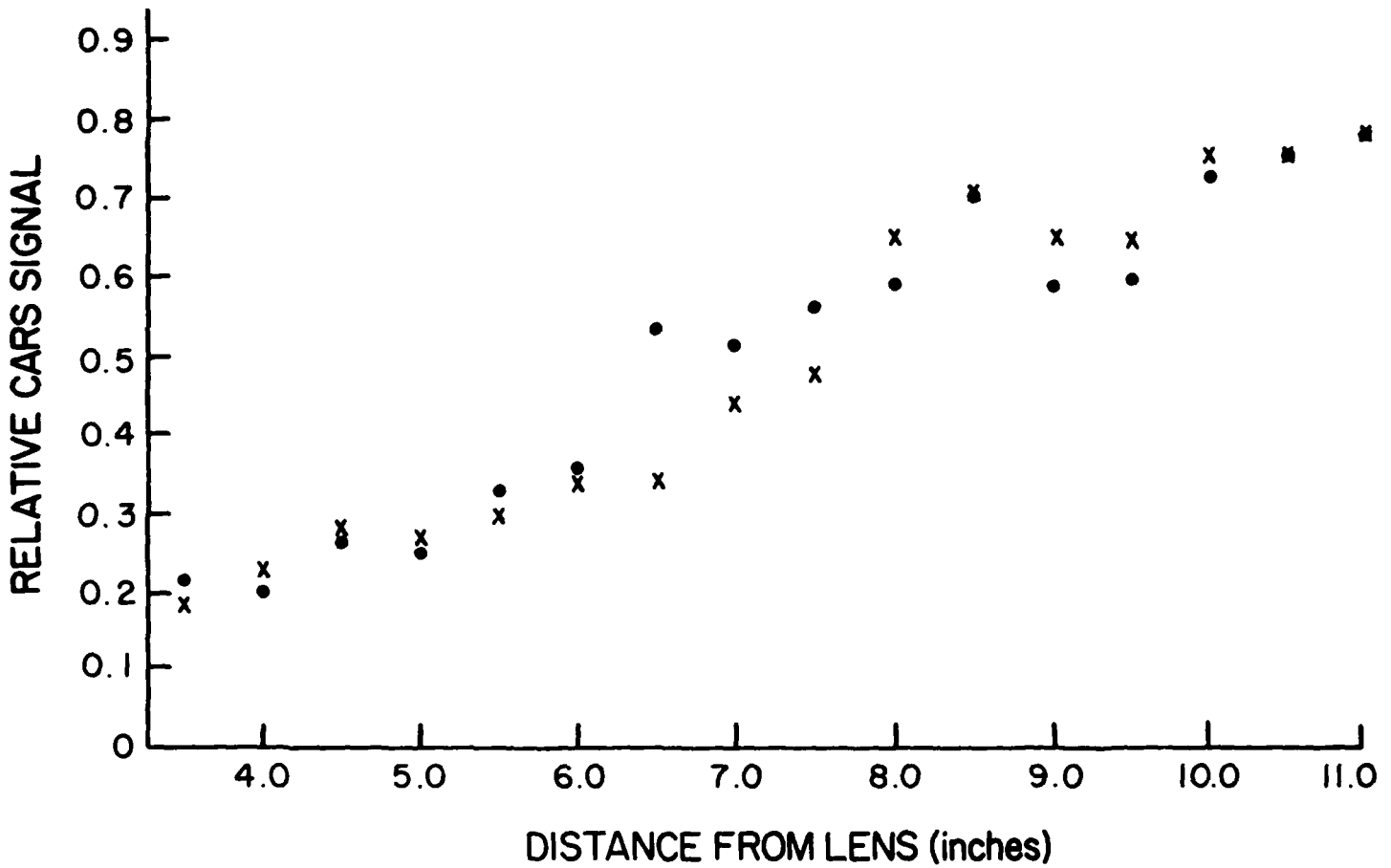

Figure 48. Correlation of the Relative CARS Signal as Experimentally Measured (·) and as Predicted (x) from the Measured Beam Diameters ($P \propto 1/D$) for a Horizontal Scan of the Turbulent Generator.

$$\frac{P_a}{P_{at}} = \frac{D_{et}}{D_e} \tag{58}$$

As can be seen, the correlation between the experimentally observed values and those predicted by Eq. (58) is quite good. An important clue concerning the reason for this result was obtained when it was noted that a 90-deg. rotation of the OMA, which resulted in the rectangular target being perpendicular to the beam propagation, gave little indication that the beam was spreading. Imaging the beam upon the laboratory wall allowed the visual assessment that the beam was spreading in only one direction. The spread, in fact, was perpendicular to the flow of the helium-air turbulence, indicating that the turbulence was not completely random in nature. This one-dimensional spreading by the turbulent field results in a linear inverse dependence of the CARS intensity upon the beam spread, as indicated.

Because of the large errors that can be introduced into the concentration measurement, it is imperative that some means of compensating for this turbulence be developed. Several such schemes have been proposed and were considered for this study. One such scheme involves taking a reference after the turbulence has been introduced in the beam, thus compensating for its effect. However, a problem with this method is that while the CARS signal is affected by the turbulence through which the beam propagates until it reaches the focus, it is unaffected by the turbulence which occurs after the focus. This, however, is not the case for the proposed reference because turbulence which occurs after the focus will affect its CARS intensity. Such a reference would tend to overcompensate for the turbulence since the reference beams would pass through twice the length of turbulence that the sample beams traversed before the respective CARS signals were produced. The reference scheme which is placed before or parallel to the sample path would not compensate for the turbulence. Therefore, it would also be, at best, a poor reference for a turbulent medium.

What was considered to be the most promising approach was a novel reference scheme proposed by Ultee and reported by Shirley[49] for background-free CARS

spectra, i.e., high major species concentrations or low concentrations with the background cancelled. This scheme involved the use of a nonresonant signal produced at the measurement location as an in situ reference. In the above-cited report, it was proposed that a two-component dye laser be employed to produce both a resonant and a nonresonant signal. The temperature could be determined from the resonant, and the nonresonant could serve as a calibration source for the concentration measurement since it is a measure of the total number of molecules present in the measurement volume. It also was noted that such a measurement approach would be immune to medium extinction and refraction effects since all beams would be similarly affected, thus making it an ideal method for turbulent compensation. The article fails to mention the fact that a power reference would still have to be employed due to the relative power fluctuations which are inevitable with such a dye-laser system.

Figure 45(b) depicts the dye-laser setup used for producing the broadband and narrow-band Stokes beams needed for the experiment. A grazing-angle prism[50] was used for beam expansion, thus allowing for one-half the beam to be incident upon a total reflector which produces the broadband Stokes output and the other half to be incident upon a 600-groove/mm 5000-Å blazed grating which accounted for the narrow nonresonant Stokes output. The output of the dye laser was then amplified and directed to the turbulent region, as shown in Fig. 45(a).

The incorporation of the additional nonresonant Stokes output results in four peaks being displayed by a Tracor-Northern 1710-DARSS multichannel analyzer.[11] The correlations without turbulent flow of the nonresonant signals in the sample and reference path and the resonant signals in the sample and reference path were better than 97%. Figure 49 shows the results obtained with this scheme with and without turbulent flow. Figure 49(b) shows the display with air flow only. The two peaks at the left of the display are from the reference path which experienced no turbulence, and the two peaks at the right are from the sample path in which the generator was located. Figure 49(a) shows the results when allowing helium to flow, thus forming a turbulent mixing region. As can be seen the peaks in the sample path are lower in

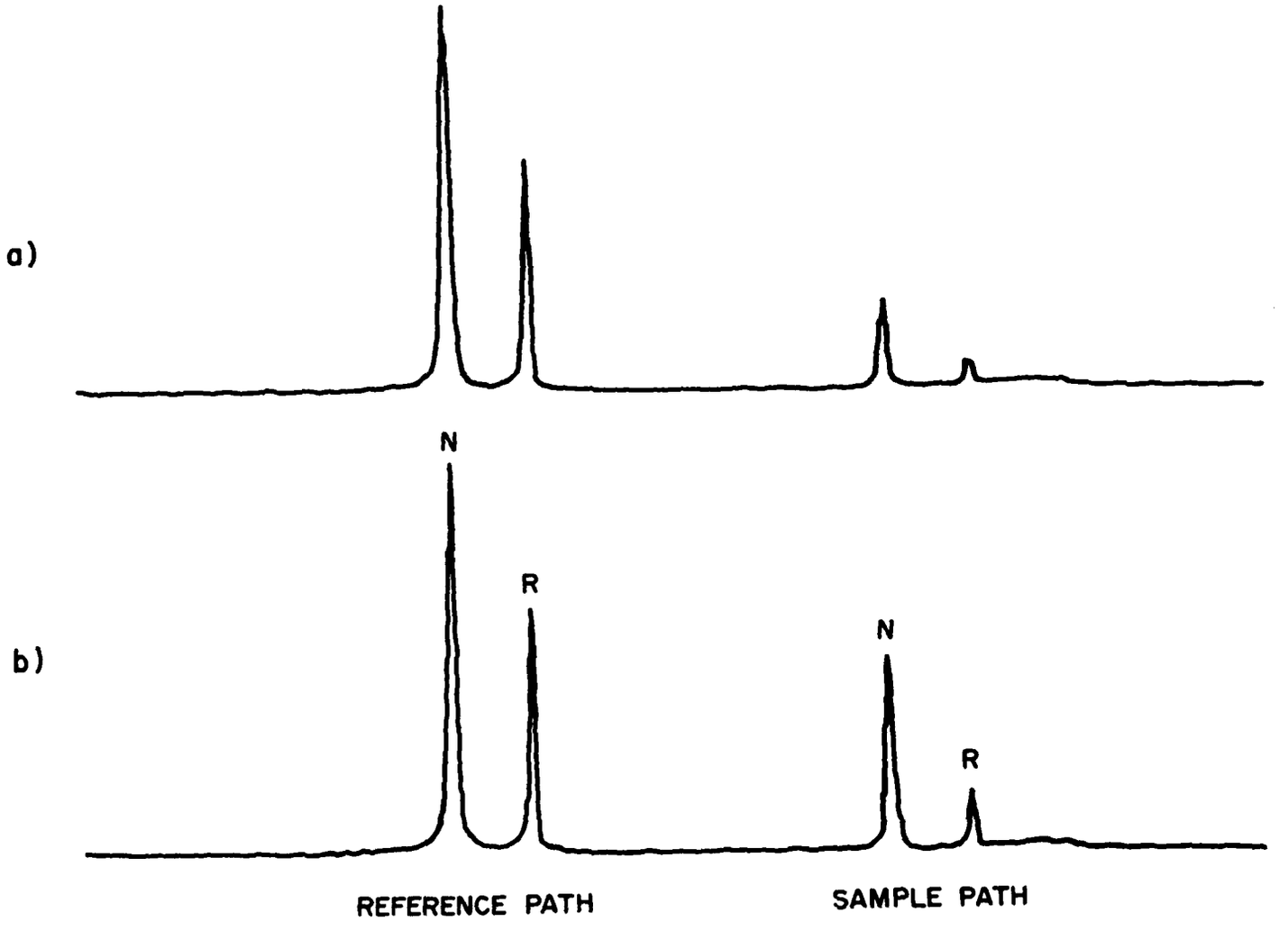

Figure 49. Display of the In Situ Reference Scheme a) With Flow and b) Without Flow. N-Nonresonant Peak, R-Resonant Peak.

intensity than those obtained without flow; however, both the nonresonant and resonant peaks decreased by the same percentage. By normalizing the resonant signal to the nonresonant *in situ* reference, one can compensate for the effect of turbulence. Tables 7 and 8 show the experimental results that were obtained with the setup described above. The variation of the relative signals increased from ~ 3% to ~ 9% when the turbulence was activated, but the ratioed results were ~ 5%, which was comparable to results obtained without turbulence. Table 8 indicates the concentrations that would have been obtained from the results listed in Table 7, with and without compensation for the turbulence. As indicated the error without compensation is quite large, while the compensated concentration is in good agreement with the nonturbulent result for ambient air. These results indicate that by using this method for turbulence compensation, accurate intensity information can be obtained without regard to the severity of the refractive-index change or beam extinction. Immediate applications for this type of method lie in concentration measurements in turbulent and particle-laden environments. This method, although demonstrated only for collinear CARS, should also be easily applicable to BOXCAR-type arrangements.

Table 7

RESULTS OF TWO SEPARATE EXPERIMENTS EMPLOYING THE IN SITU TURBULENCE COMPENSATION TECHNIQUE

No Flow*+

Resonant	Nonresonant	Ratio (R/N)
.3344	1.258	.2658
.3469	1.221	.2841
.3414	1.292	.2642
$\bar{x}$ = .3409	$\bar{x}$ = 1.257	$\bar{x}$ = .2714
σ = .0063	σ = .0355	σ = .0111
$\pm$ 1.85%	$\pm$ 2.82%	$\pm$ 4.09%

Flow

Resonant	Nonresonant	Ratio (R/N)
.2073	.7704	.2691
.2663	.9066	.2937
.2371	.8217	.2885
.2504	.8511	.2942
.2573	.9872	.2606
.2591	.9355	.2770
$\bar{x}$ = .2463	$\bar{x}$ = .8778	$\bar{x}$ = .2805
σ = .0215	σ = .0794	σ = .0139
$\pm$ 8.73%	$\pm$ 9.04%	$\pm$ 4.96%

*Values represent sum of 20 points.
+Values normalized to corresponding intensity of power reference.
$\bar{x}$ = Average value.
σ = Standard deviation.

Table 8

APPARENT N_2 CONCENTRATIONS WITH AND WITHOUT TURBULENCE COMPENSATION
(ASSUMING 78% N_2 CONCENTRATION IN AMBIENT AIR)

Without Compensation (%)	With Compensation (%)
60.82	77.69
68.94	81.18
65.05	80.46
66.85	81.24
67.76	76.47
68.00	78.82
$\bar{x}$ = 66.24	$\bar{x}$ = 79.43
σ = 2.96	σ = 1.83
$\pm$ 4.47%	$\pm$ 2.30%

Section 4

HARDENED-CARS-SYSTEM DEVELOPMENT

To extend the study of the CARS diagnostic techniques developed during this study and earlier work[4] to large-scale practical combustion environments, an environmentally hardened CARS optical system was required. The objective of this development was to produce a CARS system which could obtain temperature and major-species-concentration information while operating in the relatively uncontrolled environment of a combustor test tunnel. Following is a summary of the system design considerations and development of the CARS diagnostic capabilities.

In designing a hardened CARS system, several environmental problems were anticipated. Among these were optical problems such as nonresonant CARS generation in combustor windows, which would limit the detection of minority species, and mechanical problems connected with acoustic and seismic vibrations and thermal-gradient stresses. These problems were attacked through the system design. This design included: securely bolting all components to a common optical table; maintaining the optical axis as close to the table as possible to reduce bending moments in optics mounts; merging pump and Stokes beams as soon as possible to reduce effects of relative motion; enclosing the most sensitive components and the system as a whole in insulated housings to isolate them from the environment; and expanding the probing beams to reduce CARS generation along optical paths and in windows. The system was designed to be remotely controlled and portable, yet rugged enough to survive in the testing environment and in transport.

Preparations for the first measurement program in the AFAPL combustion tunnel[51] began with the construction of the initial system design shown in Fig. 50. Temperature measurements required spectral scanning of both sample and reference signals, but this capability was not achieved in this system because of the difficulty involved in scanning the separate sample and reference spectrometers simultaneously. Therefore, the initial system, which was used only in the laboratory, was capable of performing only CARS number-density measurements.

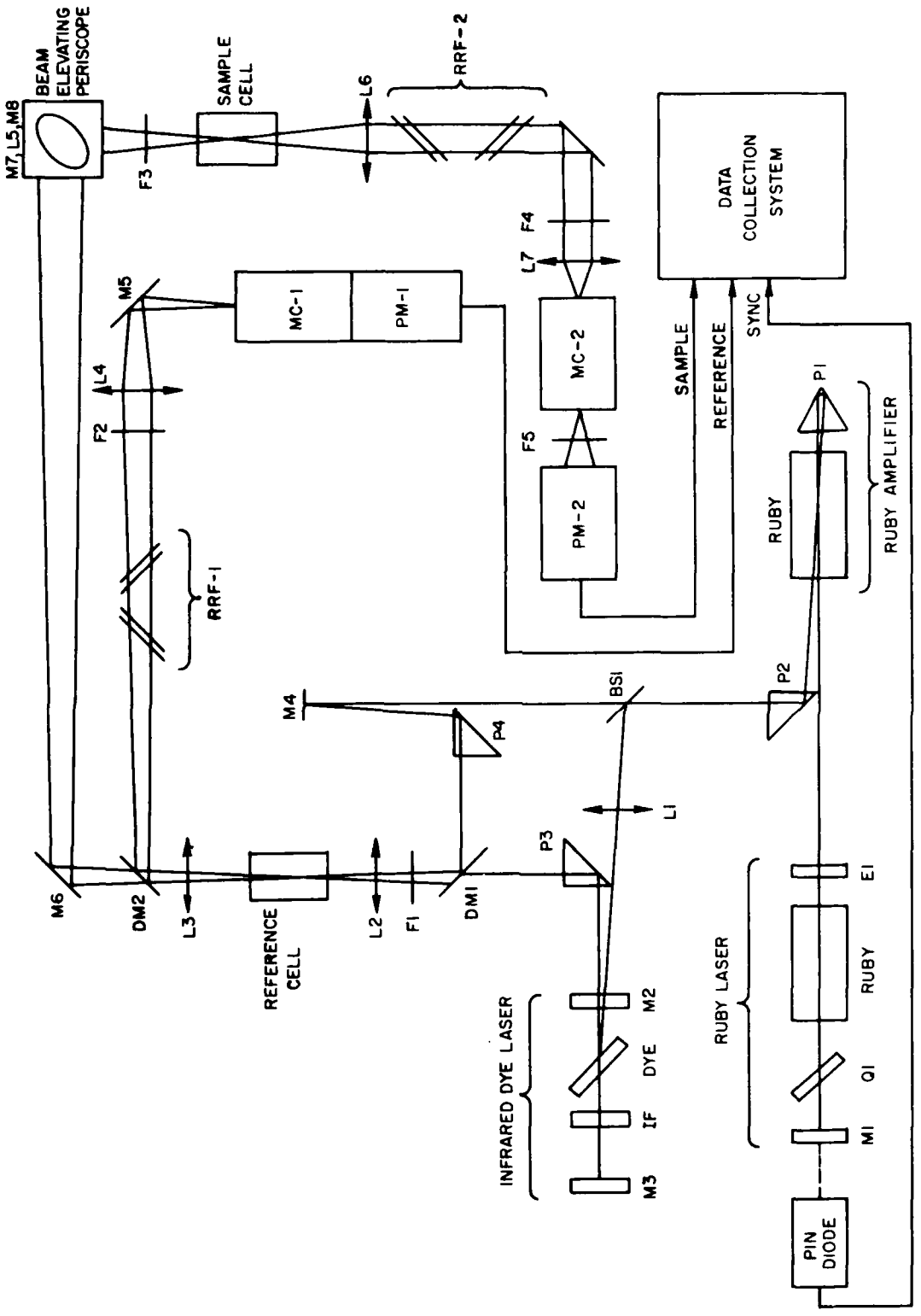

Figure 50. Initial Hardened-Optical-System Design.

Since construction of the first system went quite rapidly, there was sufficient time before beginning the tunnel experiments to modify the design to incorporate a single spectrometer to be used to analyze both sample and reference signals. This design, shown in Fig. 51, uses two photomultipliers for detection of the sample and reference signals with an optical multichannel analyzer (OMA) as an alternate sample-detection system. The two photomultipliers mounted on a common spectrometer provided a scanned temperature and single-shot concentration capability, while the OMA was used to facilitate tuning of the Stokes component of the CARS process. The primary reason for the incorporation of the OMA was to provide a means of obtaining a complete CARS spectrum in a single laser pulse, thus allowing the possibility of single-shot temperature determinations. Once this design was constructed, the system was tested in the laboratory by producing CARS signals from N_2, O_2, CO_2, CH_4, and H_2O molecules. After initial testing the system was transported to the combustor test facility to begin the first in a series of combustor tests.

The optical system for the initial test series is shown in position in the combustion facility in Fig. 52. Also shown in this figure is the optics-table support system which provides three degrees of movement about the combustion-tunnel axis. The CARS electronics control console, laser cooler, and power supplies are shown as positioned in the adjoining control room in Fig. 53. Preliminary tests in the three-month program were designed to exercise the system's capabilities in varying flame conditions to determine its ability to operate in the combustor environment. The results indicated that the CARS system suffered no apparent environmentally induced ill effects. The scope of the test program was then extended to include probing various parts of the flame structure in an attempt to identify regions where measurement difficulties such as background luminescence or laser-induced radiation from soot might be encountered. This study was performed with the aid of the OMA which was used to obtain single-shot N_2 and O_2 spectra in the flames produced by several fuel types and flow configurations. A slight difficulty in obtaining "clean", background-free spectra was encountered in the extremely luminous portions of certain flames. This problem was eliminated by operating the OMA in a 1-ms gated mode. In all cases after employing the gated OMA, these spectra were easily obtainable, indicating complete access to combustion regions for diagnostics purposes.

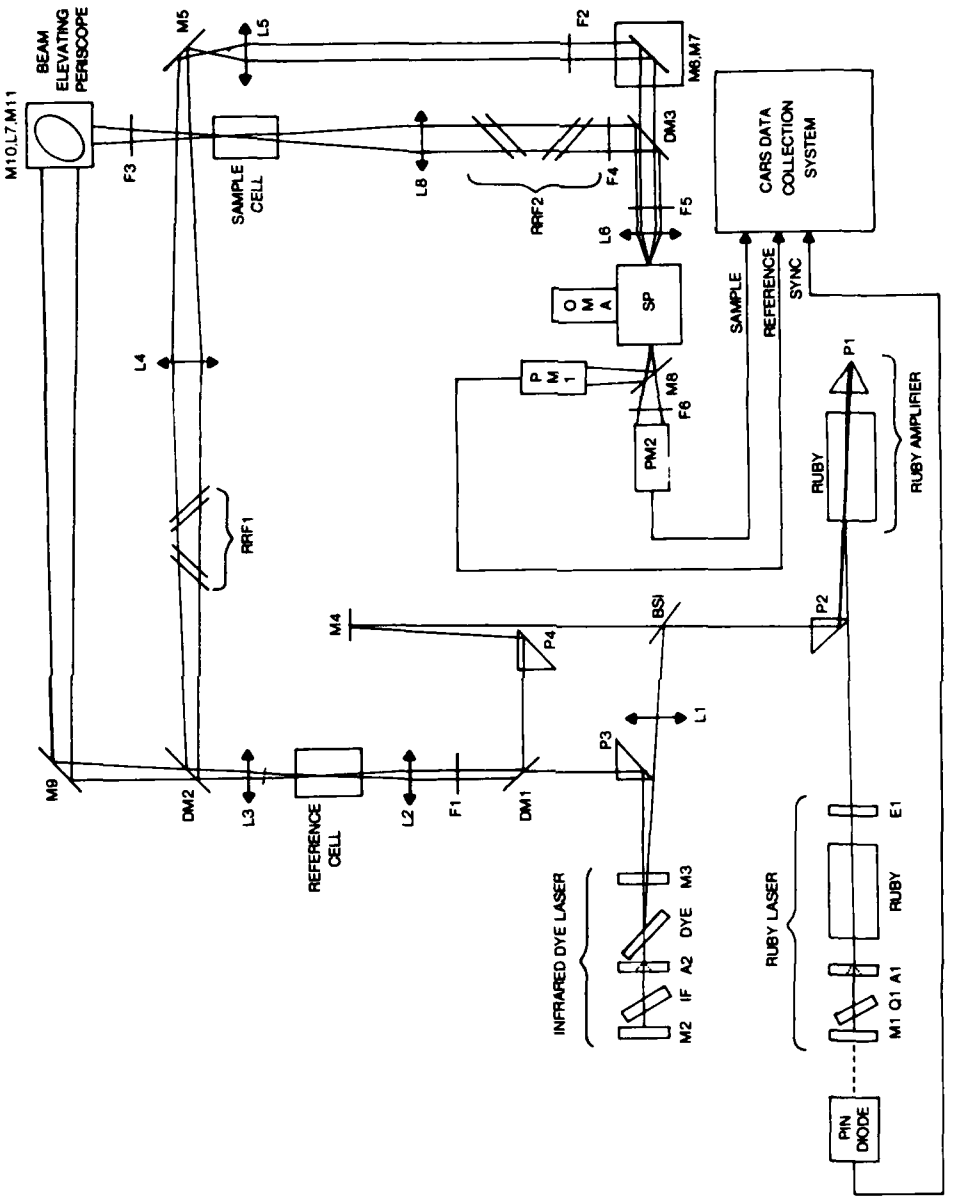

Figure 51. Second-Optical-System Design.

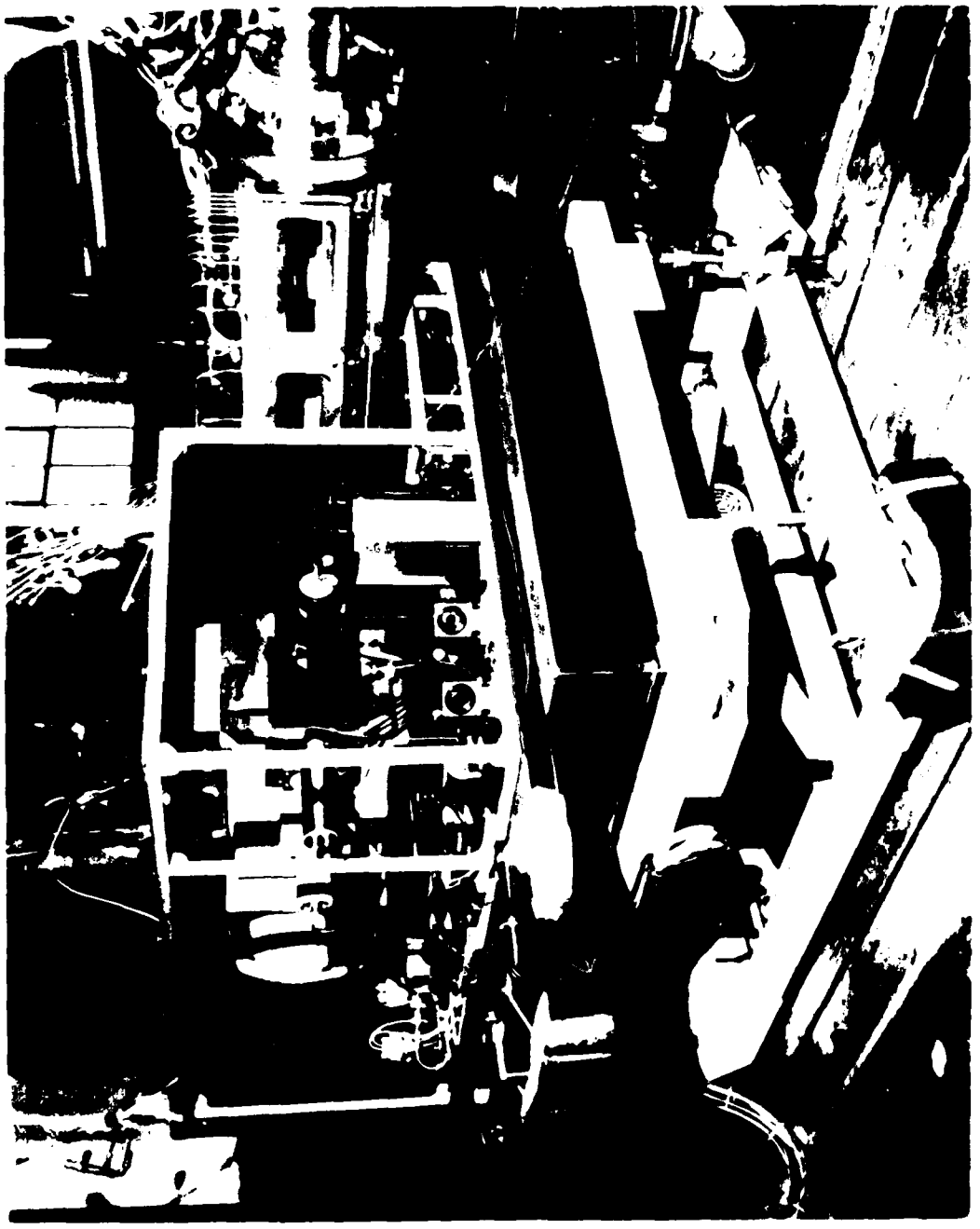

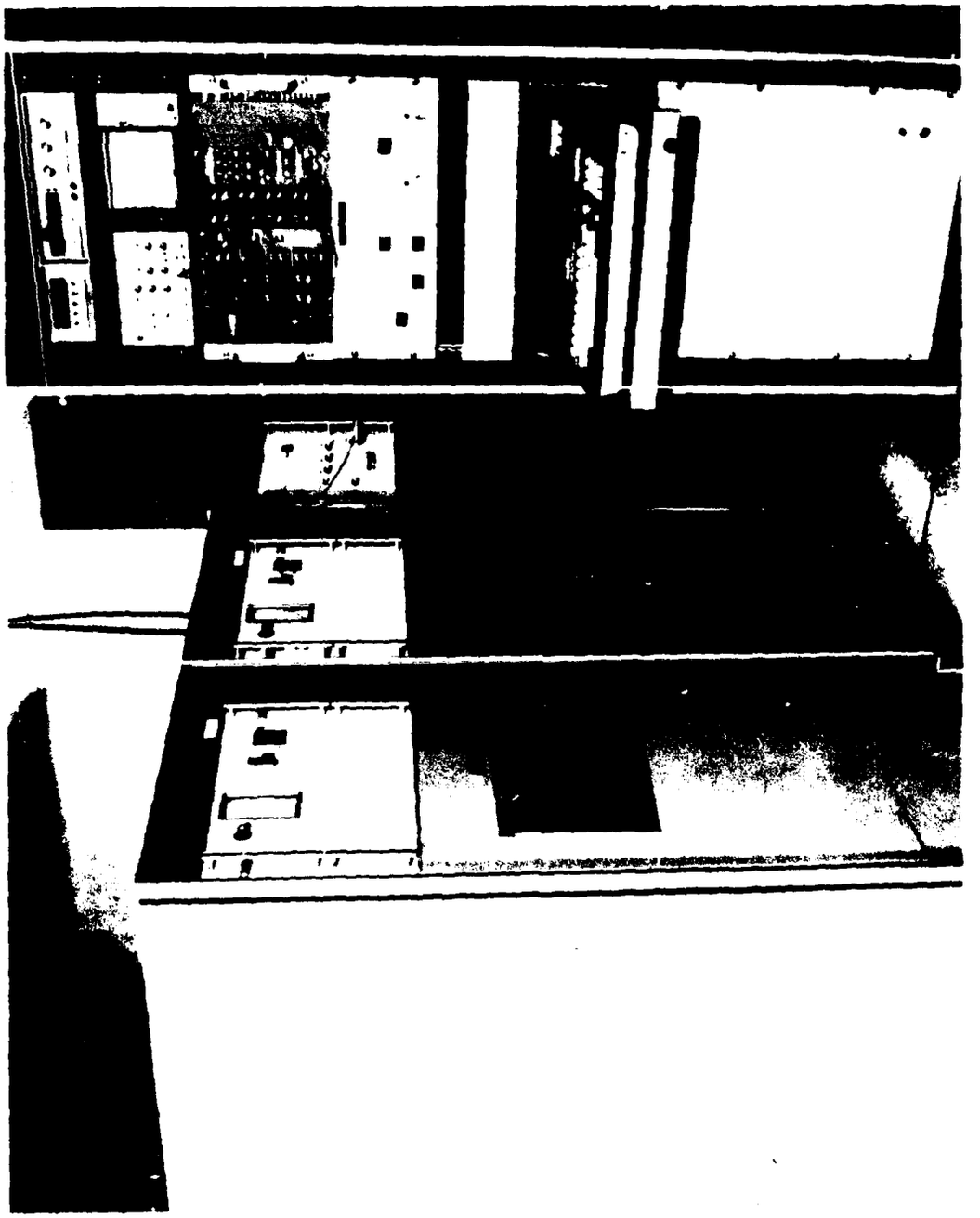

Figure 5.. Electronics Control Systems.

Scanned temperatures and N_2 and O_2 number-density data were then accumulated to produce profiles of these parameters along the combustor centerline for a well-defined flame produced by a fuel nozzle. Combustion-region temperatures were determined using the spectrum of N_2 which was generated by stepping the spectrometer in 1-Å intervals through successive N_2 anti-Stokes spectra. One such spectrum is represented by the + signs in Fig. 54. Each of these points represents the average of 30 consecutive measurements normalized with respect to the spectral-energy density of the reference anti-Stokes beam. The resulting composite spectrum was then compared with computer-generated N_2 spectra at various temperatures until the "best-fit" temperature was found. The solid overlay in Fig. 54 shows such a computer-generated N_2 CARS spectrum at a temperature of 1700 K. Since this spectral scanning and overlaying technique involves various time-averaging effects, the temperatures obtained are necessarily representative of a "weighted-average" value.

Species concentrations were determined through single-pulse integrated CARS intensity measurements involving the entire Q-branch of the N_2 and O_2 constituents of the combustion gases. The data from these measurements were reduced in conjunction with the "weighted-average" temperatures to obtain percent-by-volume concentrations. The temperature and concentration profiles obtained for the axial test positions are shown in Fig. 55. Although not indicated on this plot, the minimum detectable concentration capability of the CARS system in these experiments was determined to be ~ 2% for N_2 and 0.5% for O_2. A more complete description of these and other results of this test program is contained in Ref. 5.

After the first series of tunnel tests, the optical system was modified to allow a horizontal flame-profiling capability in addition to the vertical and longitudinal freedom already available. This capability was incorporated so that during the following two-month testing period, horizontal temperature and concentration profiles could be measured.

The purpose of this series of experiments was to obtain profiles in a given flame by means of the CARS and conventional probe techniques to allow quantitative comparison of these measurements. Figure 56 contains the CARS-developed profiles obtained through the flame diameter at a given axial position. A

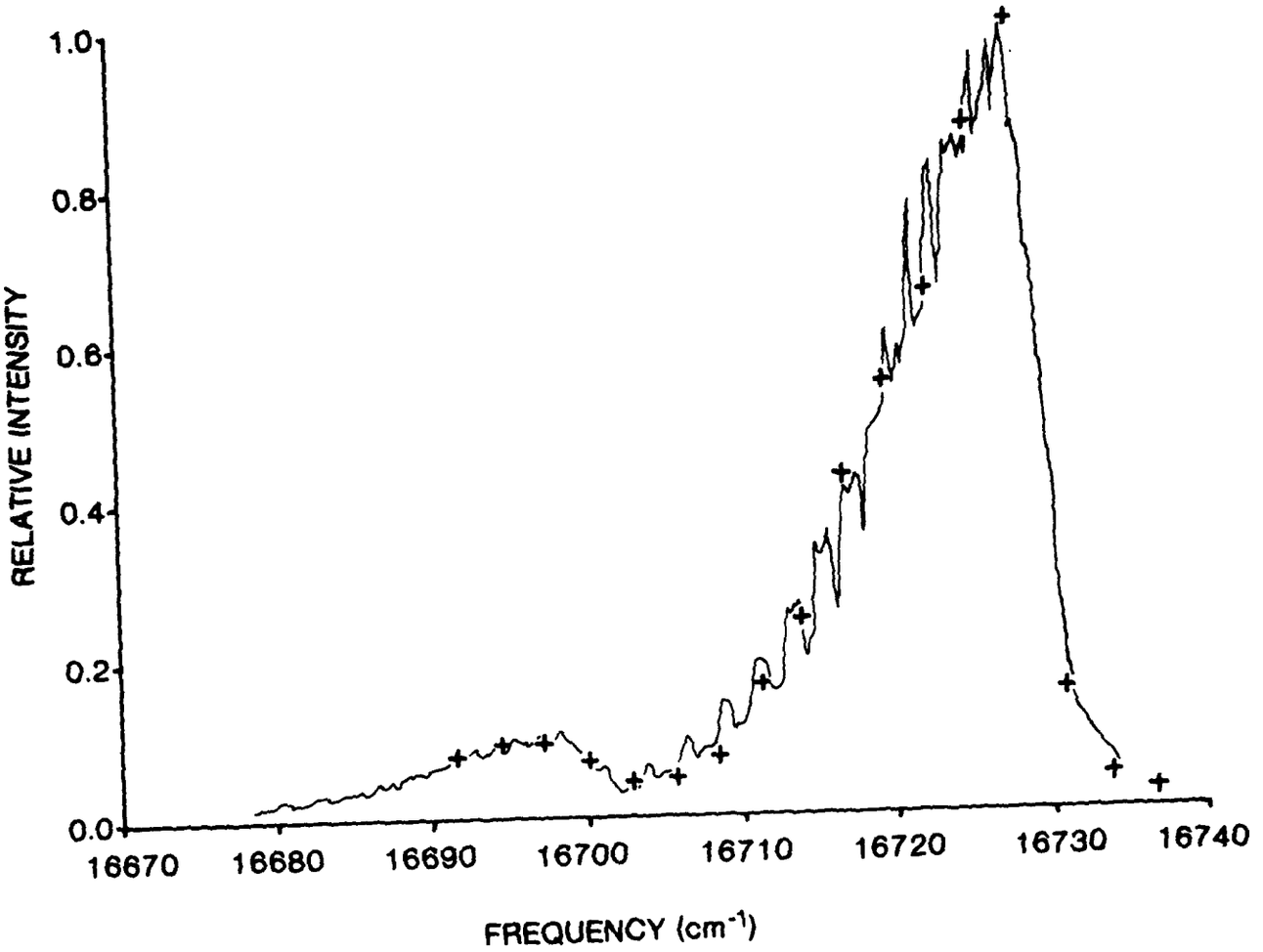

Figure 54. Overlay of Computed Spectrum of N_2 at 1700 K (Solid) *onto* Measured Spectrum (+).

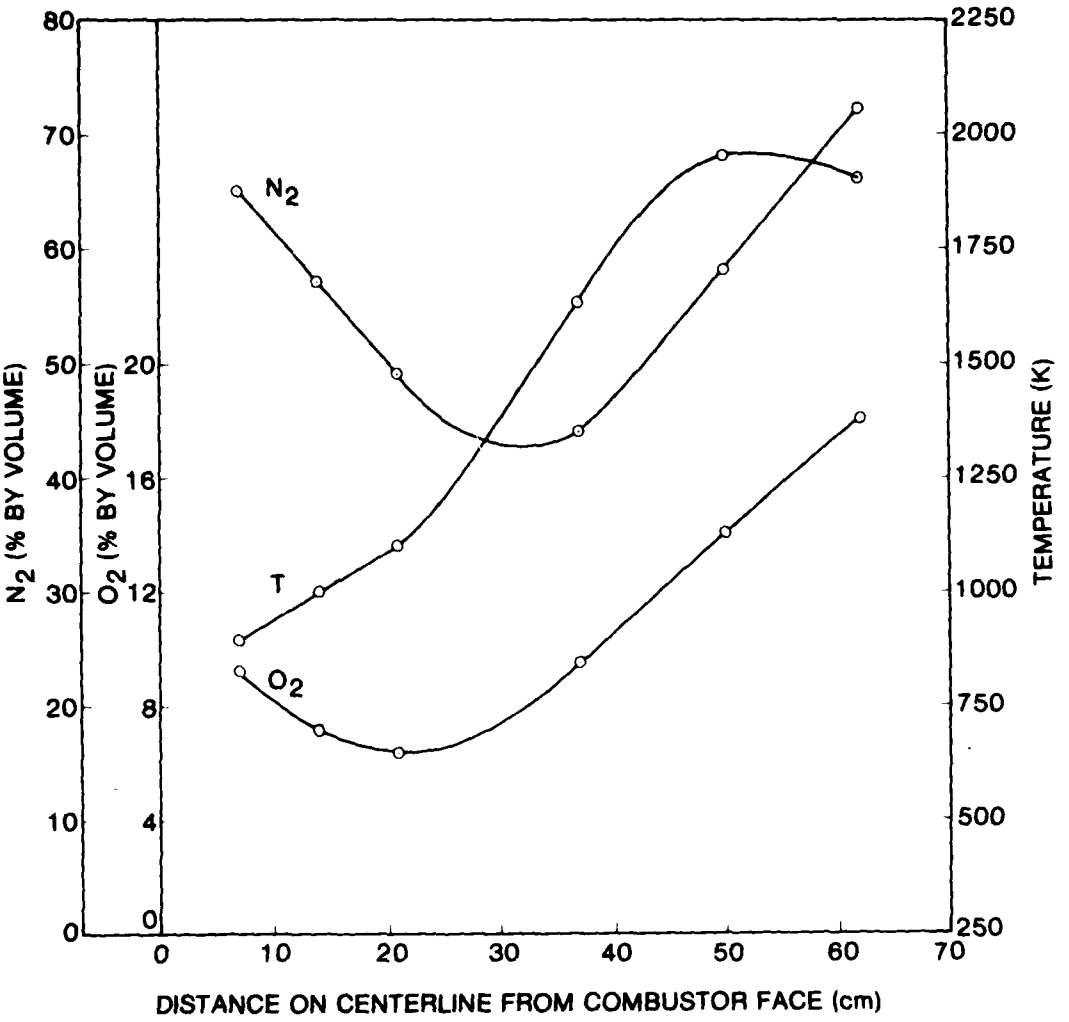

Figure 55. Axial Profiles.

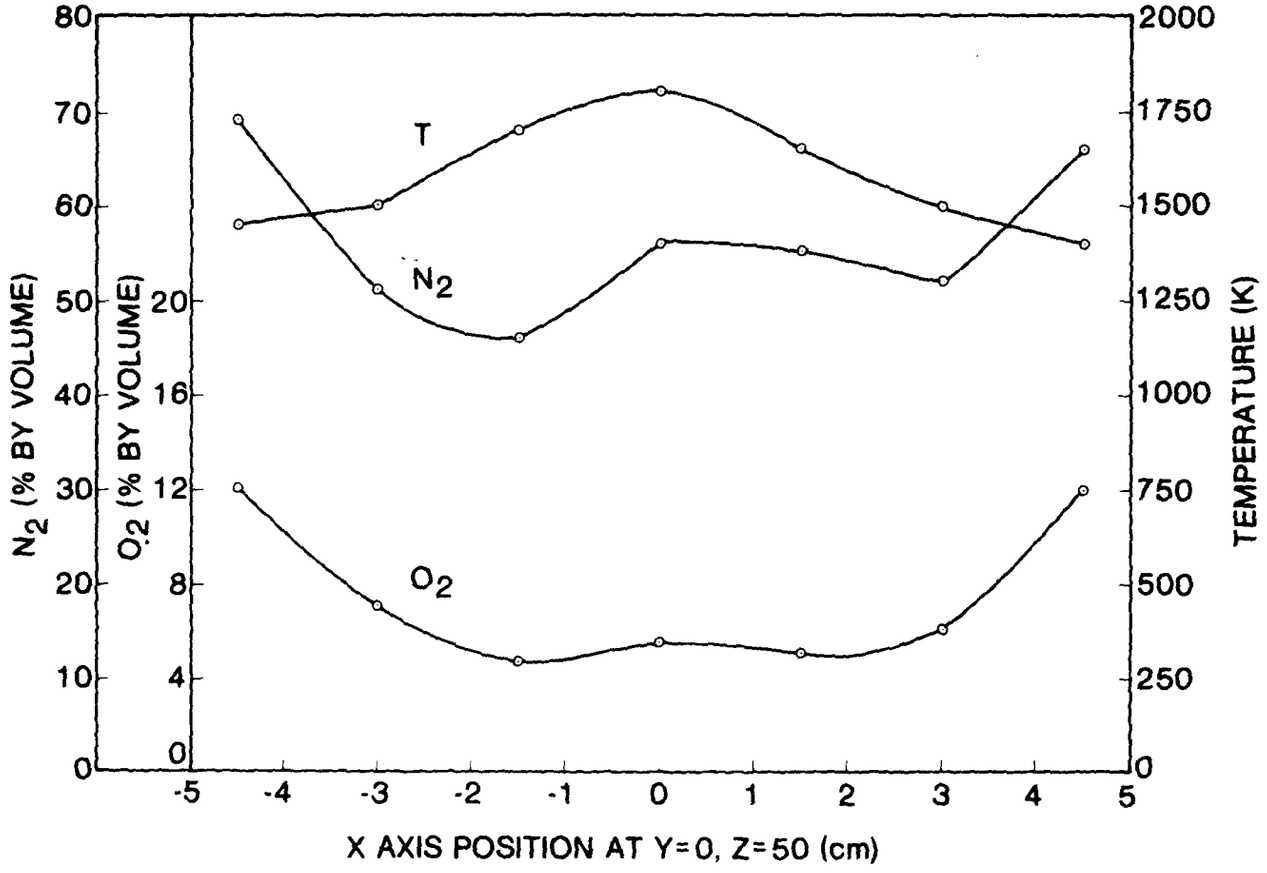

Figure 56. Radial Profiles at Y = 0, Z = 50 cm.

Pt 13%-RhPt thermocouple provided by NASA Lewis Research Center was used to profile the propane flame along the same diameter. Comparison of the CARS and thermocouple-derived temperature profiles is shown in Fig. 57. The comparison of CARS-derived O_2 concentrations and those obtained with a gas-sampling probe is shown in Fig. 58. A more detailed description of the experimental conditions and data-reduction considerations and a discussion of the results are given in Ref. 33. As can be seen from these comparative measurements, the agreement between the two methods of measurement is quite good near the flame centerline. Significant differences appear, however, for positions greater than approximately 4 cm for the centerline of the 14-cm-diam. flame. In the temperature comparisons of Fig. 57, part of this discrepancy was attributed to the effects of improper "weighting" of the observed spectra introduced by the spectral scanning technique employed for temperature measurements. To eliminate this effect and also to provide a means of obtaining true-time averaged temperature information, a single-shot "instantaneous" temperature capability was needed.

Initial attempts at single-shot temperature determination within the combustor resulted in average temperatures that were consistently lower than those measured earlier. The lower temperatures were determined to be an effect of the spectral shape of the broadband dye laser. Figure 59 shows successive shots of a nonresonant reference signal and indicates two characteristics of the dye laser output which influence single-shot spectra. The shot-to-shot profile changes visible in the figure affected measurement repeatability, while the relative-intensity distribution about the resonant frequency had a "weighting" effect on the generated CARS spectrum. This effect of nonuniform "pumping" around the resonant peak caused by improper tuning and stability of the frequency of the dye laser was believed to be partly responsible for the lowered average temperatures.

In order to correct a sample spectrum obtained with something other than a "flat-topped" dye-laser profile, a frequency normalization of the sample waveform was employed. This normalization capability was accomplished by using a dual-channel OMA detector which allowed two spectra to be recorded simultaneously. Thus, a sample waveform and a nonresonant reference were recorded and a channel-by-channel intensity normalization of the sample-to-reference

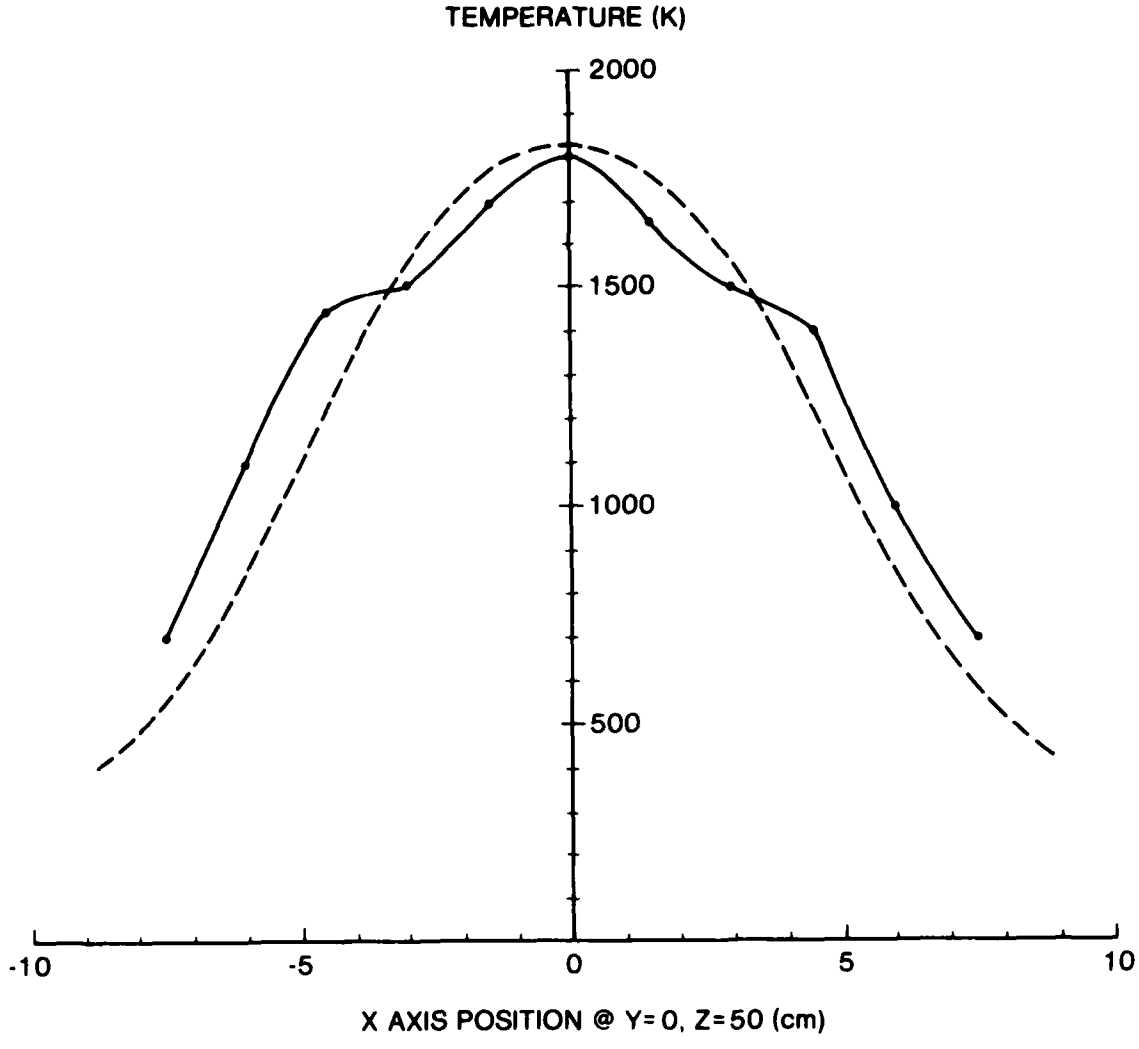

Figure 57. Comparison of CARS (Solid) and Thermocouple (Dashed) Temperatures.

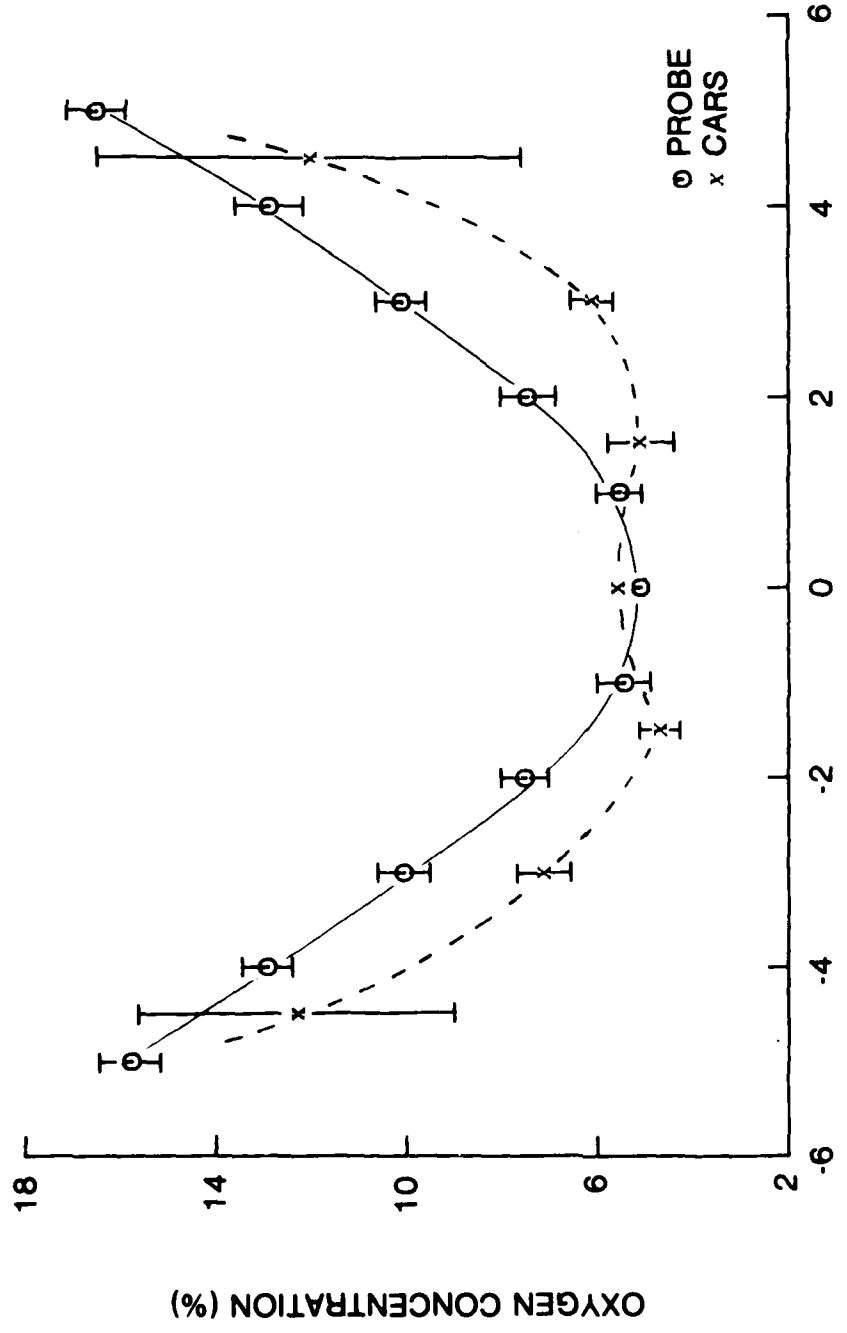

Figure 58. Comparison of CARS (Dashed) and Probe (Solid) Oxygen Concentrations.

Figure 59. Shot-to-Shot Frequency Fluctuation in Dye Laser.

signal was performed. The photographs in Fig. 60 demonstrate this dual-spectrum capability. Figure 60(a) is a room-temperature resonant N_2 CARS spectrum. Figure 60(b) is the nonresonant CARS generated in a glass substrate during the same 10-ns laser pulse. This spectrum indicates the relative frequency profile of the Stokes laser output. The absolute frequency alignment between the resonant and reference spectra can be seen in Fig. 60(c). This display represents the resonant signal minus the nonresonant and indicates the relative ease with which the proper tuning of the Stokes laser wavelength can be accomplished. Proper tuning ensures that sufficient Stokes power exists for pumping of the higher rotational and vibrational energy levels of the resonant molecule. To accomplish the spectrum normalization as well as to speed up the recording and storage of the large amounts of OMA information, the OMA was interfaced to the 9030A calculator. Several basic-language computer programs were created to collect, record, and analyze the spectral information. Figure 61(b) displays the frequency-normalized 1700 K spectrum obtained from the resonant and nonresonant signals of Fig. 61(a) and treated in the manner described above.

At this point the third and final system design changes were made. Since a single-shot temperature capability was available, only slight system modifications were necessary to acquire the sample and reference spectra and their integrated intensities from the two photomultipliers on a shot-to-shot basis, thus allowing simultaneous single-shot temperature and concentration information to be obtained. An additional modification--placing the reference generation cell after the sample volume--was made to provide better compensation for and/or demonstration of turbulence and Schlieren effects produced in the sample beam path. To date no ill effects from these disturbances have been observed. The resulting hardened CARS optical system design is shown in Fig. 62. An equipment manual[52] describing the system configuration and operation has been prepared.

Characterization of the final system configuration was carried out in the laboratory with special emphasis on determining the quality of the measured parameters. Several sets of data were accumulated to give an indication of the accuracy and precision with which the hardened system could perform N_2

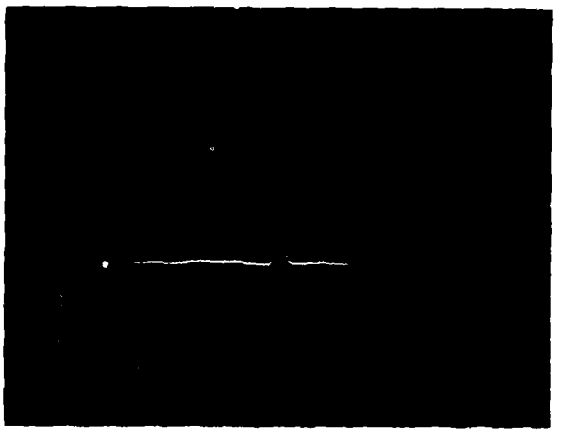

(a)

(b)

(c)

Figure [illegible] Angle-Purified XPEA Spectra.
(a) Room-temperature Ba[illegible] XPS,
(b) Room-temperature Ba[illegible] XPS,
(c) [illegible]

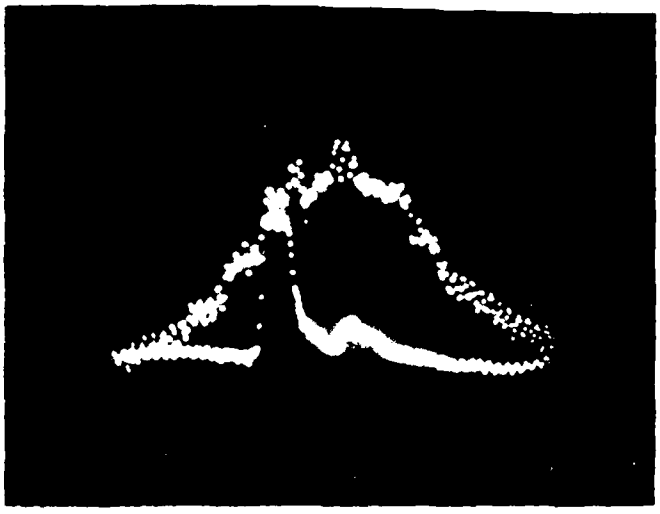

(a)

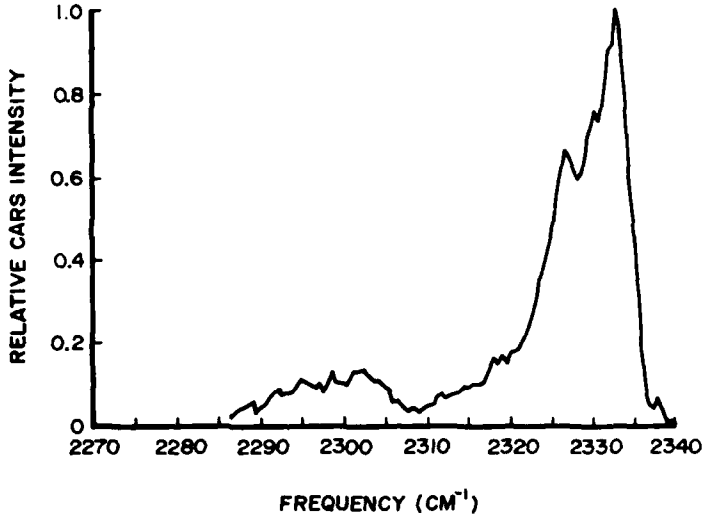

(b)

Figure 61. (a) Simultaneous Resonant and Nonresonant N_2 CARS Signals.
(b) Frequency-Normalized N_2 Spectrum Taken at 1700 K.

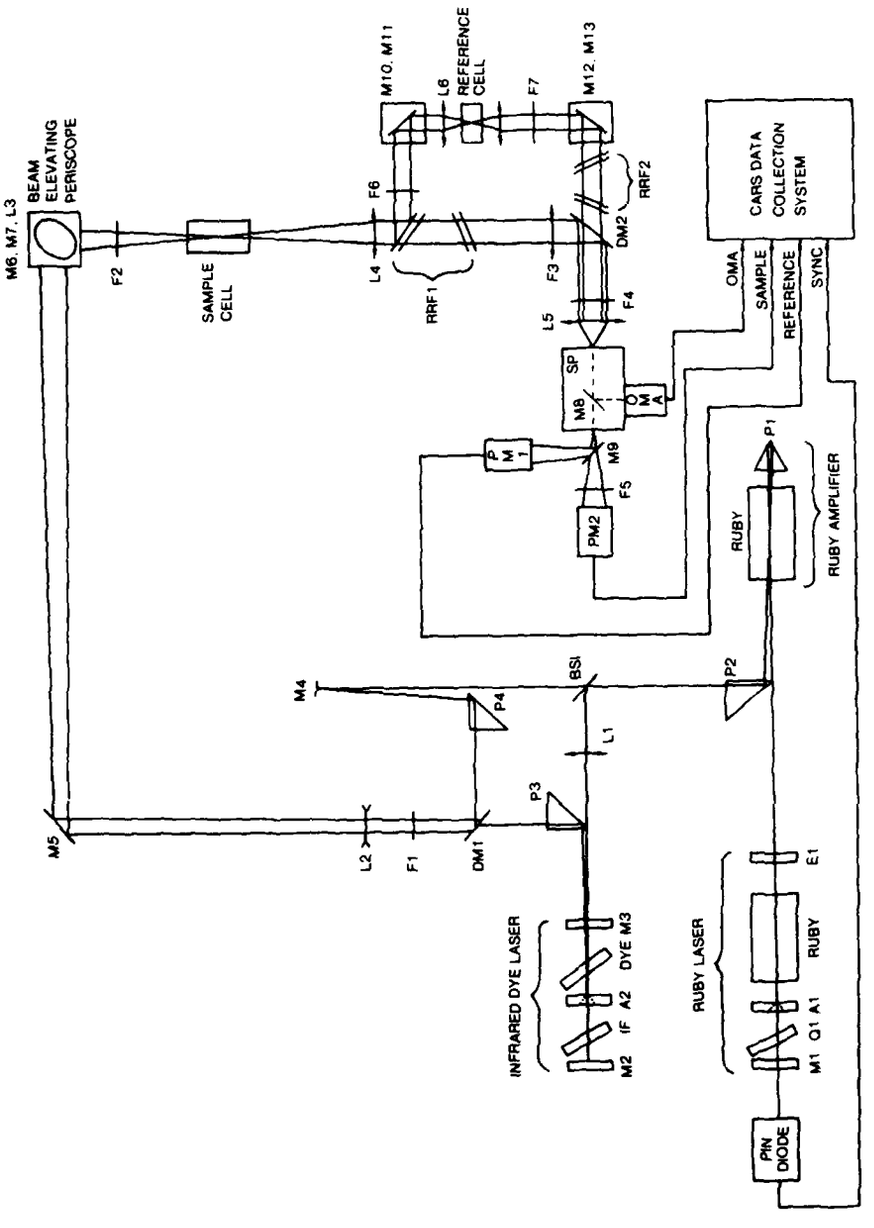

Figure 62. Final Harmed CARS Optical-System Schematic.

and O_2 concentration determinations. These results, which are summarized in Tables 9 and 10, were obtained by measurements made at room temperature and 1 atm. of pressure in a 25-cm-long × 2.5-cm-diam. cell containing N_2 and O_2 gases mixed in the stated proportions. As can be seen from this information, the accuracy of the measurements degrades at the lowest concentrations of both species, because of nonresonant background contributions.

To characterize the simultaneous single-shot temperature and concentration capability of the hardened system, a high-temperature sample environment was created by placing a 1.3-cm-diam. × 15-cm-long stainless-steel tube above a propane-fueled laboratory burner. A Pt 10%-RhPt thermocouple was inserted parallel to the tube axis to a point ≈ 2 mm below the focus of the sample beam. With this arrangement, "oven" temperatures of up to 1000 K could be attained. No thermocouple-radiation corrections were applied in these measurements since the required corrections of these temperatures were believed to be lower than other experimental uncertainties. Since the ends of the oven extended well beyond the flame zone, it was assumed that no combustion products were introduced into the tube. Thus, the mole fraction of N_2 within the tube should remain constant at 78.1% in atmosphere, while the number density and, hence, CARS intensity displays a T^{-2} dependence. The results of these measurements are summarized in Table 11.

Another parameter of the hardened CARS system which was characterized was the volume of sample gas which is active in the production of CARS signals in the given collinear optical configuration. The profile shown in Fig. 63 describes the relative intensity of resonant CARS generation as a function of distance from the focal point in the sample volume. This curve was generated by observing the integrated resonant CO_2 CARS intensity produced when a rectangular "sheet" of CO_2 gas, 1 mm in thickness, was translated along the sample optical path. These data indicate that if the concentration of the species being measured remains fairly uniform--between +3.5 cm and -3.5 cm from the sample focus--then ≈ 99% of the generated CARS signal will be produced within a path length of 12 mm. Thus, the active sample volume can be approximated by a cylinder 12 mm in length and a focal diameter which has been calculated to be ≈ 0.03 mm.

Table 9

ROOM-TEMPERATURE N_2-CONCENTRATION RESULTS

N_2 Concentration (Mixed in O_2) (%)	Measured Concentration (Average of 20 Samples) (%)	Average Concentration (Average of Five Measurements) (%)	Measurement Accuracy (Five Measurements) (%)
80	79.8 ± 4.1% 79.9 ± 6.0% 80.3 ± 6.2% 78.0 ± 4.5% 81.0 ± 3.8%	79.8 ± 1.4%	99.8
60	61.6 ± 6.9% 63.0 ± 8.6% 64.4 ± 9.8% 61.4 ± 6.1% 63.0 ± 11.2%	62.7 ± 1.9%	95.5
40	37.4 ± 5.9% 38.4 ± 7.2% 39.9 ± 9.1% 38.3 ± 7.9% 38.8 ± 6.9%	38.6 ± 2.4%	96.5
20	22.6 ± 6.8% 22.0 ± 12.3% 22.5 ± 5.8% 22.3 ± 7.1% 22.8 ± 8.4%	22.4 ± 1.4%	88.0
5	7.8 ± 6.3% 7.8 ± 6.9% 7.8 ± 6.2% 7.7 ± 5.5% 8.0 ± 7.3%	7.8 ± 1.4%	44.0

Table 10

ROOM-TEMPERATURE O_2-CONCENTRATION RESULTS

O_2 Concentration (Mixed in N_2) (%)	Measured Concentration (Average of 20 Samples) (%)	Average Concentration (Average of Five Measurements) (%)	Measurement Accuracy (Five Measurements) (%)
30	27.3 ± 4.8% 27.8 ± 4.6% 27.5 ± 6.3% 27.9 ± 4.8% 27.1 ± 7.6%	27.5 ± 1.2%	91.6
20	19.8 ± 7.9% 19.8 ± 7.5% 20.1 ± 5.9% 20.2 ± 5.0% 19.8 ± 7.4%	19.9 ± 1.0%	99.5
10	9.8 ± 7.4% 9.8 ± 7.5% 10.2 ± 4.8% 9.9 ± 9.2% 10.0 ± 8.2%	9.9 ± 1.7%	99.0
5	4.8 ± 4.4% 5.0 ± 7.1% 5.0 ± 4.7% 5.0 ± 3.2% 4.9 ± 5.0%	4.9 ± 1.8%	98.0
3	4.3 ± 4.8% 4.4 ± 6.0% 4.2 ± 6.6% 4.3 ± 7.4% 4.4 ± 8.0%	4.3 ± 1.9%	56.7

Table 11

SIMULTANEOUS TEMPERATURE AND CONCENTRATION DATA

Number of Shots	Thermocouple Temperature (K)	CARS Temperature Average (K)	Temperature Accuracy CARS (%)	N_2 Concentration Average (%)	Concentration Accuracy (%)
4	958	900	93.9	69.9	89.5
10	958	885	92.4	77.0	97.7
4	743	875	82.2	80.8	96.5
4	683	613	89.8	71.0	90.0

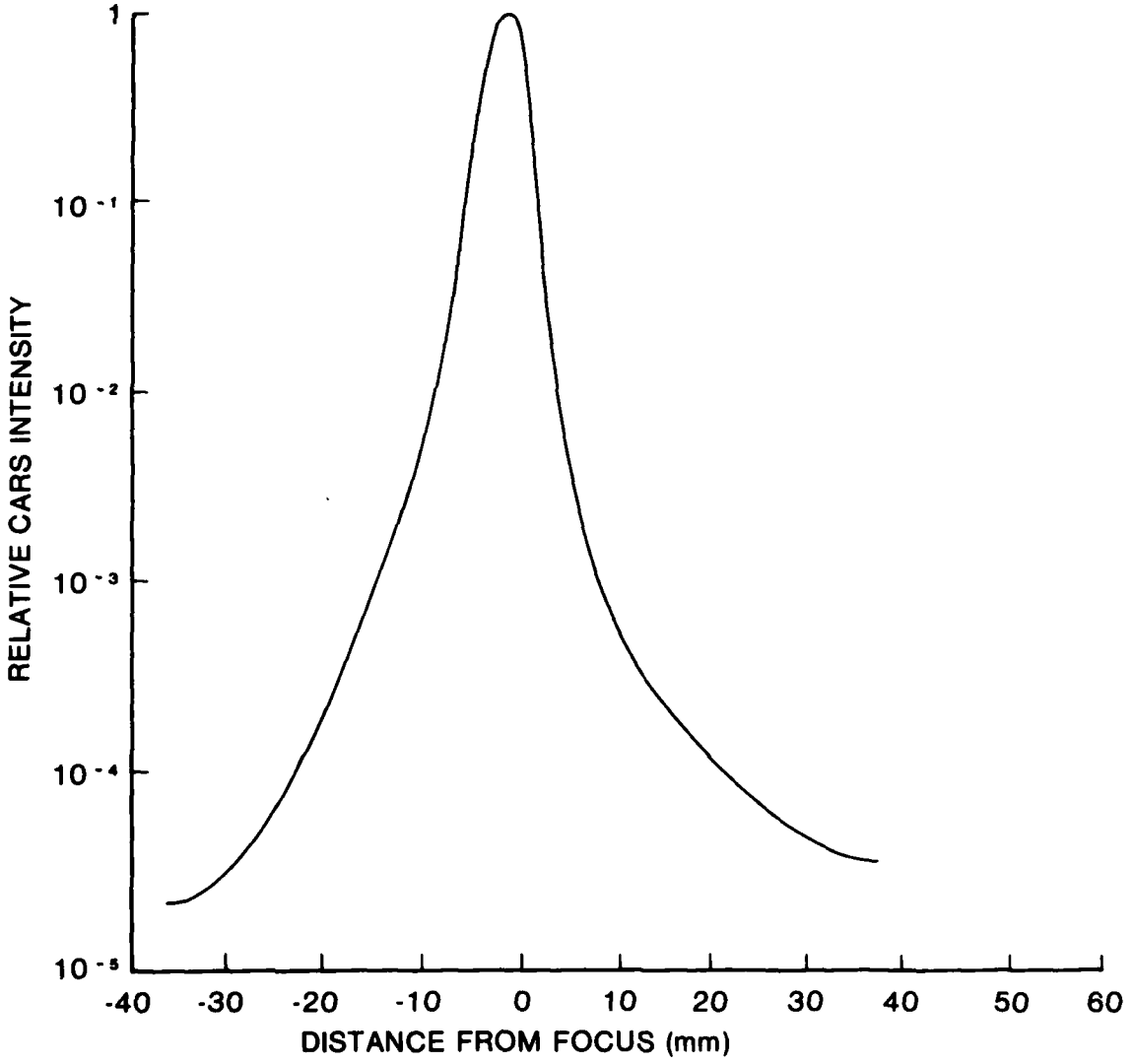

Figure 63. Distribution of Generated CARS about Sample Focus.

Section 5

CONCLUSIONS

Numerous fundamental studies have been conducted with the laboratory CARS system to determine the ability of the technique to measure temperatures and number densities in flame environments. Major emphasis has been placed upon making single-shot thermometry and density determinations. The results of single-shot thermometry studies on a propane-fueled burner have been compared with those obtained by means of the sodium-line-reversal technique with good agreement. The simultaneous temperature-number density results reported here showed good agreement with adiabatic flame calculations. The effects of turbulence upon CARS signal production have been examined, and a method for compensation has been demonstrated. Major emphasis for the future should be in the areas of broadening the range of quantifiable species for the CARS technique, increasing the data-acquisition rates of the CARS instrument to permit time histories of temperature-number density variations to be obtained, and combining the CARS technique with other techniques such as Laser Doppler Velicometry (LDV) to permit determination of velocities and thus turbulence characteristics of combustion systems.

The efforts in the hardened-CARS-system development portion of this program have culminated in an optical diagnostic system having a demonstrated ability to survive and to perform temperature and species concentration measurements in a practical combustion environment. The capability of obtaining these important parameters simultaneously and within a single shot has also been demonstrated. These results represent a very significant advancement for combustion-diagnostic techniques; however, several areas for further development can be recommended. Among these, refinements in the development of CARS theory are required for more accurate prediction of experimental observations. For measurements with finer spatial resolution, a CARS technique using small-angle CARS or BOXCARS should be considered to replace the collinear configuration used in the present system. Also, additional study is required to determine the precision and accuracy with which CARS measurements can be made in a combustion environment.

APPENDIX

LISTING OF THE CARS TEMPERATURE FITTING PROGRAM

```
      PROGRAM TFIT(INPUT,OUTPUT,TAPE5=INPUT,TAPE6=OUTPUT)                00000001
C     ******************************************************************
C
C           LEAST  SQUARES  FITTING  ROUTINE
C
C         BASED  ON  A  JACOBIAN  ITERATION
C
C           SUBROUTINES  REQUIRED FOR OPERATION
C             1  -  DELPHI
C             2  -  SPECTR
C             3  -  CONVOL
C             4  -  JMAT
C             5  -  MATINV
C             6  -  REPT
C             7  -  PLOT
C
C     ******************************************************************
C
C
C     ******************** I N P U T   D A T A ************************
C
C     C A R D  # 1                          FORMAT(I5)
C           NPLT  -  0    END OF DATA
C                 -  1  - MORE DATA
C
C     C A R D  # 2                          FORMAT(5I5)
C           NOBS  -  #OF EXPERIMENTAL OBSERVATIONS
C           NCYCLE  -  # OF CYCLES FOR THE FITTING ITERATION
C           NVMAX  -  MAX. # OF VIBRATIONAL TRANSITIONS
C           NJMAX  -  MAX. # OF ROTATIONAL TRANSITIONS
C
C     C A R D  #  3                        FORMAT(4I5)
C           PARAMETERS FOR DETERMINING THE CONVOLUTIONS TO BE TAKEN
C           NC1  -  CONVOLUTION INDICATOR FOR GAM1
C           NC2  -  CONVOLUTION INDICATOR FOR GAM2
C           NC3  -  CONVOLUTION INDICATOR FOR GAMP
C           NC4  -  CONVOLUTION INDICATOR FOR GAMS
C             -  0  -   SKIP CONVOLUTION
C             -  1  -  GAUSSIAN CONVOLUTION
C             -  2  -  LORENTZIAN CONVOLUTION
C             -  3  -  TRIANGULAR CONVOLUTION
C             -  4  -  TRAPEZOIDAL  CONVOLUTION
C
C     C  A  R  D  #  4                      FORMAT(6F10.5)
C           OINT  -  ARRAY OF THE OBSERVED INTENSITIES
C                    FROM LOW TO HIGH CM-1
```

```
C
C     C  A  R  D  #  5                    FORMAT(2F10.5)
C          STOB  -  STARTING CM-1 FOR THE EXPERIMENTAL DATA
C          OBINC  -  CM-1 INCREMENT FOR THE EXPERIMENTAL DATA
C
C     C  A  R  D  #  6                    FORMAT (I5)
C          NSW  -  WEIGHT INDICATOR FOR DATA POINTS.
C                  -  0  -  EQUAL WEIGHTS FOR DATA
C                  -  1  -  1./(OINT)**2
C                  -  2  -  WEIGHTS READ IN
C          WI(6F10.5)  -  WEIGHTS READ ONLY IF NSW = 2
C
C     C  A  R  D  #  7                    FORMAT(6F10.5)
C          GAM  -  RAMAN HWHM
C          GAM1 - HWHM FOR 1ST CONVOLUTION
C          GAM2  -  HWHM FOR 2ND CONVOLUTION
C          WINC  -  CM-1 INCREMENT FOR CALCULATED SPECTRA
C          WSTART  -  STARTING CM-1 FOR CALCULATED SPECTRA
C          T  -  INITIAL GUESS FOR THE TEMPERATURE
C
C     C  A  R  D  #  8                    FORMAT(4F10.5)
C          WFIN  -  FINAL CM-1 FOR CALCULATED SPECTRA
C          FPAR(1) -  TEMPERATURE FIT INDICATOR
C                  -  0  -  SKIP
C                  -  1  -  FIT TEMPERATURE
C          FPAR(2)  -  FREQUENCY FIT INDICATOR
C                  -  0  -  SKIP
C                  -  1  -  FIT FREQUENCY
C          FPAR(3) -  RAMAN HWHM FIT INDICATOR
C                  -  0  -  SKIP
C                  -  1  -  FIT RAMAN HWHM
C
C     C  A  R  D  #  9                    FORMAT(2F10.5)
C          GAMP  -  HWHM FOR 3RD CONVOLUTION
C          GAMS  -  HWHM FOR 4TH CONVOLUTION
C          BK  -  NONRESONANT BACKGROUND
C
C     R  E  T  U  R  N     T  O     C  A  R  D     #  1
C
C     ***************************************************************
      COMMON/AMAIN/OBS(200),O.  T(200),FPAR(3)                          00000002
      COMMON/BMAIN/GAM,T,WSTART,WINC,WFIN,BK                            00000003
      COMMON/CMAIN/NVMAX,NJMAX,NOBS                                     00000004
      COMMON/EMAIN/GAM1,GAM2,GAMP,GAMS
      COMMON/DMAIN/NC1,NC2,NC3,NC4                                      00000005
      COMMON/AOEL/WSTAR2,WM..
      DIMENSION RWO(3),RJJ(3,3),RJ(200,3),DP(200)
      DIMENSION DELF(3),P(3),SIGMA(3),WI(200)
   15 READ(5,1)NPLT
      IF(NPLT.EQ.0) GO TO 7777
      READ(5,1)NOBS,NCYCLE,NVMAX,NJMAX,NPAR
```

```
    1 FORMAT(6I5)
      READ(5,1)NC1,NC2,NC3,NC4
100   READ(5,2)(OINT(I),I=1,NOBS)
      WRITE(6,98)
   98 FORMAT(*1*)
      WRITE(6,107)
  107 FORMAT(10X,* EXPERIMENTAL DATA*,/)
105   WRITE(6,103)(OINT(I),I=1,NOBS)
  103 FORMAT(6(10X,E12.5))
      WRITE(6,144)
  144 FORMAT(1X,//)
      WMAX=OINT(1)
110   DO 10 I=1,NOBS
   10 WMAX=AMAX1(WMAX,OINT(I))
      DO 20 I=1,NOBS
   20 OINT(I)=OINT(I)/WMAX
      READ(5,2)STOB,OBINC
115   DO 16 I=1,NOBS
   16 OBS(I)=STOB+(I-1)*OBINC
    2 FORMAT(6F10.5)
      READ(5,1)NSW
      IF(NSW.GT.1)GO TO 17
120   IF(NSW.EQ.1)GO TO 21
      DO 18 I=1,NOBS
   18 WI(I)=1.
      GO TO 19
   21 DO 22 I=1,NOBS
125   IF(OINT(I).EQ.0.)OINT(I)=1.
   22 WI(I)=1./(OINT(I)**2)
      GO TO 19
   17 READ(5,3)(WI(I),I=1,NOBS)
   19 READ(5,3)GAM,GAM1,GAM2,WSTART,WINC,T
130   READ(5,3)WFIN,FPAR(1),FPAR(2),FPAR(3)
      READ(5,3)GAMP,GAMS,BK
    3 FORMAT(6F10.3)
C
C           PRINT OUT OF INPUT DATA
135 C
      WRITE(6,99)
   99 FORMAT(10X,* NOBS*,* NCYCLE*,* NVMAX*,* NJMAX*,* NPAR*)
      WRITE(6,100)NOBS,NCYCLE,NVMAX,NJMAX,NPAR
  100 FORMAT(10X,I5,2X,I5,1X,I5,1X,I5,1X,I5,//)
140   WRITE(6,101)
  101 FORMAT(10X,* NC1*,2X,* NC2*,2X,* NC3*,2X,* NC4*)
      WRITE(6,102)NC1,NC2,NC3,NC4
  102 FORMAT(9X,I5,3(1X,I5),//)
      WRITE(6,104)
```

```
      184 FORMAT(10X,* STOB*,10X,* OBINC*)
          WRITE(5,105)STOB,OBINC
      105 FORMAT(10X,F7.2,9X,F5.3,/)
          WRITE(6,106)NSW
      106 FORMAT(10X,* NSW= *,I2,/)
          WRITE(6,108)
      108 FORMAT(10X,* GAM*,7X,* GAM1*,7X,* GAM2*,5X,* WSTART*,7X,* WINC*,
         110X,* T*)
          WRITE(6,109)GAM,GAM1,GAM2,WSTART,WINC,T
      109 FORMAT(2X,6(2X,F10.5),/)
          WRITE(6,110)
      110 FORMAT(10X,* WFIN*,4X,* FPAR(1)*,4X,* FPAR(2)*,4X,* FPAR(3)*)
          WRITE(6,115)WFIN,FPAR(1),FPAR(2),FPAR(3)
      115 FORMAT(3X,4(2X,F10.5),/)
          WRITE(6,112)
      112 FORMAT(10X,* GAMP*,7X,* GAMS*,7X,* BK*)
          WRITE(6,113)GAMP,GAMS,BK
      113 FORMAT(3X,3(2X,F10.5),/)
C
C           INITIALIZATION OF PARAMETERS
C
      WSTAR2=WSTART
      P(1)=T
      P(2)=WSTAR2
      P(3)=GAM
C
C     ***** LEAST SQUARES ITERATION   ***********************************

C
      DO 999 LCYCLE=1,NCYCLE
      DO 300 K=1,NOBS
      DO 300 L=1,NPAR
      RHO(L)=0.0
      RJJ(K,L)=0.
  300 RJ(K,L)=0.
C
C           CALCULATION OF VARIANCE
C
      IF(LCYCLE.EQ.1)GO TO 6000
      SUM=0.
      DO 303 K=1,NOBS
      PP=DP(K)
  303 SUM=SUM+PP**2
      SUM=SUM/(NOBS-NPAR)
      WRITE(6,7008)SUM
 7008 FORMAT(//,10X,* VARIANCE=*,E10.3,5(/))
```

```
190         C
            C           DELPHI MATRIX
            C
            6000 CALL DELPHI(DP)
            1000 FORMAT(6E12.5)
195         C
            C           J MATRIX
            C
                 CALL JMAT(RJ)
            C
200         C           J TRANSPOSE J MATRIX
            C
                 DO 882 K=1,NPAR
                 DO 882 L=1,NPAR
                 RJJ(K,L)=0.
205              DO 882 M=1,NOBS
            882  RJJ(K,L)=RJJ(K,L)+RJ(M,K)*RJ(M,L)*WI(M)
            C
            C           CHECK FOR ZERO DIAGONAL ELEMENTS
            C
210              DO 883 K=1,NPAR
            883  IF(RJJ(K,K).EQ.0)GO TO 7776
            C
            C           J TRANSPOSE J INVERSE MATRIX
            C
215              CALL MATINV(RJJ,NPAR)
            C
            C           J TRANSPOSE DELPHI MATRIX
            C
                 DO 887 K=1,NPAR
220              RWD(K)=0.
                 DO 887 L=1,NOBS
            887  RWD(K)=RWD(K)+RJ(L,K)*DP(L)*WI(L)
            C
            C           CORRECTION MATRIX
225         C
                 DO 889 K=1,NPAR
                 DELF(K)=0.
                 DO 888 L=1,NPAR
            888  DELF(K)=DELF(K)+RJJ(K,L)*RWD(L)
230              KK=0
            C
            C           NEW PARAMETERS
            C
                 DO 889 K=1,3
235              IF(FPAR(K).EQ.0)GO TO 889
                 KK=KK+1
                 P(K)=P(K)+DELF(KK)
            889  CONTINUE
            C
```

```
C           REINITIALIZE PARAMETERS
C
      T=P(1)
      WSTAR2=P(2)
      GAM=P(3)
      WRITE(6,900)LCYCLE
  900 FORMAT(//,10X,*CYCLE=*,I5,/)
      WRITE(6,903)T
  903 FORMAT(//,10X,*TEMPERATURE=*,E12.5,/)
      WRITE(6,904)WSTAR2
  904 FORMAT(//,10X,*DISPLACEMENT=*,E12.5,/)
      WRITE(6,905)GAM
  905 FORMAT(//,10X,*RAMAN HALFWIDTH=*,E12.5,/)
  999 CONTINUE
      DO 305 K=1,NOBS
      PP=OP(K)
  305 SUM=SUM+PP**2
      SUM=SUM/(NOBS-NPAR)
      WRITE(6,7008)SUM
      KK=0
C
C           DISPERSION CALCULATION
C
      DO 914 I=1,3
      IF(FPAR(I).EQ.0)GO TO 914
      KK=KK+1
      SIGMA(I)=RJJ(KK,KK)*SUM
      SIGMA(I)=SQRT(SIGMA(I))
  914 CONTINUE
      WRITE(6,915)T,SIGMA(1)
  915 FORMAT(//,10X,*TEMP=*,E12.5,*+/-*,E12.5,/)
      WRITE(6,916)WSTAR2,SIGMA(2)
  916 FORMAT(//,10X,*DISPLACEMENT=*,E12.5,*+/-*,E12.5,/)
      WRITE(6,918)GAM,SIGMA(3)
  918 FORMAT(//,10X,*GAM=*,E12.5,*+/-*,E12.5,/)
C
C           DISPLAY OF THE RESULTS
C
      CALL REPT
      GO TO 15
 7776 WRITE(6,917)
  917 FORMAT(*1*,*ZERO DIAGONAL ELEMENT*)
 7777 STOP
      END
```

```
      SUBROUTINE DELPHI(DP)
C     ******** S U B R O U T I N E   D E L P H I  ***********
C
C           DELPHI MATRIX CALCULATION
C
C           CALCULATES DIFFERENCE OF THE OBSERVED AND CALCULATED
C           SPECTRA FOR THE INITIAL SET OF PARAMETERS
C
C     ************************  (D  P)     ******************************
C
C           DP  -  DELPHI MATRIX
C
C     ***********************************************************************
      COMMON/AMAIN/OBS(200),OINT(200),FPAR(3)
      COMMON/BMAIN/GAM,T,WSTART,WINC,WFIN,BK
      COMMON/CMAIN/NVMAX,NJMAX,NOBS
      COMMON/ADEL/WSTAR2,WMAX
      DIMENSION DP(200),WNT(6000)
C
C           CALCULATION OF SPECTRA
C
      CALL SPECTR(WNT)
C
C           FORMATION OF DELPHI MATRIX
C
      DO 70 I=1,NOBS
      K=INT((OBS(I)-WSTAR2)/WINC+1.)
   70 DP(I)=OINT(I)-WNT(K)
      RETURN
      END
```

```
      SUBROUTINE SPECTR(WINT)
C     ****** S U B R O U T I N E   S P E C T R ********
C
C
C         CALCULATION OF CARS SPECTRA
C
C           THIS SUBROUTINE USES THE LATEST CONSTANTS OF HERZBERG
C           TO CALCULATE THE RAMAN THIRD ORDER SUSCEPTIBILITY
C
C     ***************************************************************
C
C     ***********************  ( WINT )  ******************************
C
C           WINT  -  CARS SPECTRA ARRAY
C
C     ***************************************************************
      COMMON/BMAIN/GAM,T,WSTART,WINC,WFIN,BK
      COMMON/CMAIN/NVMAX,NJMAX,NOBS
      COMMON/DMAIN/NC1,NC2,NC3,NC4
      COMMON/EMAIN/GAM1,GAM2,GAMP,GAMS
      DIMENSION WINT(6000),WG(6,80),WV(6),WJ(6,80),EPVJ(6,80)
      COMPLEX CMPLX,CONJG,S,SUM,S1
      DATA BE,AE,DE,BETE/1.99824,1.7318E-2,.576E-05,.10E-08/
      DATA WE,WEXE,WEYE/2358.57,14.324,.226E-02/
      DATA EP/.69314718/
      NFREQ=(WFIN-WSTART)/WINC+1.
      HCKT=1.43977/T
      NV1=NVMAX+1
      NJ1=NJMAX+1
C
C           CALCULATION OF ENERGY LEVELS IC CM-1 UNITS
C
      DO 110 K=1,NV1
  110 WV(K)=WE*(K-.5)-WEXE*(K-.5)**2+WEYE*(K-.5)**3
      DO 100 K=1,NV1
      DO 100 I=1,NJ1
      WGG=WE-2*WEXE*K+WEYE*(3*(K-1)**2+6*(K-1)+13./4.)
      WGG=WGG-AE*(I-1)*(I)-BETE*K*((I-1)**2)*I**2
      WG(K,I)=WGG
      WJJ=(BE-AE*(K-.5))*(I-1)*I-(DE+BETE*(K-.5))*((I-1)**2)*I**2
  100 WJ(K,I)=WJJ
C
C           CALCULATION OF THE BOLTZMAN POPULATIONAL FACTORS
C
      DO 200 K=1,NVMAX
      WV1=-HCKT*WV(K)
      IF(WV1.LT.-675.)WV1=-675.
      EPV1=EXP(WV1)*K
      WV2=-HCKT*WV(K+1)
```

```
      IF(WV2.LT.-675.)WV2=-675.
      EPV2=EXP(WV2)*(K  )
      DO 200 I=1,NJMAX
      NJ=I-1
      OG=1.
      IO=MOD(NJ,2)
      IF(IO.EQ.0)OG=2.
      WJ1=-HCKT*WJ(K,I)
      IF(WJ1.LT.-675.)WJ1=-675.
      EJ1=OG*(2*NJ+1)*EXP(WJ1)
      WJ2=-HCKT*WJ(K+1,I)
      IF(WJ2.LT.-675.)WJ2=-675.
      EJ2=OG*(2*NJ+1)*EXP(WJ2)
  200 EPVJ(K,I)=EJ1*EPV1-EJ2*EPV2
C
C           CALCULATION OF THE CARS SPECTRA
C
      DO 300 I=1,NFREQ
      W=WSTART+(I-1)*WINC
      SUM=CMPLX(0.,0.)
      S=CMPLX(0.,0.)
      S1=CMPLX(0.,0.)
      DO 310 K=1,NV1
      DO 310 L=1,NJ1
      DELTA=WG(K,L)-W
      STR=DELTA
      STI=-GAM
      S=CMPLX(STR,STI)
      STR=EPVJ(K,L)
      STI=0.
      S1=CMPLX(STR,STI)
      SUM=SUM+S1/S
  310 CONTINUE
      SUM=SUM+BK
      WINT(I)=REAL(SUM*CONJG(SUM))
  300 CONTINUE
C
C           CONVOLUTION OF THE SPECTRA
C
      GAMM=GAM1
      IF(NC1.NE.0)CALL CONVOL(WINT,GAMM,NC1)
      GAMM=GAM2
      IF(NC2.NE.0)CALL CONVOL(WINT,GAMM,NC2)
      GAMM=GAMP
      IF(NC3.NE.0)CALL CONVOL(WINT,GAMM,NC3)
      GAMM=GAMS
```

```
      IF(NC4.NE.0)CALL CONVOL(WINT,GAMM,NC4)
C
C           NORMALIZATION OF THE SPECTRA
C
      WMAX=0.
      DO 10 I=1,NFREQ
   10 WMAX=AMAX1(WMAX,WINT(I))
      DO 20 I=1,NFREQ
   20 WINT(I)=WINT(I)/WMAX
      RETURN
      END



      SUBROUTINE CONVOL(WNT,GAMM,NCN)
C     ******** S U B R O U T I N E  C O N V O L ********
C
C           CONVOLUTION SUBROUTINE FOR CONVOLVING THE CALCULATED
C           SPECTRA OVER THE APPROPRIATE FUNCTIONS.
C
C     ***********************************************************************
C
C     ********************** ( WNT, GAMM, NCN ) ************************
C
C           WNT  -  MATRIX TO BE CONVOLVED
C           CONVOLVED MATRIX IS RETURNED IN THE SAME ARRAY
C           GAMM  -  HWHM OF APPROPRIATE FUNCTION
C           NCN  -  INDICATOR FOR CONVOLUTION FUNCTION
C                  -  0  -  SKIP
C                  -  1  -  GAUSSIAN
C                  -  2  -  LORENTZIAN
C                  -  3  -  TRIANGLE
C                  -  4  -  TRAPEZOID
C
C     ***********************************************************************
      COMMON/BMAIN/GAM,T,WSTART,WINC,WFIN,BK
      DIMENSION WNT(6000),WINT(6000)
      DATA EP,PI/.69314718, 3.14159/
      NFREQ=(WFIN-WSTART)/WINC+1.
      IF(NCN.EQ.0)GO TO 777
      DO 2 I=1,NFREQ
    2 WINT(I)=WNT(I)
      IF(NCN.EQ.2)GO TO 100
      IF(NCN.EQ.3)GO TO 200
      IF(NCN.EQ.4)GO TO 300
C
```

```
C           NORMALIZED GAUSSIAN
C
      K=0.
      IW2=INT(4.*GAMM/WINC)
      I22=2*IW2+1
      E2GPI=EP/(GAMM*SQRT(PI))
      E2G2=EP/(GAMM**2)
      DO 10 I=1,NFREQ
      K=K+1
      SUM=0.
      DO 20 M=1,I22
      KK0=K+M-IW2-2
      IF(KK0.LE.-1)GO TO 20
      KK1=KK0+1
      KK2=KK1+1
      IF(M.EQ.1)GO TO 25
      IF(KK0.LE.1)GO TO 25
      ED0=ED1
      ED1=ED2
      GO TO 27
   25 DEL=(-IW2-1+M)*WINC
      ED0=E2GPI*EXP(-E2G2*(DEL**2))
      DEL=DEL+WINC
      ED1=E2GPI*EXP(-E2G2*(DEL**2))
   27 DEL=DEL+WINC
      ED2=E2GPI*EXP(-E2G2*(DEL**2))
      WT0=0.
      WT1=0.
      WT2=0.
      IF(KK0.GT.0.AND.KK0.LE.NFREQ)WT0=WINT(KK0)*ED0
      IF(KK1.GT.0.AND.KK1.LE.NFREQ)WT1=WINT(KK1)*ED1
      IF(KK2.GT.0.AND.KK2.LE.NFREQ)WT2=WINT(KK2)*ED2
      SUM=SUM+WINC*(WT0+4.*WT1+WT2)/3.
   20 CONTINUE
   10 WNT(K)=SUM
      GO TO 777
C
C           NORMALIZED LORENTZIAN
C
  100 K=0.
      IW2=INT(4.*GAMM/WINC)
      I22=2*IW2+1
      GDPI=GAMM/PI
      DO 110 I=1,NFREQ
      K=K+1
      SUM=0.
      DO 120 M=1,I22
```

```
      KK0=K+M-IW2-2
      IF(KK0.LE.-1)GO TO 120
      KK1=KK0+1
      KK2=KK1+1
      IF(M.EQ.1)GO TO 125
      IF(KK0.LE.1)GO TO 125
      ED0=ED1
      ED1=ED2
      GO TO 127
  125 DEL=(-IW2-1+M)*WINC
      ED0=GDPI/(DEL**2+GAMM**2)
      DEL=DEL+WINC
      ED1=GDPI/(DEL**2+GAMM**2)
  127 DEL=DEL+WINC
      ED2=GDPI/(DEL**2+GAMM**2)
      WT0=0.
      WT1=0.
      WT2=0.
      IF(KK0.GT.0.AND.KK0.LE.NFREQ)WT0=WINT(KK0)*ED0
      IF(KK1.GT.0.AND.KK1.LE.NFREQ)WT1=WINT(KK1)*ED1
      IF(KK2.GT.0.AND.KK2.LE.NFREQ)WT2=WINT(KK2)*ED2
      SUM=SUM+WINC*(WT0+4.*WT1+WT2)/3.
  120 CONTINUE
  110 WNT(K)=SUM
      GO TO 777
C
C           NORMALIZED TRIANGLE
C
  200 K=0.
      IW2=INT(2.*GAMM/WINC)
      I22=2*IW2+1
      GD4=1./(4.*GAMM)
      DO 210 I=1,NFREQ
      K=K+1
      SUM=0.
      DO 220 M=1,I22
      KK0=K+M-IW2-2
      IF(KK0.LE.-1)GO TO 220
      KK1=KK0+1
      KK2=KK1+1
      IF(M.EQ.1)GO TO 225
      IF(KK0.LE.1)GO TO 225
      ED0=ED1
      ED1=ED2
      GO TO 227
  225 DEL=(-IW2-1+M)*WINC
      ED1=GD4*(2.*GAMM-ABS(DEL))
      DEL=DEL+WINC
      ED1=GD4*(2.*GAMM-ABS(DEL))
```

```
  227 DEL=DEL+WINC
      ED2=GD4*(2.*GAMM-ABS(DEL))
      WT0=0.
      WT1=0.
      WT2=0.
      IF(KK0.GT.0.AND.KK0.LE.NFREQ)WT0=WINT(KK0)*ED0
      IF(KK1.GT.0.AND.KK1.LE.NFREQ)WT1=WINT(KK1)*ED1
      IF(KK2.GT.0.AND.KK2.LE.NFREQ)WT2=WINT(KK2)*ED2
      SUM=SUM+WINC*(WT0+4.*WT1+WT2)/3.
  220 CONTINUE
  210 WNT(K)=SUM
      GO TO 777
C
C           NORMALIZED TRAPEZOID (SLOPE 1/1.28)
C
  300 K=0
      IW2=INT((GAMM+0.64)/WINC)
      I22=2*IW2+1
      AI2=GAMM-.64
      DO 310 I=1,NFREQ
      K=K+1
      SUM=0.
      DO 320 M=1,I22
      KKJ=K+M-IW2-2
      IF(KK0.LE.-1)GO TO 320
      KK1=KKJ+1
      KK2=KK1+1
      IF(M.EQ.1)GO TO 325
      IF(KK0.LE.1)GO TO 325
      EDJ=ED1
      ED1=ED2
      GO TO 327
  325 DEL=(-IW2-1+M)*WINC
      ED0=1./(2.*GAMM)
      IF(ABS(DEL).GT.AI2)ED0=(1.28-(ABS(DEL)-AI2))/(2.56*GAMM)
      DEL=DEL+WINC
      ED1=1./(2.*GAMM)
      IF(ABS(DEL).GT.AI2)ED1=(1.28-(ABS(DEL)-AI2))/(2.56*GAMM)
  327 DEL=DEL+WINC
      ED2=1./(2.*GAMM)
      IF(ABS(DEL).GT.AI2)ED2=(1.28-(ABS(DEL)-AI2))/(2.56*GAMM)
      WT0=0.
      WT1=0.
      WT2=0.
      IF(KK0.GT.0.AND.KK0.LE.NFREQ)WT0=WINT(KK0)*ED0
      IF(KK1.GT.0.AND.KK1.LE.NFREQ)WT1=WINT(KK1)*ED1
      IF(KK2.GT.0.AND.KK2.LE.NFREQ)WT2=WINT(KK2)*ED2
      SUM=SUM+WINC*(WT0+4.*WT1+WT2)/3.
  320 CONTINUE
  310 WNT(K)=SUM
  777 RETURN
      END
```

```
      SUBROUTINE JMAT(RJ)
C     ******* S U B R O U T I N E   J M A T *************
C
C          CALCULATION OF THE J MATRIX
C
C          A NUMERICAL CALCULATION OF THE APPROPRIATE DERIVATIVES
C          FOR THE TEMPERATURE, FREQUENCY, AND RAMAN HWHM
C
C     ***********************************************************************
C
C     ***********************************************************************
C
C
C          RJ  -  J MATRIX
C
C
C     ***********************************************************************
C
C          FPAR  -  INDICATOR FOR DERIVATIVES
C          FPAR(1) = 1  TEMPERATURE
C          FPAR(2) = 1  FREQUENCY
C          FPAR(3) = 1  RAMAN HWHM
C                  -  0  -  SKIP
C
      COMMON/AMAIN/OBS(200),OINT(200),FPAR(3)
      COMMON/BMAIN/GAM,T,WSTART,WINC,WFIN,BK
      COMMON/CMAIN/NVMAX,NJMAX,NOBS
      COMMON/ADEL/WSTAR2,WMAX
      DIMENSION RJ(200,3),WNT1(6000),WNT2(6000)
      CALL SPECTR(WNT1)
      KK=0
      DO 20 I=1,3
      IF(FPAR(I).EQ.0.)GO TO 20
      KK=KK+1.
      IF(I.EQ.2)GO TO 40
      IF(I.EQ.3)GO TO 60
C
C          TEMPERATURE DERIVATIVE
C
      T=T+100.
      CALL SPECTR(WNT2)
      T=T-100.
      DO 10 M=1,NOBS
      K=INT((OBS(M)-WSTAR2)/WINC+1.)
   10 RJ(M,KK)=(WNT2(K)-WNT1(K))/100.
      GO TO 20
C
```

```
C           FREQUENCY DERIVATIVE
C
   40 DO 50 M=1,NOBS
      K=INT((OBS(M)-WSTAR2)/WINC+1.)
      K2=INT((OBS(M)-WSTAR2-10.)/WINC+1.)
   50 RJ(M,KK)=(WNT1(K2)-WNT1(K))/10.
      GO TO 20
C
C           RAMAN HWHM DERIVATIVE
C
   60 GAM=GAM+.02
      CALL SPECTR(WNT2)
      GAM=GAM-.02
      DO 70 M=1,NOBS
      K=INT((OBS(M)-WSTAR2)/WINC+1.)
   70 RJ(M,KK)=(WNT2(K)-WNT1(K))/.02
   20 CONTINUE
      RETURN
      END


      SUBROUTINE MATINV(Y,N)
C     ***** S U B R O U T I N E   M A T I N V *********
C
C           MATRIX INVERSION SUBROUTINE
C
C           THIS SUBROUTINE CAN INVERT UP TO A THIRD ORDER MATRIX.
C           SUGGEST USING JACOB IF A HIGHER ORDER MATRIX REQUIRED
C
C     ****************************************************************
C
C     ************************  ( Y, N )  ****************************
C
C           Y  -  MATRIX TO BE INVERTED
C                 INVERTED MATRIX RETURNED IN Y ARRAY
C           N  -  ORDER OF MATRIX TO BE INVERTED
C
C     ****************************************************************
      DIMENSION Y(3,3),X(3,3)
      DO 12 I=1,N
      DO 12 J=1,N
   12 X(I,J)=Y(I,J)
      IF(N.EQ.1)GO TO 110
      IF(N.EQ.3)GO TO 20
C
```

```
C           INVERSION FOR SECOND ORDER
C
      D=X(1,1)*X(2,2)-X(1,2)*X(2,1)
      Y(1,1)=X(2,2)/D
      Y(1,2)=X(1,2)/D
      Y(2,1)=X(2,1)/D
      Y(2,2)=X(1,1)/D
      GO TO 100
C
C           INVERSION FOR THIRD ORDER MATRIX
C
   20 D=X(1,1)*(X(2,2)*X(3,3)-X(2,3)*X(3,2))
      D=D-X(1,2)*(X(2,1)*X(3,3)-X(2,3)*X(3,1))
      D=D+X(1,3)*(X(2,1)*X(3,2)-X(2,2)*X(3,1))
      Y(1,1)=(X(2,2)*X(3,3)-X(2,3)*X(3,2))/D
      Y(1,2)=(X(1,2)*X(3,3)-X(3,2)*X(1,3))/D
      Y(1,3)=(X(1,2)*X(2,3)-X(2,2)*X(1,3))/D
      Y(2,1)=(X(2,1)*X(3,3)-X(2,3)*X(3,1))/D
      Y(2,2)=(X(1,1)*X(3,3)-X(1,3)*X(3,1))/D
      Y(2,3)=(X(1,1)*X(2,3)-X(2,1)*X(1,3))/D
      Y(3,1)=(X(2,1)*X(3,2)-X(2,2)*X(3,1))/D
      Y(3,2)=(X(1,1)*X(3,2)-X(3,1)*X(1,2))/D
      Y(3,3)=(X(1,1)*X(2,2)-X(2,1)*X(1,2))/D
      GO TO 100
C
C           INVERSION FOR FIRST ORDER MATRIX
C
  110 Y(1,1)=1./Y(1,1)
  100 RETURN
      END
```

```
      SUBROUTINE REPT
C     ****************************************************************
C
C
C           OUTPUT SUBROUTINE
C
C           USES LINE PLOT SUBROUTINE PLOT
C
C     ****************************************************************
      COMMON/AMAIN/OBS(200),OINT(200),FPAR(3)
      COMMON/BMAIN/GAM,T,WSTART,WINC,WFIN,BK
      COMMON/CMAIN/NVMAX,NJMAX,NOBS
      COMMON/ADEL/WSTAR2,WMAX
      DIMENSION ONNT(200),RINT(200),WNT(6000)
      CALL SPECTR(WNT)
      IHIST=1
      ICNT=1
      WRITE(6,10)
   10 FORMAT('1')
      WT=OBS(1)
      WNC=OBS(2)-OBS(1)
      DO 20 I=1,NOBS
   20 ONNT(I)=OINT(I)
      NBBS=NOBS
C
C           PLOT OF EXPERIMENTAL DATA
C
      WRITE(6,30)
   30 FORMAT(30X,' EXPERIMENTAL  SPECTRA ',/)
      CALL PLOT(ONNT,WT,WNC,NBBS,IHIST,ICNT)
      DO 100 I=1,NOBS
      K=INT((OBS(I)-WSTAR2)/WINC+1.)
      RINT(I)=WNT(K)
  100 CONTINUE
      WRITE(6,10)
C
C           PLOT OF CALCULATED SPECTRA
C
      WRITE(6,40)
   40 FORMAT(30X,' CALCULATED  SPECTRA ',/)
      CALL PLOT(RINT,WT,WNC,NBBS,IHIST,ICNT)
      RETURN
      END
```

```
      SUBROUTINE PLOT(Y,XMIN,XINT,NPTS,IHIST,ICNT)
C     ****** S U B R O U T I N E   P L O T **************
C
C          LINE PLOT SUBROUTINE
C
C     ***********************************************************************
C
C     ***********  ( Y, XMIN, XINT, NPTS, IHIST, ICNT )  ***************
C
C          Y   -  Y ARRAY TO BE PLOTTED
C          XMIN  -  SMALLEST X VALUE
C          XINT  -  INCREMENT FOR X AXIS
C          NPTS  -  # OF POINTS TO BE PLOTTED
C          IHIST  -  0  - NO HISTOGRAM
C                 -  1  -  HISTOGRAM
C          ICNT  -  0  -  CENTER 0 ON PLOT
C                 -  1  -  0 ANYWHERE
C
C     ***********************************************************************
      DIMENSION Y(2000),TITLE(36),APT(103),YSCL(11),PMRK(11)
      DATA STAR,BLNK,PLUS,ZERO,HRTX,HRTI/1H*,1H ,1H+,1H0,1HX,1HI/,APT/
     1103*1HX/,PMRK/11*1H+/
      WRITE(6,1000)(Y(I),I=1,NPTS)
 1000 FORMAT(6E12.5)
      YMAX=Y(1)
      YMIN=Y(1)
      DO 2 I=1,NPTS
      YMAX=AMAX1(YMAX,Y(I))
    2 YMIN=AMIN1(YMIN,Y(I))
      IF(YMAX.EQ.YMIN)GO TO 29
      RANGE=YMAX-YMIN
      YMNM=-YMIN
      CODM=YMAX
      IF(YMNM.GT.YMAX)CODM=YMNM
      A=RANGE/10.
      IF(ICNT.EQ.0)A=CODM/5.
      B=YMIN
      IF(ICNT.EQ.0)B=-CODM
      DO 5 I=1,11
      AI=I-1
    5 YSCL(I)=A*AI+B
      PRINT 6,(YSCL(I),I=1,11)
    6 FORMAT(16X,1P11E10.2)
      PRINT 7,(PMRK(I),I=1,11),(APT(K),K=1,103)
    7 FORMAT(/,22X,11(A1,9X),/,21X,103A1)
      DO 27 J=1,NPTS
      NPNT=MOD(J,10)
      DO 8 K=2,102
```

```
      8 APT(K)=BLNK
   50   IF(NPMT.NE.1)GO TO 10
        DO 9 K=1,11
        KM=10*(K-1)+2
      9 APT(KM)=PLUS
     10 IF(Y(J).LT.YMIN.OR.Y(J).GT.YMAX)GO TO 31
   55   IF(ICNT.EQ.0)GO TO 15
        YJ=(Y(J)-YMIN)*100./RANGE+2.5
        IYJ=INT(YJ)
        YPRD=YMAX*YMIN
        IF(YPRD.LT.0..AND.ICNT.NE.-1)GO TO 14
   60 11 IF(IHIST.EQ.0)GO TO 13
        DO 12 K=2,IYJ
     12 APT(K)=STAR
        GO TO 23
     13 APT(IYJ)=STAR
   65   GO TO 23
     14 BLN=2.5-YMIN*100./RANGE
        IBLN=INT(BLN)
        IF(IBLN.LT.2.OR.IBLN.GT.102)GO TO 11
        GO TO 16
   70 15 IBLN=52
        YJ=Y(J)*50./COOM+52.5
        IYJ=INT(YJ)
     16 IF(IYJ.GT.IBLN)GO TO 17
        IF(IYJ.LT.IBLN)GO TO 19
   75   APT(IBLN)=STAR
        GO TO 23
     17 IF(IHIST.EQ.0)GO TO 21
        IBLNP=IBLN+1
        DO 18 K=IBLNP,IYJ
   80 18 APT(K)=STAR
        GO TO 22
     19 IF(IHIST.EQ.0)GO TO 21
        IBLNM=IBLN-1
        DO 20 K=IYJ,IBLNM
   85 20 APT(K)=STAR
        GO TO 22
     21 APT(IYJ)=STAR
     22 APT(IBLN)=WRTI
        IF(NPMT.EQ.1.OR.NPMT.EQ.6)APT(IBLN)=ZERO
   90 23 IF(NPMT.NE.1)GO TO 25
        ZJM=J-1
        XJ=XMIN+ZJM*XINT
        PRINT 24,XJ,(APT(K),K=1,103)
```

```
      24 FORMAT(9X,1PE10.3,2X,103A1)
   95    GO TO 27
      25 PRINT 26,(APT(K),K=1,103)
      26 FORMAT(21X,103A1)
      27 CONTINUE
         DO 281 I=1,103
  100 281 APT(I)=WRTX
         PRINT 28, (APT(I),I=1,103),(PMRK(K),K=1,11),(YSCL(J),J=1,11)
      28 FORMAT(21X,103A1,/,22X,11(A1,9X),//,16X,1P11E10.2,///)
         RETURN
      29 PRINT 30
  105 30 FORMAT(//,10X,*ERROR IN PLOT SUBROUTINE -YMAX=YMIN*)
         RETURN
      31 PRINT 32
      32 FORMAT(//,10X,*ERROR IN PLOT SUBROUTINE-Y EXCEDES YMAX,YMIN
        1LIMITS*)
  110    RETURN
         END
```

References

1. A. C. Eckbreth, R. J. Hall, and J. A. Shirley, "Investigations of Coherent Anti-Stokes Raman Spectroscopy (CARS) for Combustion Diagnostics," Paper 79-0083, presented at the 17th AIAA Conference on Aerospace Sciences, New Orleans, LA, 15-17 June 1979.

2. F. Moya, S. A. J. Druet, and J. P. E. Taran, "Gas Spectroscopy and Temperature Measurement by Coherent Raman Anti-Stokes Scattering," Opt. Commun. 13, 169 (1975).

3. J. W. Nibler, J. R. McDonald, and A. B. Harvey, "CARS Measurements of Vibrational Temperatures in Electric Discharges," Opt. Commun. 18, 371 (1976).

4. W. B. Roh, "Coherent Anti-Stokes Raman Scattering of Molecular Gases," AFAPL-TR-77-47 (Air Force Aero Propulsion Laboratory, Wright-Patterson Air Force Base, OH, August 1977).

5. G. L. Switzer, W. M. Roquemore, R. B. Bradley, P. W. Schreiber, and W. B. Roh, "CARS Measurements in a Bluff-Body-Stabilized Diffusion Flame," Appl. Opt. 18, 2343 (1979).

6. G. L. Switzer, W. M. Roquemore, R. B. Bradley, P. W. Schreiber, and W. B. Roh, "CARS Measurements in Simulated Practical Combustion Environments," Presented at the 178th ACS National Meeting, Washington, D.C., 9-14 September 1979.

7. A. E. Eckbreth, "Spatially Precise Laser Diagnostics for Practical Combustor Probing," Presented at Annual Meeting of the American Chemical Society, Washington, D.C., 9-14 September 1979.

8. I. A. Stenhouse, D. R. Williams, J. B. Cole, and M. D. Swords, "CARS Measurements in an Internal Combustion Engine," Appl. Opt. 18, 3819 (1979).

9. W. M. Tolles, J. W. Nibler, J. R. McDonald, and A. B. Harvey, "A Review of the Theory and Application of Coherent Anti-Stokes Raman Spectroscopy (CARS)," Appl. Spec. 31, 253 (1977).

10. J. W. Nibler and G. V. Knighten, "Coherent Anti-Stokes Raman Spectroscopy," in Raman Spectroscopy of Gases and Liquids (A. Weber, Ed.) (Springer-Verlag, NY, 1979).

11. "Application of Coherent Anti-Stokes Raman Scattering to Laser and Combustion Media," SRL R&D Report 6948-11 covering period 9 December 1979 - 9 March 1980, prepared under Contract F33615-77-C-2019 for the Air Force Aero Propulsion Laboratory (AFAPL/SFF), Wright-Patterson Air Force Base, OH (Systems Research Laboratories, Inc., Dayton, OH, 7 March 1980).

12. W. Koechner, Solid-State Laser Engineering, Springer Series in Optical Sciences (Springer-Verlag, NY, 1976).

13. A. Kim, "Computer Programming in Physical Chemistry Laboratory: Least Squares Analysis," J. Chem. Ed. 47, 120 (1970).

14. R. J. Hall, "CARS Spectra of Combustion Gases," Comb. and Flame 35, 47 (1979).

15. R. J. Hall, Private communication.

16. L. P. Goss, G. L. Switzer, and P. W. Schreiber, Paper 80-1543 presented at the 15th AIAA Thermophysics Conference, Snowmass, CO, 14-16 July 1980.

17. W. B. Roh, R. Weber, and P. W. Schreiber, Opt. Commun. 27, 142 (1978).

18. Quantitative Molecular Spectroscopy and Gas Emissivities (S. S. Penner, Ed.) (Addison-Wesley Publishing Co., Reading, MA, 1959).

19. W. B. Roh, "Coherent Anti-Stokes Raman Scattering of Molecular Gases," AFAPL-TR-77-47 (Air Force Aero Propulsion Laboratory, Wright-Patterson Air Force Base, OH, August 1977).

20. R. Srivastava and H. Zoidi, "Intermolecular Forces Revealed by Raman Scattering," in Raman Spectroscopy of Gases and Liquids (A. Weber, Ed.) (Springer-Verlag, NY, 1979).

21. L. Rahn, A. Owyoung, M. Coltrin, and M. Koszykowski, "The J Dependence of Nitrogen 'Q' Branch Linewidths," presented at the 7th International Conference on Raman Spectroscopy, Ottawa, Canada, 4-9 August 1980.

22. Handbook of Mathematical Functions (M. Abramowitz and I. A. Segun, Eds.) (Power Publications, Inc., NY, 1964).

23. M. A. Henesian, L. A. Kulevsky, R. L. Byer, and R. L. Herbst, Opt. Commun. 18, 225 (1976).

24. W. B. Roh, "Application of Coherent Anti-Stokes Raman Scattering to Laser and Combustion Media," SRL R&D Status Report 6948-1 covering the period 31 May - 31 August 1977, prepared under contract F33615-77-C-2019 for the Air Force Aero Propulsion Laboratory (AFAPL/SFF), Wright-Patterson Air Force Base, OH, (Systems Research Laboratories, Inc., Dayton, OH, 9 September 1977).

25. G. Herzberg, Infrared and Raman Spectra of Polyatomic Molecules, (Van Nostrand, NY, 1945), p. 215.

26. L. S. Rothman and W. S. Bennet, Appl. Opt. 17, 2606 (1978).

27. H. R. Gordon and T. K. McCubbin, Jr., J. Mol. Spectry. 19, 137 (1966).

28. H. E. Howard-Lock and B. P. Stoicheff, J. Mol. Spectry. 37, 321 (1971).

29. H. Haraguchi, et al., "Measurement of Small Volume Flame Temperatures by the Two-Line Atomic Fluorescence Method," Appl. Spectry. 31, 156 (1977).

30. H. Haraguchi and J. D. Winefordner, Appl. Spectry. 31, 330 (1977).

31. A. C. Gaydon and H. G. Wolfhard, Flames: Their Structure, Radiation, and Temperature, 3rd Ed. (Chapman and Hall, London, 1970).

32. R. L. St. Peters, Opt. Lett. 12, 401 (1979).

33. G. L. Switzer, L. P. Goss, W. M. Roquemore, R. B. Bradley, P. W. Schreiber, and W. B. Roh, "The Application of CARS to Simulated Practical Combustion Systems," Paper No. 80-0353, presented at the 18th AIAA Aerospace Sciences Meeting, Pasadena, CA, 14-16 January 1980.

34. W. B. Roh and G. L. Switzer, "Application of Coherent Anti-Stokes Scattering to Laser and Combustion Media," SRL R&D Report 6948-4 covering period 1 March 1978 - 31 May 1978, prepared under contract F33615-77-C-2019 for the Air Force Aero Propulsion Laboratory (AFAPL/SFF), Wright-Patterson Air Force Base, OH (Systems Research Laboratories, Inc., Dayton, OH, 28 June 1978).

35. W. S. Blazowski, "Fundamentals of Combustion," in The Aerothermodynamics of Aircraft Gas Turbine Engines, AFAPL-TR-78-53 (Air Force Aero Propulsion Laboratory, Wright-Patterson Air Force Base, OH, July 1978).

36. "Procedure for the Continuous Sampling and Measurement of Gaseous Emissions from Aircraft Turbine Engines," Society of Automotive Engineers, Aerospace Recommended Practices No. 1256 (Society of Automotive Engineers, Oct. 1971).

37. R. W. Morris, Jr., Private communication.

38. W. M. Roquemore, Private communication.

39. R. T. Lynch, S. D. Kramer, H. Lotens, and N. Bloembergen, Opt. Commun. 16, 372 (1976).

40. J. J. Song, G. L. Eesley, and M. D. Levenson, Appl. Phys. Lett. 29, 567 (1976).

41. A. Owyoung, IEEE J. Quantum Electron. QE-14, 192 (1978).

42. J. L. Onder, R. W. Smith, and Y. S. Shem, Appl. Phys. Lett. 34, 758 (1979).

43. L. A. Rahn, J. L. Zynch, and P. L. Mattern, "Background-Free CARS Studies of Carbon Monoxide in a Flame," Sandia Report SAND 79-8650, prepared for United States Department of Energy under Contract DE-AC04-76DP00789 (Sandia Laboratories, Albuquerque, NM, 1979).

44. B. Hogge and W. Visinsky, Appl. Opt. 10, 899 (1971).

45. W. B. Roh and P. Schreiber, Appl. Opt. 17, 1418 (1978).

46. D. Jackson, Classical Electrodynamics (John Wiley and Sons, Inc., NY, 1967), p. 186.

47. R. Schmeltzer, Appl. Opt. 10, 1652 (1971).

48. P. Regnier, F. Moya, and J. P. E. Taran, AIAA J. 12, 826 (1974).

49. J. A. Shirley, R. J. Hall, J. F. Verdieck, and A. C. Eckbreth, Paper 80-1542, presented at the 15th AIAA Thermophysics Conference, Snowmass, CO, 14-16 July 1980.

50. S. Chandra and A. Compaan, Opt. Commun. 31, 73 (1979).

51. W. M. Roquemore, R. B. Bradley, J. S. Stutrud, C. M. Reeves, and L. Krishnamurthy, "Preliminary Evaluation of a Combustor for use in Modeling and Diagnostics Development," Paper 80-GT-93, presented at ASME 25th Annual International Gas Turbine Conference, New Orleans, LA, March 1980.

52. G. L. Switzer, "Hardened CARS System Equipment Manual," Prepared for Aero Propulsion Laboratory (AFWAL/POSF), Wright-Patterson Air Force Base, OH, under Contract F33615-77-C-2019 (Systems Research Laboratories, Inc., Dayton, OH, May 1980)

☆ U.S. GOVERNMENT PRINTING OFFICE: 1981—757-002/16

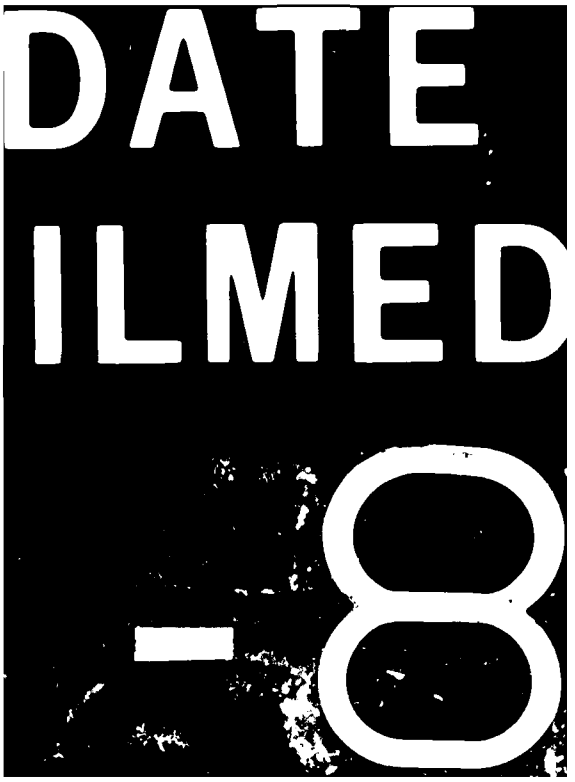
DATE
ILMED
-8